Aus der Abteilung für Experimentelle Chirurgie

des Abteilungsleiters Prof. Edward Geissler, PhD

der Fakultät für Medizin

der Universität Regensburg

The Mechanism of lncRNAs in Cell Death after Hepatic Ischemia-Reperfusion Injury

Inaugural-Dissertation

zur Erlangung des Doktorgrades

der Medizin

der

Fakultät für Medizin

der Universität Regensburg

vorgelegt von

Fan Yang

2026

Dekan: Prof. Dr. Dirk Hellwig

1. Berichterstatterin: Prof. Dr. rer. nat. Elke Eggenhofer

2. Berichterstatterin: Prof. Dr. med. Miriam Banas

Tag der mündlichen Prüfung: 28.04.2026

Content

I. Abbreviations

4HNE	4-Hydroxynonenal
AA	Arachidonic acid
ABCC1	ATP binding cassette subfamily C member 1
ACD	Accidental cell death
ACSL4	Acyl-CoA synthetase long chain family member 4
ACTB	β-actin
AdA	Adrenic acid
ADMET	Adsorption, distribution, metabolism, elimination, toxicity
AIFM	Apoptosis-inducing factor mitochondria -associated
AK	Adenylate kinase
AKR1C1/2/3	Aldo-keto reductase family 1 member C1/2/3
ALOX	Arachidonate lipoxygenase
ARNTL	Aryl hydrocarbon receptor nuclear translocator -like protein 1
ATP	Adenosine triphosphate

BBH4	Tetrahydrobiopterin
CBS	Cystathionine beta-synthase
CD	Cluster of differentiation
cDNA	Complementary DNA
CHAC1	ChaC glutathione specific gamma -glutamylcyclotransferase 1
CHMP	Charged multivesicular body protein
CoQ10	Coenzyme Q10
Ctrl	Control
DAMP	Damage-associated molecular pattern
DPBS	Dulbecco's phosphate buffered saline
DPI	Diphenylene iodonium chloride
DPP4	Dipeptidyl peptidase-4
DSO	Deutsche Stiftung Organtransplantation
ECD	Extended criteria donors
ECM	Extracellular matrix
EDTA	Ethylenediaminetetraacetic acid
EGOT	Eosinophil Ontogeny Transcript

eNOS	Endothelial NO synthase
ESCRT	Endosomal sorting complexes required for transport
Fer-1	Ferrostatin-1
FIN56	Ferroptosis inducer 56
$FINO_2$	Ferroptosis inducer endoperoxide
FPN	Ferroportin
FSP1	Ferroptosis suppressor protein1
FTH1	Ferritin heavy chain 1
GCH1	GTP cyclohydrolase-1
GMP	Good manufacturing practice
GODT	Global Observatory on Donation and Transplantation
GPX4	Glutathione peroxidase 4
GS	Goat serum
GSDMD	Gasdermin D
GSH	Glutathione
HCl	Hydrogen chloride

HIF1α	Hypoxia-inducible factor 1 alpha
HIRI	Hepatic ischemia-reperfusion injury
HLMA	Human lymphocyte micronucleus assay
HMGB1	High mobility group box 1
HMOX1	Heme oxygenase 1
HRP	Horseradish peroxidase
HSC	Hepatic stellate cells
HSF1	Heat shock factor 1
HSPB1	Heat shock protein beta 1
IC_{50}	Mean inhibitory concentration
ICAM1	Intercellular adhesion molecule 1
ICH	International council for harmonisation of technical requirements for pharmaceuticals for human use
IFNγ	Interferon γ
IL	Interleukin
INR	International normalized ratio
IRI	Ischemia reperfusion injury

KC	Kupffer cells
KEAP1	Kelch like ECH associated protein 1
KLF2	Krüppel-like factor 2
Lip-1	Liproxstatin-1
LncRNA	Long non-coding RNA
LOH	Lipid alcohols
LOOH	Lipid hydroperoxides
LPCAT3	Lysophosphatidylcholine acyltransferase 3
LSEC	Liver sinusoidal endothelial cells
LTF	Lactotransferrin
MDA	Malondialdehyde
MELD	Model for end stage liver disease
MFD	Maximum feasible dose
MHH	Medical school Hannover
MLKL	Mixed lineage kinase domain-like protein
MMP	Matrix metalloprotease
MT1G	Metallothionein 1 G
MTD	Maximum tolerable dose

MUFA	Monounsaturated fatty acids
Na_2HPO_4	Disodium phosphate
NaCl	Sodium chloride
NAD^+	Nicotinamide adenine dinucleotide
NADPH	Nicotinamide adenine dinucleotide phosphate hydrogen
NAFLD	Non-alcoholic fatty liver disease
NaH_2PO4	Monosodium phosphate
NCCD	Nomenclature Committee on Cell Death
NCOA4	Nuclear receptor coactivator 4
NEAT1	Nuclear Paraspeckle Assembly Transcript 1
Nec-1	Necrostatin-1
NEDD4	Neuronal precursor cell-expressed developmentally downregulated 4
NEDD4L	NEDD4-like E3 ubiquitin ligase
NO	Nitric oxide
NOX	NADPH oxidase
NQO1	NADPH quinone dehydrogenase 1

NRF2	Nuclear factor erythroid 2–related factor 2
OPTN	Organ Procurement and Transplantation Network
PARP	Poly(ADP-ribose)-polymerase
PBMC	Peripheral blood mononuclear cell
PCR	Polymerase chain reaction
PE	Phosphatidylethanolamine
PMSF	Phenylmetansulfonylfluoride
POR	Cytochrome P450 oxidoreductase
PRDX	Peroxiredoxin
PTGS2	Prostaglandin endoperoxide synthase 2
UCA1	Urothelial Cancer Associated 1

II. Abstract

Hepatic ischemia-reperfusion injury (HIRI) represents a significant clinical challenge, particularly in the context of liver transplantation, resection, and marginal donor organ utilization. While the pathogenesis of HIRI involves a complex interplay of hypoxia, oxidative stress, inflammation, and various forms of regulated cell death, emerging evidence underscores the pivotal role of long non-coding RNAs (lncRNAs) in orchestrating these processes. Despite extensive advances in our understanding of the mechanisms of hepatocellular damage, the specific regulatory contributions of lncRNAs to the modalities of programmed cell death—namely apoptosis, necroptosis, and ferroptosis—are not yet fully understood. This study aimed to elucidate the mechanistic involvement of lncRNAs in hepatocyte death following ischemia-reperfusion, with a particular focus on identifying functional lncRNAs that may serve as biomarkers or therapeutic targets in marginal donor liver grafts.

Using a human hepatocyte-derived cell line (HepaRG) exposed to hypoxic and steatotic conditions mimicking marginal graft physiology, we employed a high-throughput RT^2 lncRNA PCR Array to profile the expression of 114 candidate lncRNAs previously implicated in liver pathophysiology. We identified 28 lncRNAs with significant differential expression under hypoxia and/or fatty acid overload, comprising 11 up-regulated and 17 down-regulated transcripts. Integration of this dataset with the

ncFO database—an established compendium of lncRNAs associated with ferroptosis—revealed seven up-regulated ferroptosis-related lncRNAs (H19, UCA1, PVT1, LUCAT1, LINC00673, ZFAS1, MALAT1) and nine down-regulated counterparts (e.g., NEAT1, TUG1, XIST). Parallel screening using the LncPCD database, which catalogs lncRNAs linked to broader cell death mechanisms, yielded nine up- and twelve down-regulated PCD-associated lncRNAs. Cross-validation across datasets, combined with literature-based functional annotation, narrowed our focus to four lncRNAs—UCA1, H19, EGOT, and NEAT1—as high-priority candidates.

Functional studies demonstrated that knockdown or overexpression of these lncRNAs significantly modulated cell viability, ROS generation, mitochondrial membrane potential, and the expression of key apoptotic and ferroptotic markers, including caspase-3, caspase-9, GPX4, and ACSL4. UCA1, a well-characterized oncogenic lncRNA, exerted anti-apoptotic effects via the PI3K/Akt pathway and suppressed ferroptotic damage by regulating miR-143 and glutathione metabolism. H19, originally identified as an imprinted transcript, promoted ferroptosis through miRNA sponging (e.g., miR-675) and modulated inflammatory responses via NF-κB and STAT3 signaling. EGOT, an antisense intronic lncRNA previously implicated in eosinophil biology and cancer, was found to regulate hypoxia-induced autophagy and promote mitochondrial dysfunction, exacerbating IRI-related damage. NEAT1, a nuclear lncRNA central to paraspeckle

formation, influenced both apoptosis and ferroptosis by altering expression of SLC7A11, c-Met/Akt signaling, and pro-inflammatory cytokine cascades.

Our results support a paradigm in which lncRNAs act as master regulators of hepatic cell fate during IRI, functioning through diverse mechanisms including miRNA sponging, transcriptional scaffolding, and post-transcriptional modulation. Mechanistically, the lncRNA-mRNA-miRNA axis forms a critical regulatory triad in hypoxia-reoxygenation settings, wherein lncRNAs serve as both signal integrators and amplifiers of stress responses. Moreover, the cross-talk between apoptosis, ferroptosis, and necroptosis, as modulated by these lncRNAs, suggests a networked model of cell death regulation in the ischemic liver, challenging the traditional view of linear, pathway-isolated cell death modalities.

To translate these insights into potential therapeutic strategies, we evaluated the impact of pharmacologic inhibitors targeting ferroptosis (e.g., ferrostatin-1), necroptosis (e.g., necrostatin-1), and apoptosis (e.g., caspase inhibitors) in conjunction with siRNA-mediated lncRNA silencing. Combined modulation revealed synergistic effects, particularly when UCA1 or NEAT1 was suppressed alongside ferroptosis inhibition, indicating that lncRNA-targeted interventions may enhance cytoprotective strategies in liver transplantation.

Taken together, our findings reveal that lncRNAs are not merely bystanders but active participants in the molecular orchestration of hepatic ischemia-reperfusion injury. The identified lncRNAs—

UCA1, H19, EGOT, and NEAT1—serve as key regulators of hepatocellular resilience or vulnerability under ischemic stress and represent promising biomarkers and targets for therapeutic intervention. Future studies should extend these insights into in vivo models and clinical cohorts to validate translational potential and inform strategies for improving marginal liver graft outcomes.

III. Zusammenfassung

Die ischämisch-reperfusionsbedingte Leberschädigung (HIRI) stellt eine erhebliche klinische Herausforderung dar, insbesondere im Kontext der Lebertransplantation, Leberresektion und der Verwendung von marginalen Spenderorganen. Obwohl die Pathogenese der HIRI ein komplexes Zusammenspiel von Hypoxie, oxidativem Stress, Entzündungsreaktionen und verschiedenen Formen des regulierten Zelltods umfasst, rückt die zentrale Rolle von langen nicht-kodierenden RNAs (lncRNAs) zunehmend in den Fokus der Forschung. Trotz bedeutender Fortschritte im Verständnis hepatotoxischer Mechanismen sind die spezifischen regulatorischen Funktionen von lncRNAs im Rahmen des programmierten Zelltods – insbesondere Apoptose, Nekroptose und Ferroptose – noch unzureichend geklärt. Ziel dieser Arbeit war es, die mechanistische Beteiligung von lncRNAs am Hepatozytentod nach ischämischer Reperfusion zu untersuchen und funktionell relevante lncRNAs zu identifizieren, die als Biomarker oder therapeutische Zielmoleküle bei der Nutzung marginaler Spenderlebern dienen könnten.

Unter Verwendung einer aus humanen Hepatozyten abgeleiteten Zelllinie (HepaRG), die hypoxischen und steatotischen Bedingungen ausgesetzt wurde, welche die Physiologie marginaler Lebertransplantate nachahmen, führten wir ein Hochdurchsatz-RT2-lncRNA-PCR-Array durch, um das Expressionsprofil von 114 Kandidaten-lncRNAs zu analysieren,

die zuvor mit leberassoziierter Pathophysiologie in Verbindung gebracht worden waren. Dabei identifizierten wir 28 lncRNAs mit signifikant veränderter Expression unter Hypoxie und/oder Fettsäureüberladung, darunter 11 hochregulierte und 17 herunterregulierte Transkripte. Die Integration dieses Datensatzes mit der ncFO-Datenbank – einer etablierten Sammlung ferroptoseassoziierter lncRNAs – ergab sieben hochregulierte ferroptosebezogene lncRNAs (H19, UCA1, PVT1, LUCAT1, LINC00673, ZFAS1, MALAT1) sowie neun herunterregulierte Gegenstücke (u. a. NEAT1, TUG1, XIST). Eine parallele Analyse mithilfe der LncPCD-Datenbank, die lncRNAs im Zusammenhang mit allgemeinen Zelltodmechanismen katalogisiert, identifizierte neun hoch- und zwölf herunterregulierte PCD-assoziierte lncRNAs. Durch Kreuzvalidierung der Datensätze in Kombination mit literaturbasierter funktioneller Annotation wurde der Fokus schließlich auf vier lncRNAs – UCA1, H19, EGOT und NEAT1 – als hochprioritäre Kandidaten eingegrenzt.

Funktionelle Untersuchungen zeigten, dass der Knockdown oder die Überexpression dieser lncRNAs die Zellviabilität, die ROS-Produktion, das mitochondriale Membranpotenzial sowie die Expression zentraler apoptotischer und ferroptotischer Marker, darunter Caspase-3, Caspase-9, GPX4 und ACSL4, signifikant beeinflusste. UCA1, eine gut charakterisierte onkogene lncRNA, vermittelte antiapoptotische Effekte über den PI3K/Akt-Signalweg und unterdrückte ferroptotische Schädigung durch Regulation von miR-143 und des Glutathionstoffwechsels. H19, ursprünglich als

geprägtes Transkript identifiziert, förderte die Ferroptose durch miRNA-Sponge-Mechanismen (z. B. miR-675) und modulierte inflammatorische Antworten über NF-κB- und STAT3-Signalwege. EGOT, eine antisense-intronspezifische lncRNA, die zuvor mit der Eosinophilenbiologie und malignen Erkrankungen in Verbindung gebracht wurde, regulierte hypoxieinduzierte Autophagie und förderte mitochondriale Dysfunktion, wodurch ischämie-reperfusionsbedingte Zellschädigung verstärkt wurde. NEAT1, eine nukleäre lncRNA mit zentraler Bedeutung für die Paraspeckle-Bildung, beeinflusste sowohl Apoptose als auch Ferroptose durch Veränderung der Expression von SLC7A11, der c-Met/Akt-Signaltransduktion sowie proinflammatorischer Zytokinkaskaden.

Unsere Ergebnisse unterstützen ein Paradigma, dem zufolge lncRNAs als übergeordnete Regulatoren des hepatischen Zellschicksals während der Ischämie-Reperfusions-Schädigung fungieren und dabei über vielfältige Mechanismen wie miRNA-Sponging, transkriptionelle Gerüstbildung und posttranskriptionelle Modulation wirken. Mechanistisch bildet die lncRNA-mRNA-miRNA Achse eine entscheidende regulatorische Triade unter Hypoxie-Reoxygenierungsbedingungen, wobei lncRNAs sowohl als Signal-Integratoren als auch als Verstärker zellulärer Stressantworten agieren. Darüber hinaus legt das durch lncRNAs modulierte Zusammenspiel von Apoptose, Ferroptose und Nekroptose ein vernetztes Modell der Zelltodregulation in der ischämischen Leber nahe und stellt damit die traditionelle

Auffassung linearer, voneinander isolierter Zelltodwege infrage.

Zur Übertragung dieser Erkenntnisse in potenzielle therapeutische Strategien untersuchten wir den Effekt pharmakologischer Inhibitoren der Ferroptose (z. B. Ferrostatin-1), der Nekroptose (z. B. Necrostatin-1) und der Apoptose (z. B. Caspase-Inhibitoren) in Kombination mit siRNA-vermittelter lncRNA-Silenzierung. Die kombinierte Modulation zeigte synergistische Effekte, insbesondere bei gleichzeitiger Suppression von UCA1 oder NEAT1 und Hemmung der Ferroptose, was darauf hindeutet, dass lncRNA-gerichtete Interventionen zytoprotektive Strategien in der Lebertransplantation verstärken können.

Zusammenfassend zeigen unsere Ergebnisse, dass lncRNAs keine passiven Begleiterscheinungen, sondern aktive Akteure in der molekularen Orchestrierung der hepatischen Ischämie-Reperfusions-Schädigung sind. Die identifizierten lncRNAs – UCA1, H19, EGOT und NEAT1 – fungieren als zentrale Regulatoren der hepatozellulären Resistenz oder Vulnerabilität unter ischämischem Stress und stellen vielversprechende Biomarker sowie therapeutische Zielstrukturen dar. Zukünftige Studien sollten diese Erkenntnisse auf in-vivo-Modelle und klinische Kohorten ausweiten, um das translationale Potenzial zu validieren und Strategien zur Verbesserung der Ergebnisse marginaler Lebertransplantate zu entwickeln.

1. Introduction

1.1 Hepatic Ischaemia-Reperfusion Injury

Liver diseases are reported to cause up to 2 million deaths worldwide each year[1]. With the increasing global incidence of liver disease in recent years, the prevalence of hepatic ischaemia-reperfusion injury (IRI), a serious complication of liver transplantation, liver resection and systemic hypoperfusion, has remained persistently high[1]. Consequently, the mitigation of hepatic IRI has received increasing attention. Since Jennings first introduced the concept of ischaemia-reperfusion injury in 1960[2], IRI has been recognised in organs such as the heart, kidney, brain, intestine and liver[2–5]. In the liver, ischaemia-reperfusion injury was identified by Toledo-Pereyra and colleagues in 1975 as a pathological change with significant clinical relevance in experimental liver transplantation[3]. However, it wasn't until the mid-1980s that the term "hepatic ischaemia-reperfusion injury" became widely used in the literature[6–8].

IRI is defined as the exacerbation of cellular damage following restoration of oxygen after a period of hypoxia[9]. In the liver, IRI manifests as an inflammatory and immune response triggered by hypoxia and reoxygenation, ultimately leading to hepatocyte damage or even death[10]. Multiple cell types are involved in this process, including hepatocytes, liver sinusoidal endothelial cells (LSECs), Kupffer cells, hepatic stellate cells (HSCs), extrahepatic macrophages, neutrophils and platelets[11,12].

Pathways involved in hepatic IRI include anaerobic metabolism,

oxidative stress, intracellular calcium overload, endothelial injury, activation of Kupffer cells and infiltration of neutrophils, CD4+ T cells, interleukins and chemokines as shown in Figure 1. During hypoxia, hepatocytes switch from aerobic ATP production to anaerobic ATP-dependent metabolism. This depletion of ATP and accelerated glycolysis leads to the accumulation of lactate and ketone bodies[13], causing the intracellular pH to drop. The accumulation of acidic metabolites disrupts signalling, cellular homeostasis and sodium/potassium ATPase activity, leading to reduced activity of phospholipases, proteases and Na+/K+ ATPase, ultimately altering the balance of intracellular H+, Na+ and Ca2+, resulting in cytoplasmic pH decline and calcium overload[13–15].

Figure 1 illustrates that, in the early stages of reperfusion, the restoration of aerobic metabolism facilitates the removal of lactate and ketones by perfusion or blood flow, gradually normalising pH. However, this also triggers the activation of pH-dependent enzymes, such as proteases and phospholipases, which exacerbate cellular organelle damage by increasing reactive oxygen species (ROS)[16]. Damaged mitochondria further release calcium, which converts xanthine dehydrogenase (XDH) to xanthine oxidase (XOD), which generates oxygen free radicals. ROS in turn interact with Ca2+, promoting the opening of mitochondrial permeability transition pores (MPTP), further mitochondrial damage, cytochrome C release, apoptotic body formation and promotion of apoptosis[17].

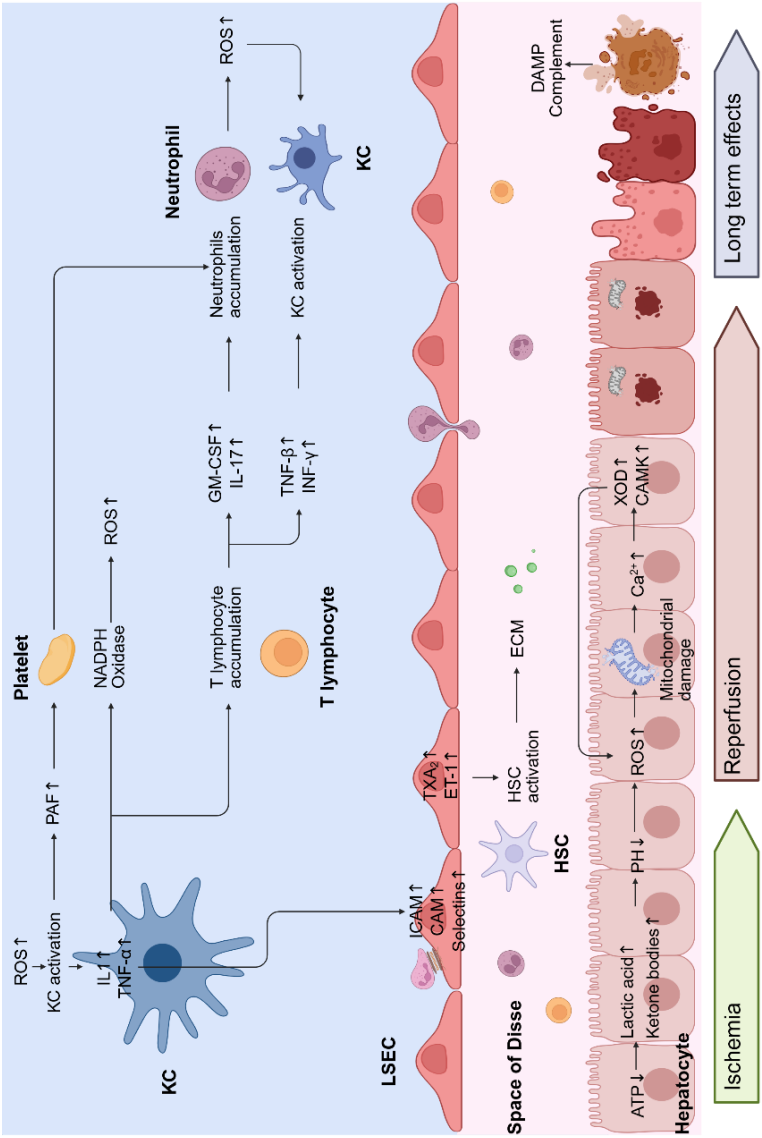

Figure 1. The regulation of liver microenvironment during different periods of hepatic ischemia/reperfusion injury. A summary of the immune components of liver microenvironment during the continuous phase of ischemia/reperfusion injury is manifested. LSEC, liver sinusoidal endothelial

cell; HSC, hepatic stellate cell; KC, kupffer cell; ROS, reactive oxygen species; ECM, extracellular matrix. Created with BioRender.com.

Cells damaged by ROS release damage-associated molecular patterns (DAMPs) such as HMGB1, mROS and histone/DNA complexes. HMGB1, passively released from necrotic cells, binds to LR4 or TLR9 on Kupffer cells (KCs), activating the NF-κB pathway and inducing the production of pro-inflammatory cytokines such as tumour necrosis factor-α (TNF-α) and interleukin-1 (IL-1)[18–21]. Elevated levels of TNF-α and IL-1 further activate NADPH oxidase, producing hydrogen peroxide (H_2O_2) and hydroxyl radicals (HO-), which propagate ROS-mediated damage to hepatocytes, leading to mitochondrial dysfunction and cell death[9]. Inhibition of NADPH oxidase significantly attenuates liver injury after ischaemia-reperfusion[22–24].

In addition, IL-1 and TNF-α recruit and activate CD4+ T lymphocytes[25,26], which produce granulocyte-macrophage colony-stimulating factor (GM-CSF), interferon-γ (INF-γ), TNF-β and IL-17[11,27]. INF-γ and TNF-β enhance KC activation, which further promotes TNF-α and IL-1 secretion, thereby exacerbating IRI progression[28,29]. IL-17 and GM-CSF contribute to neutrophil recruitment and ROS release[30,31].

TNF-α also induces P-selectin expression in liver sinusoidal endothelial cells (LSECs), facilitating neutrophil aggregation and adhesion[32]. As key cells during liver ischaemia-reperfusion, activated Kupffer cells release platelet-activating factor (PAF),

which mediates platelet adhesion and triggers neutrophil recruitment[31,33,34]. Kupffer cells also release oxygen free radicals (OFRs) and cytokines that promote the shedding of protein-polysaccharide complexes from the endothelial surface of liver sinusoids and increase the activation of adhesion molecules such as ICAM, VCAM, L-selectin and PAF. Studies have shown that ICAM and VCAM promote neutrophil aggregation in reperfused livers[35]. Activated LSECs release thromboxane A2 (TXA2) and endothelin-1 (ET-1), leading to activation of HSCs, their transdifferentiation into proliferative, contractile and pro-inflammatory myofibroblasts characterised by extracellular matrix (ECM) secretion[36]. In this state, HSCs express α-smooth muscle actin (α-SMA), causing sinusoidal contraction and microcirculatory disturbances that exacerbate hepatic IRI.

In the later stages of reperfusion, hepatic IRI is characterised by immune cell infiltration. Approximately 30% of recruited CD4+ T cells reside in the hepatic sinusoids where they enhance platelet adhesion and neutrophil recruitment, intensifying local inflammatory responses, microvascular injury and hepatocyte death, ultimately leading to severe liver injury[37].

1.2 Cell Death In The Liver

The liver is composed of a heterogeneous population of cells, which can be broadly classified into two main categories: parenchymal and non-parenchymal cells. Approximately 78–80% of the liver's total volume is constituted by parenchymal cells

(hepatocytes), whereas non-parenchymal cells account for a mere 5–6%. The non-parenchymal population includes Kupffer cells (KCs), liver sinusoidal endothelial cells (LSECs), and hepatic stellate cells[38–40]. During ischemia-reperfusion, these cellular constituents engage in the process at distinct temporal phases, involving various modalities of cell death.

Until the early twenty-first century, it was widely accepted that HIRI induced cell death exclusively through necrosis and apoptosis. It was further postulated that necrosis was responsible for 90% of cell death post-hepatic IRI[41]. However, as our understanding of hepatic IRI has deepened, research has revealed that although necroptosis appears to be the predominant form of cell death in this context, multiple regulated cell death pathways are typically complementary or overlapping across different liver regions[42]. Ischemia and reperfusion injury can activate a number of cell death mechanisms, including necrosis, apoptosis, necroptosis, ferroptosis, pyroptosis, autophagy, and NETosis.

In the initial phase of ischaemia-reperfusion, the disruption of the respiratory chain within hepatocytes results in the generation of reactive oxygen species (ROS) by the mitochondria. These ROS directly affect biological membranes through lipid peroxidation and induce protein denaturation, which ultimately leads to necrosis[43]. Apoptosis can be divided into two main pathways: intrinsic and extrinsic. The intrinsic pathway is activated in response to stressors such as hypoxia during ischaemia, resulting in the release of pro-apoptotic factors (e.g. cytochrome c, caspase-

activated DNase G, apoptosis-inducing factor) from the mitochondria into the cytoplasm. This induces apoptosis via caspase-dependent and -independent pathways. In contrast, the extrinsic pathway is triggered by extracellular death ligands, including TNF-α, Fas ligand and TNF-related apoptosis-inducing ligand (TRAIL), which bind to death receptors and induce cytotoxic signalling, leading to apoptosis in damaged cells by proteolysis[44]. The morphological similarities between necroptosis and necrosis are evident; however, the biochemical distinctions are more pronounced. Necroptosis is induced in the presence of caspase inhibitors and is mediated by receptor-interacting serine/threonine protein kinase 3 (RIPK3)[43,44]. Following reperfusion, the accumulation of ROS promotes the formation of inflammasomes, which have the potential to trigger pyroptosis. This process is distinct from apoptosis in that it is exclusively dependent on caspase-1 and results in the substantial release of pro-inflammatory cytokines[45]. Ferroptosis is an iron-dependent oxidative form of cell death that is triggered by the inactivation of cellular glutathione (GSH). It is mediated by erastin, which induces iron-dependent ROS accumulation, iron overload and lipid peroxidation[46]. Autophagy, a lysosome-mediated mode of cell death, is utilised by both healthy and damaged hepatocytes to eliminate long-lived or misshapen proteins and organelles[47]. NETosis is induced by various stimuli (such as DAMPs), whereby neutrophils shed chromatin to form adhesive neutrophil extracellular traps (NETs) with the capacity to trap and neutralise

pathogens[48].

The triggers, main mechanisms and morphological characteristics of the different cell death modalities are listed in Table 1. The following sections will discuss the mechanisms of four prototypical forms of cell death in hepatic ischaemia-reperfusion injury in detail.

	Necrosis	Apoptosis intrinsic	Apoptosis extrinsic	Necroptosis	Ferroptosis	Pyroptosis	Autophagy	NETosis
Triggers	Ischemia	Intracellular signals	TNF-α	TLR3/4 receptor activation	Fe2+ overload	Inflammation	Ischemia	ROS
Associated inflammatory response?	Yes	No	NO	Yes	Yes	Yes	Unknown	Yes
Main mechanism	ATP depletion	Caspase-3 cleavage	Caspase cascade	Necrosome complex	Lipid peroxidation	Caspase-1 activation	Autolysosomes	Inflammation
Key players	ROS	Caspase-3 and 9	Caspase-8	RIPK1, RIPK3, MLKL	LPO and ROS	Caspase-1, caspase-4 and 11, Gasdermin D	ATGs	Activated neutrophils
Inhibitors	amino acid glycine	Bcl-2	Bcl-2	Caspase-8	GPX4	Inflammation inhibitors	Bcl-2	NETs inhibitors
Morphology	Cell swelling, Karyolysis, Vacuolization	Nuclear condensation, Apoptotic bodies	Outer mitochondrial membrane pores	Cell swelling, Membrane rupture	Smaller mitochondria	Chromatin condensation	Double-membraned vacuoles	Neutrophil release of chromatin fibers

Table 1 : Characterization of different forms of cell death in hepatic ischemia-reperfusion injury

ROS: reactive oxygen species; MPTP: Mitochondrial Permeability Transition Pore; Bcl-2:B-cell lymphoma-2; TNF:tumor necrosis factor; TLR:Toll-like receptors; RIPK: Receptor-interacting serine/ threonine-protein kinase; MLKL: mixed lineage kinase domain-like; LPO:lipid peroxide; GPX4:glutathione peroxidase-4; ATGs: autophagyrelated genes; NETs: Neutrophil extracellular traps.

1.2.1 Necrosis

Necrosis, also known as permeable necrosis or tumour deposition, represents an irreversible, non-apoptotic form of cell death. It accounts for approximately 90% of all cell death forms in hepatic ischemia-reperfusion injury (HIRI)[49]. In the initial stages of hepatic ischemia, the hypoxic environment resulting from global or localized liver ischemia causes intracellular ATP depletion and a reduction in pH within minutes to hours, leading to disturbances in ionic homeostasis within cells. This imbalance results in mitochondrial permeability changes, lysosomal rupture, cell swelling, and endoplasmic reticulum expansion (Figure 2). Prolonged hypoxia results in irreversible cellular damage and ultimately leads to cell death[29,50]. It is notable that necrotic cell death induces a significant inflammatory response as a result of the release of cellular contents.

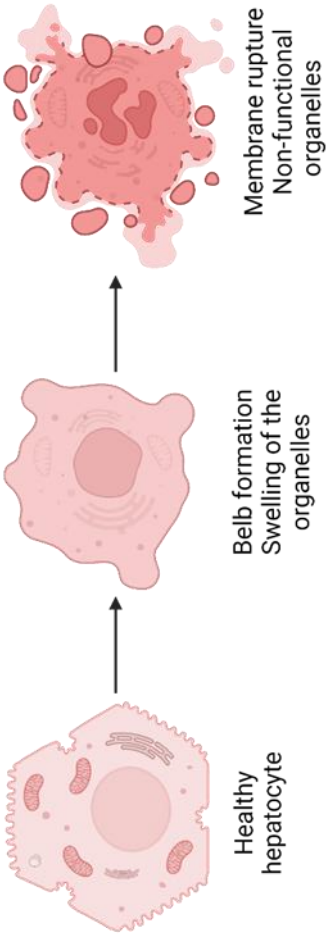

Figure 2. Morphologic changes associated with necrosis after hepatic IRI. Necrosis occurs from injury or stress with uncontrolled consequences. In morphology necrosis involves swelling, organelle damage, and the release of cellular contents. Created with BioRender.com.

Hypoxia in hepatocytes disrupts the mitochondrial respiratory chain, resulting in the generation of excessive reactive oxygen species (ROS). These ROS compromise membrane integrity and lead to a loss of selective mitochondrial permeability. During reperfusion, the irreversible depletion of cellular ATP exacerbates ROS accumulation, which in turn provokes neutrophil infiltration within hepatic tissue and exacerbates widespread hepatocyte injury and inflammatory response[51]. The release of cellular components, including damage-associated molecular patterns (DAMPs), following necrosis activates Kupffer cells and releases pro-inflammatory mediators, eliciting a robust sterile inflammatory reaction. In the liver, necrosis affects a substantial number of adjacent cells, thereby intensifying tissue injury through the inflammatory response that it provokes. Morphological and histological characteristics indicative of cell death include cellular swelling, vacuolisation, karyolysis, diffuse areas of cellular content release, and pronounced inflammatory responses[29].

In light of the advancements in scientific knowledge and the enhanced comprehension of cell death mechanisms, researchers have noted that necrosis and necroptosis exhibit analogous ultrastructural characteristics when observed under electron microscopy. Consequently, the initial assumption that necrosis was occurring in the context of hepatic ischemia-reperfusion may now be revised to include the possibility of necroptosis and other forms of cell death.

In the context of hepatic ischemia-reperfusion injury, studies have identified molecular mechanisms that are capable of modulating necrosis. For example, the inhibition of MPT pore opening and the application of glycine to block anion channel activation have been demonstrated to mitigate cell necrosis induced by liver ischemia-reperfusion injury[17,27,52]. These strategies provide a degree of protection against hepatic ischemia-reperfusion injury.

Given that necrosis is a vigorous and irreversible form of cell death induced by severe extrinsic factors, its modulation is influenced by a number of factors. In light of the multitude of influencing factors and the difficulties in accurately defining necrosis in an experimental setting, therapeutic approaches targeting necrosis to protect against post-reperfusion liver injury remain limited. Consequently, researchers frequently direct their attention towards programmed cell death as a principal area of inquiry.

1.2.2 Apoptosis

Apoptosis is a highly regulated form of cell death that plays a crucial role in physiological and pathological processes in multicellular organisms. It is regulated by two main pathways, the extrinsic and intrinsic pathways (Figure 3). In hepatic ischaemia-reperfusion (IR) injury, the mechanism of apoptosis is particularly important because it is closely related to tissue damage and repair. The intrinsic pathway of apoptosis is mainly mediated by mitochondria. The intrinsic pathway is normally activated by intracellular insults such as oxidative stress, DNA damage and ER

stress[29,41], and these stimuli trigger the activation of pro-apoptotic proteins such as Bax and Bak, leading to an increase in the permeability of the mitochondrial outer membrane and the release of apoptotic factors such as cytochrome c into the cytoplasm. These factors further bind to Apaf-1 to form apoptotic bodies, which in turn activate caspase-9, initiating a series of caspase cascade reactions that ultimately lead to apoptotic cell death (apoptosis)[11,51,53]. Extrinsic pathway activated by death receptor signalling. Binding of tumour necrosis factor (TNF-α) or Fas ligand to its receptor activates caspase-8, which in turn signals the intrinsic pathway via cleavage of Bid proteins, further amplifying apoptotic signalling. This pathway is dependent on the formation of the death-inducing signalling complex (DISC) (apoptosis)[53,54].

Figure 3 shows that mitochondrialitochondrial dysfunction induced by excessive production of reactive oxygen species (ROS) during IRI is the main cause of the intrinsic pathway of apoptosis. Excessive ROS attack the mitochondria, leading to the opening of the mitochondrial membrane permeability transition pore (MPTP), which causes a decrease in the mitochondrial membrane potential and results in the release of pro-apoptotic factors such as cytochrome c, which initiates the caspase-9 cascade reaction. This mechanism is particularly prominent in the early stages of IRI[38,55,56].

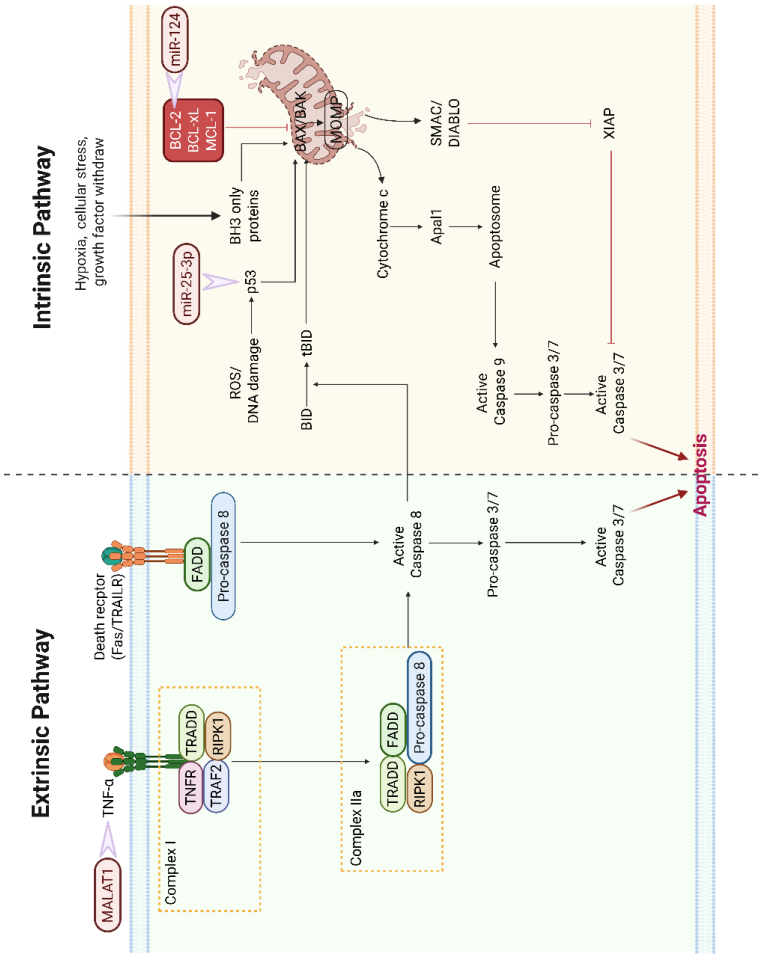

Figure 3. Molecular mechanisms and regulation pathways of Apoptosis. Apoptosis is a programmed cell death mechanism that can be triggered through two pathways: extrinsic and intrinsic. The extrinsic pathway starts with external signals binding to death receptors on the cell surface (i.e. FAS receptor), activating a caspase cascade that leads to cell death. Conversely, the intrinsic pathway is initiated from within the cell due to stress signals, causing mitochondria to release pro-apoptotic proteins, like SMAC and cytochrome C, that activate caspases, resulting in apoptosis. Both pathways play crucial roles

in maintaining cellular homeostasis and eliminating damaged or unwanted cells. Created with BioRender.com.

During reperfusion, TNF-α levels are significantly elevated, a process that induces oxidative stress.TNF-α activates the c-Jun N-terminal kinase (JNK) signalling pathway through its receptor, which further increases ROS production and leads to sustained opening of the MPTP, exacerbating mitochondrial damage and apoptosis in IRI[57,58].

Extrinsic pathways also play a key role in HIRI. Kupffer cells and lymphocytes release large amounts of TNF-α during reperfusion, a cytokine that initiates the extrinsic pathway by binding to specific receptors.Upon binding to its receptor, TNF-α forms a death signalling complex that activates caspase-8, which in turn initiates the apoptotic cascade. In addition, increased expression of the Fas ligand promotes activation of the death receptor pathway, particularly during reperfusion. Notably, the extrinsic pathway not only directly activates caspase-8, but also transmits extrinsic signals to the intrinsic pathway via Bid protein cleavage, leading to the release of pro-apoptotic factors from mitochondria, which ultimately triggers widespread apoptosis[59,60], as also illustrated in Figure 3.

The mechanism of apoptosis in liver ischaemia-reperfusion injury is complex and involves the reciprocal regulation of the intrinsic mitochondrial pathway and the extrinsic death receptor pathway. Therefore, intervention at the molecular targets of these pathways

is expected to provide new therapeutic ideas for hepatic ischaemia-reperfusion injury. For example, inhibition of caspase-3 and caspase-9 activity significantly reduces apoptosis and attenuates tissue damage caused by IRI. In addition, cyclosporine A, an inhibitor of MPTP, has been shown to block the initiation of the mitochondrial pathway, thereby reducing apoptosis during HIRI[58]. It has been found that non-coding RNAs, especially long non-coding RNAs (lncRNAs) and microRNAs (miRNAs), play an important role in HIRI by regulating apoptosis.Zhou et al. found that CCAT1 reduces apoptosis by upregulating the cell cycle protein D1, which provides protection under oxygen-glucose deprivation/reperfusion perfusion conditions[61]. Zhang et al. found that MALAT1 promotes apoptosis through the HMGB1-TLR4 pathway and exacerbates cell death and inflammation through its pro-apoptotic effects[62]. Sun et al. found that miR-494 protected human liver L02 cells from hypoxia-induced apoptosis through activation of the PI3K/Akt pathway[63]. Li et al. found that the BMSC exosome miR-25-3p inhibited apoptosis and ameliorated liver ischaemia/reperfusion injury by regulating the p53 signalling pathway through PTEN[64]. These regulatory non-coding RNAs function in a complex network affecting multiple signalling pathways and thus represent potential therapeutic targets for intervention in HIRI via apoptosis and other related mechanisms[65]. Given the critical role of apoptosis in hepatic IRI, future research and therapies may focus on targeting apoptosis-related molecules to reduce tissue damage.

1.2.3 Necroptosis

Necrotic apoptosis was first proposed in 2005 by Degtyrev et al. who found that tumour necrosis factor alpha (TNFα) induced a non-apoptotic form of cell death in the presence of caspase-8 inhibition[66]. The researchers found that necrotic apoptosis is a form of programmed cell death with morphological features of necrosis, including cell swelling, mitochondrial dysfunction, increased cell membrane permeability and release of cytoplasmic contents, but that this form of death differs from conventional necrosis in that it is modifiable and has specific signalling pathways[67]. Necrotic apoptosis is usually triggered by extracellular signals such as tumour necrosis factor (TNF), interferon, toll-like receptor (TLR) and depends on the activation and interactions of key molecules such as receptor-interacting protein kinase 1 (RIPK1), receptor-interacting protein kinase 3 (RIPK3) and mixed-spectrum kinase structural domain-like proteins (MLKL)[68,69] (Figure 4).

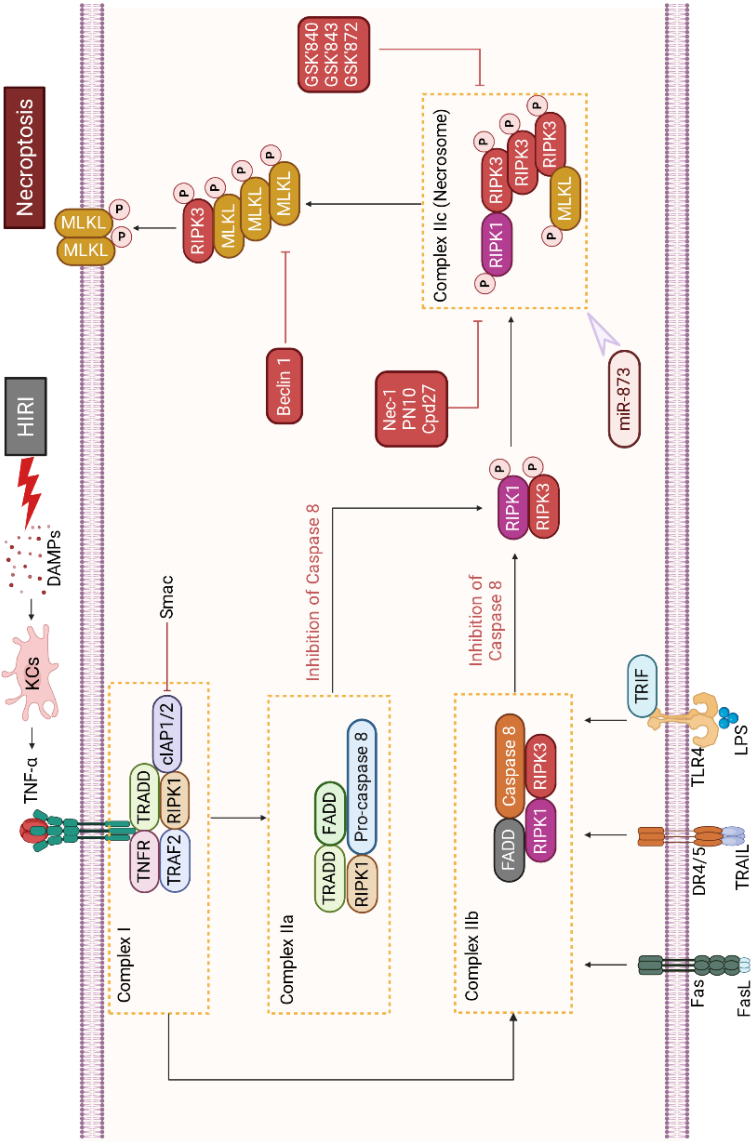

Figure 4. Hepatic ischemia-reperfusion injury–mediated necroptosis pathway. Necroptosis can be induced by various stimuli such as TNFa. In short

ubiquitination of RIPK1 leads to cell survival through activation of NF-kB, whereas deubiquitination of RIPK1 leads to the formation of complex II. The necrosome, a complex consisting of RIPK1, RIPK3, and MLKL is formed from complex IIa or IIb by inhibition of caspase 8. Created with BioRender.com.

Necrotic apoptosis is currently implicated in a variety of pathological conditions, including cancer, inflammatory responses, cerebral ischaemia, myocardial infarction, renal and hepatic injury[70–75]. In this article we focus on the mechanisms of necrotic apoptosis in hepatic ischaemia-reperfusion. Recent studies have shown that hepatic I ischemia-reperfusion significantly increases RIP3 levels, phosphorylated RIP1 and RIP3 protein expression, and RIP1/RIP3 necrosome formation, and these are attenuated by Nec-1[76]. Meanwhile, Ni et al. showed that necroptosis is involved in the process of hepatic ischaemia-reperfusion injury in liver transplantation[77]. As shown in Figure 4, when hepatocytes experience a period of hypoxia, some cells undergo irreversible necrosis, ruptured cells release DAMPs, which induces the release of TNF-α from KCs after reperfusion, and the binding of TNF-α to its receptor TNFR1 leads to the activation of RIPK1, which, due to the limitation of caspase-dependent protein kinase (CDPK), is involved in the activation of apoptosis, interacts with RIPK3 to form necrosomes due to the restriction of caspase-8 function caused by ischaemia and reperfusion, activated RIPK3 recruits and phosphorylates MLKL, and phosphorylated MLKL oligomerises on the cell membrane to form pore structures,

leading to increased cell membrane permeability and triggering cell rupture and necrotic apoptosis[76,78]. Necrotic apoptosis leads to the release of intracellular ATP, HMGB1 and nucleic acids, etc. DAMPs induce the activation of Kupffer cells and neutrophils, which release a large amount of inflammatory factors (e.g. TNFα, IL-1β), leading to further necrotic apoptosis and exacerbating liver injury.

Recent experiments have shown that Necrostatin-1, as well as compounds such as GSK'840, GSK'843 and GSK'872, can protect local tissue from severe injury by inhibiting necrotic apoptosis to some extent[79] (Figure 4). Yang et al. found that pretreatment with Necrostatin-1 and GSK'872 significantly reduced hepatic IRI and ROS production in mice by studying the hepatic IRI model in mice fed a high-fat diet[80]. As an important RNA molecule in the body, lncRNA has been found by researchers to play a role in necrotic apoptosis. Khan et al. found that TRINGS binds to STRAP (Serine-Threonine Kinase Receptor-Associated Protein) and inhibits the STRAP-GSK3β-NF-κB pathway, which inhibits necrotic apoptosis in tumours[81]. Another study found that NRF (necrosis-related factor) protects cardiomyocytes from necrotic apoptosis by binding to miR-873 and inhibiting the expression of RIPK1 and RIPK3[82]. Tran et al. found that knockdown of Linc00176 increased the phosphorylation of MLKL, triggering necrotic apoptosis, a process that inhibits the growth of HCC cells and ultimately leads to cell death[78]. The above study found that lncRNAs can regulate necroptosis by directly affecting the activity

of RIPK1, RIPK3 or MLKL, or participate in the process of necroptosis by binding to miRNAs and regulating the inhibitory effect of miRNAs on target genes.

Necrotic apoptosis, a novel form of programmed cell death, plays a key role in hepatic ischaemia-reperfusion injury. A thorough understanding of the molecular mechanisms of necrotic apoptosis may help to develop targeted clinical interventions and improve the prognosis of liver surgery and transplantation.

1.2.4 Ferroptosis

Beyond the commonly recognized forms of cell death, recent studies have highlighted the involvement of ferroptosis in HIRI[83]. Ferroptosis, a term first introduced by Stockwell and Dixon et al. in 2012[84], represents a distinct form of cell death driven by iron-dependent lipid peroxidation[83]. Unlike necrosis, apoptosis, and necroptosis, ferroptotic cell death is characterized by mitochondrial shrinkage, increased inner mitochondrial membrane density, rupture of the inner mitochondrial membrane, and an intact nucleus during the process[85].

The occurrence of ferroptosis involves multiple molecular pathways, notably redox homeostasis, iron metabolism, the GSH, and mitochondrial function (Figure 5). Due to the reliance of polyunsaturated fatty acid (PUFA) peroxidation on iron, the exhaustion of interconnected antioxidant mechanisms leads to the lethal accumulation of lipid peroxides, ultimately triggering

ferroptosis. The process is initiated by intracellular iron accumulation and the inactivation of glutathione peroxidase 4 (GPX4). The susceptibility to ferroptosis depends on the balance between iron-catalyzed reactive oxygen species (ROS) production and the clearance capacity of antioxidant defenses. Given the inevitable oxidative stress associated with ischemia-reperfusion (IR), ferroptosis is mechanistically implicated in this process.

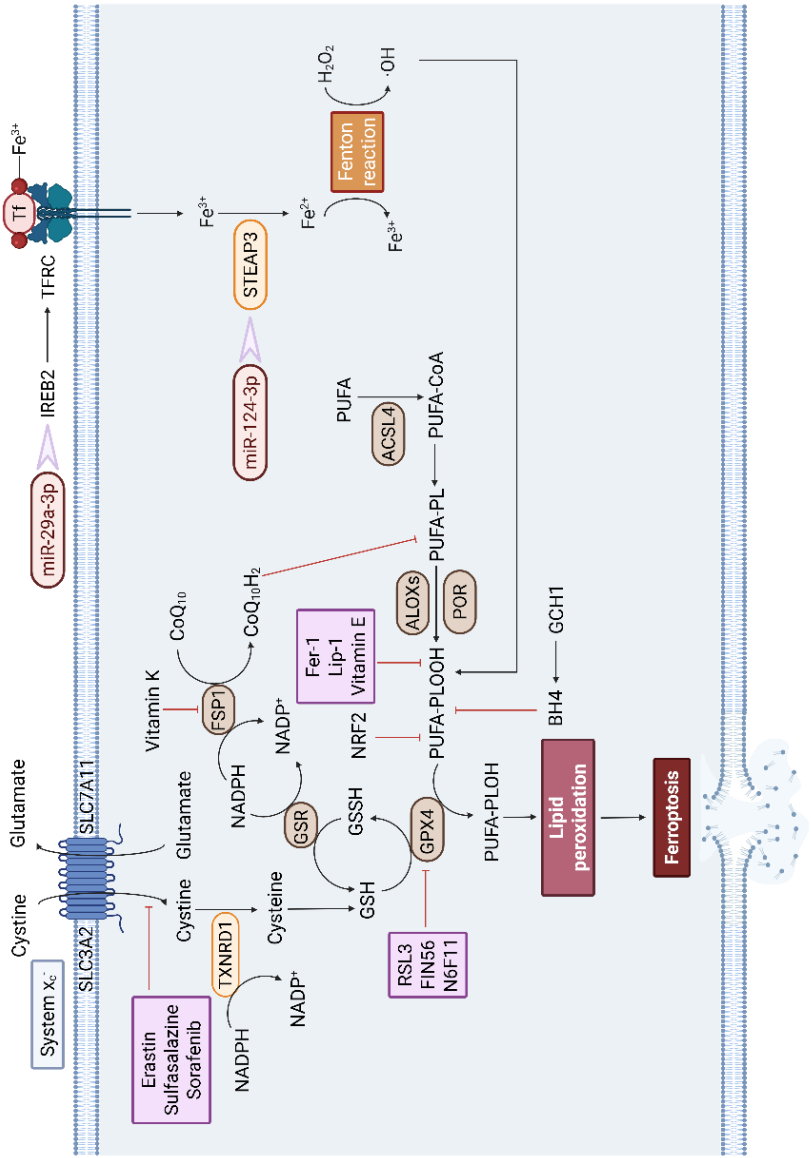

Figure 5. **Molecular mechanisms and regulation pathways of ferroptosis**. Ferroptosis is triggered by the excessive lipid peroxidation (LPO). Cysteine and

reduced glutathione (GSH) availability are regulated by cystine-glutamate antiporter system Xc– or the transsulfuration pathway. The transsulfuration pathway is a metabolic pathway for the production of cysteine (Cys)-containing amino acids and the synthesis of GSH through the interconversion of cysteine and homocysteine. Glutamine can be transported into intracellular places by SLC1A5 transporter, and then converted into glutamate by glutaminase (GLS) to affect the GSH availability. GSH is a key cofactor of GPX4 for clearing lipid peroxides. The suppression of system Xc− by erastin or GPX4 activity by RSL3, which ultimately leads to cell ferroptosis. On the one hand, the peroxidation of PUFAs and excess irons is considered to be an important contributor. Iron uptake via the transferrin receptor-like TFR1 or degradation of ferritin iron stores enhances the labile iron pool, thereby cells are susceptible to ferroptosis via lipid hydroperoxides generation from the Fenton-like reaction. In addition, the mevalonate pathway is also involved in ferroptosis process by generating a series of biomolecules with potential anti-ferroptotic activity such as squalene, coenzyme Q10 (CoQ10), isopentenyl- pyrophosphate (IPP), and farnesyl pyrophosphate (FPP), which in part influences the ferroptosis occurrences. POR cytochrome P450 oxidoreductase, LOX lipoxygenase. Created with BioRender.com.

During hepatic ischemia, the deprivation of oxygen and nutrients disrupts cellular metabolism and escalates ROS production. Upon reperfusion, the restoration of oxygen supply degrades ferritin, elevating intracellular free iron levels. Ferrous ions (Fe^{2+}) catalyze ROS production through the Fenton reaction, amplifying ROS generation, inducing PUFA peroxidation, and compromising cell membrane stability. Studies reveal that the mechanical properties of the membrane are altered by increased peroxidation, reducing phospholipid density and causing irreversible thinning. However,

whether this increased permeability directly causes membrane rupture remains unclear[86].

We hypothesize that the rising instability of cellular membranes exacerbates liver injury through ferroptotic cell death. Indeed, Linkermann et al., in studies on liver transplantation, demonstrated a significant correlation between elevated systemic iron levels and increased risk of hepatic injury post-allogeneic liver transplantation, affirming the role of ferroptosis in liver IRI[87]. Furthermore, during the late reperfusion phase, the release of damage-associated molecular patterns (DAMPs) from ferroptotic cells intensifies local inflammation. Free lipid peroxides not only directly induce cell death but also activate macrophages and other inflammatory cells, promoting the release of cytokines such as TNF-α and IL-6, thereby exacerbating liver damage.

GPX4 is a pivotal regulator that suppresses ferroptosis by reducing lipid hydroperoxides into non-toxic lipid alcohols, preventing lipid peroxidation. However, oxidative stress during hepatic IR injury depletes GSH, impairing GPX4 activity. The reduction in GSH is largely attributed to the dysfunction of the system Xc^- antiporter, responsible for cystine uptake from the extracellular environment for GSH synthesis. Insufficient cystine supply further limits GSH synthesis, aggravating ferroptosis[88]. Targeting molecular pathways involved in ferroptosis presents significant therapeutic potential for managing hepatic ischemia-reperfusion injury.

In addition to GPX4 and the GSH system, lipid oxidases (LOX), ACSL4, and the system Xc^- are promising intervention targets. Researchers are exploring strategies to inhibit ROS and mitigate lipid peroxidation-induced ferroptosis, employing agents such as ferrostatin-1 (Fer-1), liproxstatin-1 (Lip-1), vitamin E, and coenzyme Q10[84,89–91] (Figure 5). Xu et al. demonstrated that inhibiting nuclear factor erythroid 2-related factor 2 (Nrf2) signaling promotes ferroptosis, underscoring the role of Nrf2 in mitigating ROS generation through antioxidant regulation, thereby inhibiting ferroptosis in hepatic IR injury[92]. Similarly, Wu et al., using a rat model of fatty donor liver transplantation, revealed that miR-124-3p attenuates ferroptosis by downregulating prostate six transmembrane epithelial antigen 3 (STEAP3) expression, alleviating hepatic IRI[93]. Li et al. further identified that miR-29a-3p suppresses ferroptosis by downregulating iron response element-binding protein 2 (IREB2) expression in a fatty liver ischemia-reperfusion model[94].

As established, ferroptosis plays a critical role in hepatic ischemia-reperfusion injury by promoting iron-dependent lipid peroxidation and suppressing antioxidant defenses. With an enhanced understanding of ferroptosis, our efforts aim to identify long non-coding RNAs (lncRNAs) capable of suppressing ferroptosis, thereby ameliorating liver ischemia-reperfusion injury and improving patient outcomes.

1.3 Long Non-coding RNA

It is estimated that only approximately 1.9% of the human genome encodes proteins, while the remaining 98% is transcribed into non-coding RNAs (ncRNAs)[95]. Despite the fact that these RNAs are not translated into proteins, they are regarded as being of vital importance in the regulation of gene expression[96]. The category of non-coding RNAs encompasses a number of distinct types, including microRNAs (miRNAs), long non-coding RNAs (lncRNAs), circular RNAs (circRNAs), and small nucleolar RNAs (snoRNAs)[97]. Each of these plays a role in a diverse array of biological processes through a range of interactions with proteins and other types of RNAs. MicroRNAs (miRNAs) are typically 20 to 25 nucleotides in length and generally inhibit the translation of target messenger RNAs (mRNAs) by binding complementarily to the 3′ untranslated region (3′UTR) of these mRNAs[92]. lncRNAs, defined as RNAs longer than 200 nucleotides, predominantly function as molecular sponges for miRNAs, indirectly regulating the genes targeted by miRNAs. Additionally, some lncRNAs interact with DNA, RNA, or proteins to modulate gene expression[98]. CircRNAs, a distinct class of ncRNAs with covalently closed structures, contribute to gene expression regulation by sponging miRNAs or interacting with specific proteins[99,100]. Recent research has increasingly focused on the role of lncRNAs[101]. lncRNAs can be categorised into five types based on their position relative to coding genes: (1) sense lncRNA; (2) antisense lncRNA;

(3) intronic lncRNA; (4) bidirectional non-coding lncRNA; and (5) intergenic lncRNA[102]. As depicted in Figure 6, lncRNAs can operate through various mechanisms and are classified into several functional subtypes, with the most frequently reported being sponge, scaffold, guide, and decoy types[103,104]. Sponge lncRNAs can bind to microRNAs, thereby preventing these microRNAs from interacting with their target mRNAs and regulating post-transcriptional processes. lncRNAs can also aid in the assembly of chromatin remodeling complexes and facilitate subsequent gene transcription (scaffold). They may function as guides by directing transcription factors to specific DNA sites to modulate transcription. Additionally, lncRNAs can act as decoys by binding transcription factors and obstructing their binding to DNA[105]. It has been reported that lncRNAs might be involved in the pathogenesis of a range of diseases, such as cancer, autoimmune disorders, metabolic conditions, and neurological diseases, with their function in ischemia-reperfusion injury particularly drawing our attention[101,106–108].

Figure 6. The principal mechanisms of lncRNAs. (A) guiding proteins to specific regions to perform their functions; (B) serving as scaffolds to assemble

macromolecular complexes at target sites; (C) acting as sponges for microRNAs, preventing their interaction with mRNA targets; (D) functioning as decoys to inhibit protein regulation of DNA and mRNA or to compete with miRNAs, thereby reducing miRNA-mediated repression of mRNA. Created with BioRender.com.

In this thesis, our research centers on four lncRNAs: Urothelial Cancer Associated 1 (UCA1), H19, Eosinophil Granule Ontogeny Transcript (EGOT), and Nuclear Paraspeckle Assembly Transcript 1 (NEAT1). In the following, I will elaborate on my research findings regarding the involvement of lncRNAs UCA1, H19, EGOT, and NEAT1 in the processes of apoptosis, necroptosis, and ferroptosis during hepatic ischemia-reperfusion injury.

1.3.1 UCA1

LncRNA UCA1 was first cloned and identified in the bladder cancer cell line BLZ-211. This gene fragment is located on the short arm of chromosome 19 and comprises three exons and two introns. Notably, the UCA1 sequence contains multiple termination sequences and lacks any conserved long open reading frames (ORFs)[109]. UCA1 exists in three transcript isoforms: lncRNA UCA1 (1.4 kb), lncRNA UCA1a (also referred to as lncRNA CUDR, 2.3 kb), and a 2.7 kb variant[110,111]. Most studies have primarily focused on the 1.4 kb isoform due to its predominant expression across various cancers, including bladder cancer, breast cancer, and

hepatocellular carcinoma[112,113].

Emerging evidence suggests that UCA1 expression is regulated by transcription factors, transcriptional complexes, hypoxia-inducible transcription factors, and microRNAs. Beyond its role in cancer progression, UCA1 is also implicated in non-cancerous diseases such as ischemia-reperfusion (I/R) injury, systemic lupus erythematosus (SLE), diabetic nephropathy (DN), and Parkinson's disease (PD)[114–116]. UCA1 exerts its influence through diverse pathways. For instance, in acute myocardial infarction, UCA1 mitigates OGD-induced apoptosis and injury by downregulating miR-122 expression and suppressing the downstream JNK/p38 MAPK signaling pathway[117]. Additionally, UCA1 reduces arsenic-induced hepatocyte death via the activation of the OSGIN1/mTOR/p70S6K autophagy suppression pathway[118].

Depletion of UCA1 induces hypoxia-mediated apoptosis in bladder cancer cells by upregulating pro-apoptotic Bax and downregulating anti-apoptotic Bcl-2, both of which are downstream effectors of AKT[119]. In cardiomyocytes subjected to hypoxia/reoxygenation (H/R), UCA1 downregulation exacerbates apoptosis and autophagy through miR-128 enhancement[120]. Conversely, Chen et al. reported that UCA1 overexpression in H9C2 cells following I/R treatment protects cardiomyocytes from endoplasmic reticulum stress and apoptosis[121]. Yan JY et al. demonstrated that UCA1 exacerbates acute ischemic stroke by inhibiting miR-18a-5p, thereby promoting apoptosis[122]. Furthermore, Wang QS et al. found that UCA1 protects

cardiomyocytes from hypoxia-induced apoptosis by inhibiting miR-143, highlighting its potential to prevent myocardial infarction[123].

These findings underscore UCA1's involvement in cell death mechanisms under ischemia-reperfusion conditions. However, its role in ischemia-reperfusion injury of marginal donor livers remains unclear.

1.3.2 H19

H19 was first identified in mouse cells by Pachnis et al. in 1984[124] and was subsequently found to be highly expressed during human embryonic development, predominantly in mesoderm- and endoderm-derived tissues. Its expression is markedly downregulated after birth, except in cardiac and skeletal muscle[125]. H19 is a maternally expressed imprinted gene located on chromosome 7 in mice and chromosome 11p15.5 in humans. The H19 gene comprises five exons and four introns, encoding a 2.2 kb fully capped, spliced, and polyadenylated transcript[126–128]. While present in both the cytoplasm and nucleus, H19 primarily exerts its functions in the cytoplasm[129].

H19 expression is regulated in a co-regulatory manner with insulin-like growth factor 2 (IGF2), located upstream on the same locus. The imprinting control region (ICR) between these genes, along with the differential methylation status of the ICR on each allele, determines the expression of H19 and IGF2[130,131].

H19 fulfills diverse biological roles, including the regulation of cell

proliferation and differentiation[132,133], and functions as both an oncogene and a tumor suppressor in various cancers[134–136]. These roles are mediated through interactions with proteins and RNA. For instance, H19 collaborates with PTBP1 to regulate hepatic metabolic homeostasis by enhancing the mRNA stability, proteolytic activation, and nuclear transcriptional activity of sterol regulatory element-binding protein 1c (SREBP-1c)[137]. Furthermore, H19 is downregulated during aging and controls endothelial cell senescence, proliferation, inflammatory activation, and angiogenic sprouting by inhibiting STAT3 activation[138]. In myocardial infarction models, H19 overexpression promotes physiological autophagy by increasing the expression of Beclin-1, ATG7, and the LC3 II/I ratio[139].

H19 also interferes with miRNA-mediated post-transcriptional regulation. It acts as a precursor for miRNA, with its first exon encoding miR-675, which is processed into two mature forms, miR-675-3p and miR-675-5p, via DNase III enzymes[135]. miR-675 plays a critical role in tissue development, tumorigenesis, and cancer progression, suggesting the potential involvement of H19 in these processes[130,132,140]. Additionally, H19 sponges a variety of miRNAs, including miR-200, miR-106, miR-141, miR-22, miR-181, and miR-326, among others, thereby influencing processes such as cell proliferation, differentiation, death, and tumorigenesis[141–144]. A growing body of research links H19 to cell death during IRI. Wu et al. demonstrated that under hypoxic conditions, Hif-1α directly enhances H19 expression by binding to its promoter, while SP1-

mediated transcriptional activation indirectly promotes H19 transcription in glioblastoma cells during hypoxia[144]. Wang found that H19 depletion during oxygen-glucose deprivation/reoxygenation (OGD/R) reduces histone deacetylase 1 (HDAC1) and increases acetylation of histones H3 and H4, promoting the polarization of microglia from the M1 to the M2 phenotype. This polarization suppresses inflammatory responses and alleviates tissue damage[145]. Recent studies by Wan et al. revealed that I/R-induced upregulation of H19 disrupts the balance of NLRP3/6 inflammasomes, leading to pro-inflammatory cytokine responses, microglial pyroptosis, and ultimately, neuronal apoptosis due to excessive immune activation[146]. Furthermore, Cui et al. observed that H19 expression is significantly elevated in Hep G2 and HCCLM3 cells after H/R induction, while H19 knockout reduces the expression of cleaved caspase-3 and caspase-9, thereby preventing H/R-induced apoptosis and cellular damage[147].

Despite evidence suggesting H19's involvement in programmed cell death across various organs during ischemia-reperfusion injury, its role in hepatocyte death following HIRI remains poorly understood, sparking significant interest in further investigation.

1.3.3 EGOT

EGOT is a long non-coding RNA encoded at 3p26.1. It is an antisense intronic RNA located within the intronic region of the ITPR1 gene in the antisense orientation. Highly conserved at the

nucleotide level, ITPR1 encodes a ligand-gated ion channel that mediates calcium release from intracellular stores[148]. Wagner et al. demonstrated that EGOT plays a role in eosinophil development[149] and is expressed in mature eosinophils. Recent studies have focused on EGOT's roles in glioblastoma, breast cancer, renal carcinoma, gastric cancer, hematologic malignancies, viral infections, and cardiology[148,150–158].

EGOT expression is inducible under various stress conditions, such as hypoxia, radiotherapy, chemotherapy, or growth factor depletion. It has been implicated in the activation of the PI3K/AKT, MAPK, and NF-κB pathways, contributing to antiviral responses, inflammation, and cell death[159]. Carnero et al. observed increased EGOT expression in hepatocytes[156]. Wu et al. found that EGOT overexpression in human glioblastoma cells inhibits cell proliferation and migration while promoting apoptosis[150]. Similarly, Jin et al. reported that EGOT upregulation suppresses proliferation, migration, and invasion in 786-O and ACHN renal cell lines, inducing apoptosis[148]. Wang et al. discovered EGOT's involvement in autophagic processes in renal tubular cells under hypoxic conditions[160]. Zhang et al.'s recent study highlighted EGOT's role in cardiac ischemia-reperfusion injury, demonstrating that elevated EGOT expression is a protective mechanism of rhBNP against hypoxia-induced heart failure[158]. However, the involvement of EGOT in programmed cell death during hepatic ischemia-reperfusion injury remains unclear, warranting further investigation.

1.3.4 NEAT1

NEAT1, a nuclear lncRNA, was first identified in 2007 through a genome-wide screening of mammalian species by Hutchinson et al. It is abundantly expressed in tissues such as the prostate, pancreas, ovary, and colon[161]. NEAT1 is transcribed by RNA polymerase II from the familial multiple endocrine neoplasia type 1 (MEN1) locus on chromosome 11q13.1 in humans. It exists in two isoforms: the short isoform (lncRNA NEAT1-1, 3.7 kb), which undergoes polyadenylation, and the long isoform (lncRNA NEAT1-2, 23 kb), which remains non-polyadenylated[162]. NEAT1 serves as the structural scaffold for paraspeckles through its interactions with paraspeckle proteins such as paraspeckle component 1 (PSPC1), proline/glutamine-rich splicing factor (SFPQ), and 54 kDa nuclear RNA and DNA-binding protein (p54nrb)[163]. Paraspeckles are subnuclear ribonucleoprotein complexes that play critical roles in transcriptional regulation and RNA processing by modulating RNA and protein editing within the nucleus. Additionally, paraspeckles act as sponges for various microRNAs[164]. Given their essential function in controlling gene expression during processes like cell differentiation, proliferation, and death, NEAT1, as an integral component of paraspeckles, is likely indispensable in certain cellular processes[165,166].

Since its discovery, numerous biological functions of NEAT1 have been reported, including roles in cell differentiation, immune responses, and organ development[18,165,167,168]. Increasing

evidence suggests that NEAT1 dysregulation contributes to the progression of various diseases, including cancer, neurological disorders, metabolic diseases, and immune-related conditions[169–174]. Yan et al. demonstrated that NEAT1 and Tim-3 levels are elevated in PBMCs from HCC patients. Silencing NEAT1 in CD8+ T cells from healthy donor PBMCs (via si-NEAT1) reduced apoptosis and enhanced cytolytic activity, accompanied by decreased cleaved caspase-3 levels, suggesting that NEAT1 promotes CD8+ T cell apoptosis through a caspase-dependent pathway[175]. Kong et al. found that NEAT1 sponges miR-29b to promote Atg9a expression, enhancing autophagy in Ad-IGFBPrP1-treated hepatocytes in mice[176]. Yamazaki et al. showed that NEAT1 supports sustained cancer cell proliferation by inhibiting apoptosis via activation of the Akt/mTOR and ERK pathways[177]. Similarly, Li et al. demonstrated that NEAT1 suppresses apoptosis in HepG2 cells and mouse HCC models by inhibiting the miR-335/c-Met/Akt pathway[178]. Ren et al. reported that NEAT1 knockdown promotes proliferation and reduces apoptosis in I/R-induced H9c2 cells[179]. Wang et al. observed that NEAT1 overexpression diminishes hepatocyte proliferation, increases apoptosis, and elevates inflammatory cytokine production (e.g., IL-1, IL-6, TNF-α), suggesting that NEAT1 exacerbates hepatocyte inflammation and could serve as a therapeutic target in HIRI[180]. Moreover, Wang et al. identified NEAT1's involvement in ferroptosis via the SLC7A11 pathway[181].

Numerous studies confirm NEAT1's role in various forms of programmed cell death in hepatocytes. Thus, we aim to further elucidate the mechanisms by which NEAT1 modulates programmed cell death pathways in HIRI through experimental research.

1.4 Study Aim and Objectives

The overall aim of this study was to elucidate the roles of hypoxia-responsive lncRNAs in HIRI and to define their mechanistic links with regulated cell death pathways under hypoxia–reoxygenation stress.

To achieve this aim, the present study was designed with the following specific objectives:

(1) To characterize the dynamic expression profiles of UCA1, H19, EGOT, and NEAT1 during hypoxia and subsequent reoxygenation in hepatocyte models.

(2) To investigate the associations between these hypoxia-responsive lncRNAs and key molecular markers of ferroptosis, apoptosis, and necroptosis.

(3) To delineate the role of NEAT1 in modulating ferroptosis susceptibility through regulation of cystine transport, lipid peroxidation defense, and antioxidant capacity.

(4) To establish a molecular framework linking lncRNA-mediated hypoxic responses to hepatocyte vulnerability, with relevance to graft injury risk stratification in liver transplantation.

2. Materials And Methods

2.1 Items list for experiments

2.1.1 Company directory

Company	Headquarters
3DHISTECH	Budapest, Hungary
Abcam	Cambridge, UK
Agilent	Santa Clara, California, USA
Antibodies-online.com	Aachen, Germany
Bandelin electronic	Berlin, Germany
BD Pharmingen	San Diego, CA, USA
Bertin Technologies	Montigny-le-Bretonneux, France
Bioer Technology	Hangzhou, China
Biomol	Hamburg, Germany
Bio-Rad Laboratories	Hercules, California, USA
Biotium	Fremont, California, USA
Biozym Scientific	Hessisch Oldendorf, Germany
Carl Roth	Karlsruhe, Germany
Carl Zeiss	Oberkochen, Germany
Cell Signaling Technology	Cambridge, UK
Eppendorf	Hamburg, Germany
Epredia	Portmouth, New Hampshire, USA
FabGennix	Frisco, Texas, USA
Feather	Osaka, Japan
Graphpad Software	San Diego, California, USA
Greiner Bio-One	Kremsmünster, Austria
Heraeus	Hanau, Germany
Hirschmann Laborgeräte	Eberstadt, Germany
IKA	Staufen, Germany
Interchim	Montlucon, France
Leica Biosystems	Nussloch, Germany
Medite medical	Burgdorf, Germany
Merck Millipore	St. Louis, Missouri, USA
Merck Sigma-Aldrich	St. Louis, Missouri, USA

Merck Supelco	St. Louis, Missouri, USA
Microsoft Corporation	Redmond, Washington, USA
Molecular Devices	San Jose, California, USA
MP Biomedicals	Irvine, California, USA
PAN Biotech	Aidenbach, Germany
Proteintech	Rosemont, Illinois, USA
QIAGEN	Venlo, Netherlands
R. Langenbrinck	Emmendingen, Germany
Roche	Basel, Schweiz
Sakura Finetek	Alphen aan den Rijn, Netherlands
Santa Cruz	Dallas, Texas, USA
SLEE medical	Nieder-Olm, Germany
Thermo Fisher Scientific	Waltham, Massachusetts, USA
Vector Laboratories	Burlingame, California, USA
VWR International	Radnor, Pennsylvania, USA
Zytomed Systems	Berlin, Germany

2.1.2 Reagents and Kits

Reagents/Kits	Company
4,6-Diamidino-2-phenyl-indol (DAPI) dihydrochloride	Merck Sigma-Aldrich
1x Dulbecco's phosphate buffered saline (DPBS)	PAN Biotech
4x Laemmli sample buffer	Bio-Rad Laboratories
10x ReBlot Plus Strong Antibody Stripping solution	Merck Millipore
10x Tris/Glycine/Sodium dodecyl sulfate (SDS) buffer	Bio-Rad Laboratories
10x HIER T-EDTA buffer (pH 9.0)	Zytomed Systems
20x TrueBlack® Lipofuscin Autofluorescence Quencher	Biotium
Acetic acid (glacial), 100%	Merck Supelco
Acetone	Merck Sigma-Aldrich
AllProtect tissue reagent	QIAGEN

BLOXALL® Blocking Solution	Vector Laboratories
β-Mercaptoethanol	Carl Roth
Bovine serum albumin (BSA), fraction V	Biomol
Clarity™ Western ECL Substrate	Bio-Rad Laboratories
cOmplete™ Mini Proteaseinhibitor cocktail	Roche
Criterion™ TGX stain-free™ precast gels (12%)	Bio-Rad Laboratories
Disodium phosphate (Na_2HPO_4)	Carl Roth
Entellan™	Merck Sigma-Aldrich
Eosin G solution, 0.5% aqueous	Carl Roth
Ethanol (100%)	Carl Roth
Ethylenediaminetetraacetic acid (EDTA)	Thermo Fisher Scientific
Fluorescence Mounting Medium	Agilent
Formalin	Pathology of Regensburg
Goat serum	Merck Sigma-Aldrich
High-Capacity cDNA Reverse Transcription Kit	Thermo Fisher Scientific
Hydrogen chloride (HCl)	Carl Roth
ImmEdge Hydrophobic Barrier (PAP) pen	Vector Laboratories
Mayer's hemalum solution	Merck Sigma-Aldrich
Milk powder, blotting grade	Carl Roth
Monosodium phosphate (NaH_2Po_4)	Merck Sigma-Aldrich
Nuclease-free water	Bio-Rad Laboratories
PeqGOLD pre-stained Protein Marker IV	VWR International
Phenylmetansulfonylfluoride (PMSF)	Merck Sigma-Aldrich
Phosphatase inhibitor cocktail	Cell Signaling Technology

QIAshredder™	QIAGEN
QuantiNova SYBR® Green PCR Kit	QIAGEN
Roti® Histol	Carl Roth
Sodium chloride (NaCl)	Carl Roth
Tissue-Tek®	Sakura Finetek
Trans-Blot Turbo transfer pack	Bio-Rad
Tris base	Merck Sigma-Aldrich
Triton X-100	Merck Sigma-Aldrich
TWEEN® 20 viscous liquid	Merck Sigma-Aldrich
Uptima BC Assay Protein Quantification Kit	Interchim
Urea	Merck Sigma-Aldrich

2.1.3 Ingredients of chemical solutions

Chemical solutions	Ingredients
10x Tris-buffered saline (TBS) (pH 7.58)	137 mM NaCl 20 mM Tris base in millipore water pH 7.58 adjusted with HCl
BSA solution (BS)	5% BSA, fraction V in TBS-T
Goat solution (GS)	10% Goat serum in DPBS
Lysis buffer for soluble proteins	cOmplete™ Mini Proteaseinhibitor cocktail (1 tablet/ 10 ml) Phosphatase inhibitor cocktail (1:100) 20 mM PMSF in RIPA-B-buffer
Lysis buffer for insoluble proteins	cOmplete™ Mini Proteaseinhibitor cocktail (1 tablet/ 10 ml) Phosphatase inhibitor cocktail (1:100) 20 mM PMSF

	6.32 M urea in RIPA-B-buffer
Milk solution (MS)	5% Milk powder, blotting grade in TBS-T
RIPA-B-buffer	50 mM NaCl 5 mM EDTA 2 mM sodium-phosphate buffer 1% Triton X-100 in millipore water
Sodium-phosphate buffer (pH 7.4)	200 mM NaH_2PO_4 200 mM Na_2HPO_4 in millipore water
Tris-buffered saline + Tween 20 (TBS-T)	10% 10x TBS 0.1% TWEEN® 20 in millipore water

2.1.4 Antibodies for western blot and immunohistochemistry

1st Antibody	Host	Dilution	Cat. number	Company
4HNE	mouse	1:500 in BS	MA5-27570	Thermo Fisher Scientific
ACSL4	rabbit	1:500 in MS	ABIN2854678	antibodies-online.com
Caspase 3	rabbit	1:500 in MS	#9662	Cell Signaling
Caspase 9	mouse	1:500 in MS	#9508	Cell Signaling
FSP1	rabbit	1:500 in MS	PA5-28727	Thermo Fisher Scientific
GPX4	rabbit	1:500 in MS	ab125066	Abcam
HIF1α	rabbit	1:1000 in MS	PA1-16601	Thermo Fisher Scientific
MDA	mouse	1:500 in BS	MA5-	Thermo Fisher

			27560	Scientific
xCT	rabbit	1:1000 in MS	ab175186	Abcam

2nd Antibody	**Host**	**Dilution**	**Cat. number**	**Company**
Anti-mouse IgG, HRP-linked	horse	1:1000 in MS	#7076	Cell Signaling
Anti-rabbit IgG, HRP-linked	goat	1:1000 in MS	#7074	Cell Signaling

2.1.5 Primer for quantitative real-time-PCR

RT² Primer	**RefSeq**	**Cat. number**	**Product**	**Company**
ACSL4	NM_001038694	PPS01233A-200	330001	QIAGEN
ACTB	XM_00312480	PPS71698A-200	330001	QIAGEN
FSP1	XM_005657396	PPS08443A-200	330001	QIAGEN
GPX4	NM_214407	PPS01006A-200	330001	QIAGEN
HIF1α	NM_001123124	PPS00112A-200	330001	QIAGEN
IFNγ	NM_213948	PPS00334A-200	330001	QIAGEN
Il-17A	NM001005729	PPS01245A-200	330001	QIAGEN
SLC2A1	XM_013977359	PPS00716B-200	330001	QIAGEN
TNF	NM_214022	PPS00426A-200	330001	QIAGEN

VEGF A	NM_214084	PPS00495A-200	330001	QIAGEN

2.1.6 Software

Software	Company
AxioVision Rel. 4.8	Carl Zeiss
CaseViewer	3DHISTECH
GraphPad Prism 9.0.1	Graphpad Software
ImageLab 6.1	Bio-Rad Laboratories
LightCycler® 480 SW 1.5.1	Roche
Microsoft Excel 2013	Microsoft Corporation
WSoftMax	Molecular Devices

2.2.1 Cell Culture

HepaRG cells were obtained from Biopredic International (France) as cryopreserved vials. Upon thawing in a 37 °C water bath, cells were transferred into pre-warmed HepaRG growth medium and seeded into T75 culture flasks. The HepaRG growth medium consisted of William's E medium supplemented with 10% HyClone FetalClone II serum, 1% penicillin/streptomycin, 1% L-glutamine, 0.023 IU/mL insulin, 4.7 µg/mL hydrocortisone, and 80 µg/mL gentamicin. After attachment, cultures were expanded at 37 °C in a humidified 5% CO_2 cubator until reaching approximately 80–90% confluence. Cells were then detached with 0.05% trypsin–EDTA, pelleted at 300 g for 5 minutes, resuspended in growth medium, counted, and seeded into 6-well plates at 2×10^5 cells/well in 2–3 mL of medium. Cells were maintained in the same HepaRG growth medium for 2 weeks, with medium changes every 2–3 days, to complete the proliferative phase. Hepatic differentiation was

induced by switching the cultures to HepaRG growth medium supplemented with 1.8% DMSO, which was applied continuously for an additional 2 weeks, again with medium refreshment every 2–3 days. This DMSO-driven differentiation phase induced hepatic polarization, bile-canaliculus–like structures, and metabolic competence characteristic of mature HepaRG cells. After 4 weeks total (2 weeks proliferation + 2 weeks differentiation), cells were considered fully differentiated and were subjected to downstream steatosis induction, hypoxia–reoxygenation, siRNA knockdown, NEAT1 overexpression, or ferroptosis experiments according to the study design.

2.2.2 Fatty Acid (PA/OA) Treatment

To induce steatosis, fully differentiated HepaRG cells were first incubated for 24 hours in diet medium, defined as HepaRG growth medium containing 1% fatty acid-free BSA. Following this pre-conditioning step, cells were treated for 24 hours with a 0.5 mM mixture of palmitic acid (PA) and oleic acid (OA) in a 1:2 molar ratio, prepared in diet medium. Unloaded control HepaRG cells were treated with diet medium containing the same final concentration of isopropanol but without fatty acids. After 24 hours of PA/OA exposure, cells were subjected to subsequent treatments.

2.2.3 Hypoxia Treatment

Hypoxia was induced using a sealed hypoxia chamber system,

Modular Incubator Chamber (Billups-Rothenberg). Differentiated HepaRG cells were incubated inside the chamber and exposed to a controlled hypoxic environment of <0.5% O_2 5% CO_2, and balanced N_2. To establish these conditions, the chamber was flushed with the hypoxic gas mixture for several minutes at a constant inflow rate and then sealed according to the manufacturer's guidelines. The cells were maintained under hypoxia for 48 hours, ensuring stable and reproducible low-oxygen exposure. At the end of the hypoxia period, the chamber was opened and the culture plates were immediately transferred back to normoxic conditions (37°C, 5% CO_2) to simulate reperfusion. The cells were maintained under these reoxygenation conditions for 24 hours. After hypoxia or reoxygenation, cells were washed with ice-cold PBS and subsequently collected for downstream applications such as RNA extraction, protein isolation, or additional experimental treatments, as described in the respective analyses.

2.2.4 RNA Analysis

RNA Harvesting and Isolation

After the previous treatments, culture supernatants were discarded and the cells were washed twice with 3–4 mL ice-cold PBS per well. Cells were detached by scraping in cold PBS, and the entire wash solution was transferred into 50-mL centrifugation tubes, including an additional PBS rinse of each well to ensure complete cell recovery.

Cell suspensions were centrifuged at 1500 rpm for 5 minutes at 4 °C in a Megafuge system. Supernatants were aspirated, and cell pellets were gently loosened and resuspended in 1.5 mL ice-cold PBS. The resuspended cells were divided into:

0.5 mL for RNA extraction (into an RLT-plus tube),

1.0 mL for protein extraction (into a protein lysis tube).

Residual PBS from the 50-mL tubes was used to rinse down remaining cells and was equally distributed into the RNA and protein tubes.

For RNA processing, RLT-plus lysis buffer was prepared freshly each day by mixing 1000 µL RLT-plus with 10 µL β-mercaptoethanol (β-ME). A volume of 350 µL RLT-plus/β-ME was added to each RNA pellet, followed by soft vortexing. Tubes were centrifuged at 2000 rpm for 5 minutes at 4 °C, the supernatant was checked for clarity, and samples were stored at –20 °C or processed immediately for RNA purification.

RNA concentration and purity were quantified using a NanoDrop spectrophotometer.

cDNA Synthesis

cDNA synthesis was performed using the High-Capacity cDNA Reverse Transcription Kit (Thermo Fisher Scientific, USA). Up to 1000 ng RNA was diluted to 14.2 µL with RNase-free water, and 5.8 µL RT master mix (2 µL 10× RT buffer, 2 µL random primers, 1 µL MultiScribe RT, 0.8 µL dNTPs) was added to a final reaction volume of 20 µL.

Cycling conditions:

25°C for 10 min

37°C for 120 min

85°C for 5 min

Hold at 4°C

cDNA was stored at –20°C.

Quantitative Real-Time PCR (qRT-PCR)

qRT-PCR was performed using the QuantiNova SYBR Green PCR Kit on the LightCycler® 480 II platform. Each 20 µL reaction contained:

10 µL SYBR Green Master Mix

1 µL forward primer

1 µL reverse primer

6 µL nuclease-free water

2 µL cDNA

Cycling program:

95 °C for 5 sec

40 cycles of:

95 °C for 10 sec

60 °C for 30 sec

Melt curve analysis

Relative expression levels were calculated using the Pfaffl method.

2.2.5 Western Blot Analysis

Protein Collection and Lysis. Protein collection followed the same harvesting steps as described for RNA extraction. After pelleting, the protein-designated cell fraction was resuspended in

200 µL freshly prepared RIPA-based lysis buffer. The lysis buffer was prepared daily and consisted of:

RIPA Lysis Buffer Composition (per 2.5 mL working solution)

1,987.5 µL RIPA buffer (commercial; containing Tris-HCl, NaCl, NP-40/Triton X-100, SDS, sodium deoxycholate)

100 µL protease inhibitor cocktail (4% v/v final)

12.5 µL 0.1 M Na_3VO_4 (final concentration 0.5 mM)

250 µL PMSF (20 mM stock) (final concentration 2 mM)

Cell pellets were lysed in this buffer by gentle vortexing and pipette shearing (avoiding foam formation). Lysates were incubated briefly on ice and centrifuged at 12,000 rpm for 15 minutes at 4°C. The clarified supernatants were transferred to clean tubes and stored at −80°C until further analysis.

Protein concentrations were measured using the BCA assay.

Sample Preparation. To ensure equal protein loading across all lanes, the volume of each sample was adjusted based on BCA quantification so that an identical amount of total protein (15–20 µg per lane) was loaded onto the SDS-PAGE gel. This step ensures valid comparison between experimental conditions. Protein samples were then mixed with 2× Laemmli sample buffer containing 5% β-mercaptoethanol, heated at 95°C for 5 minutes, and briefly centrifuged before loading.

SDS-PAGE. Equal total protein amounts (15–20 µg) were loaded per lane onto 12% TGX stain-free polyacrylamide gels (Bio-Rad)

and electrophoresed at 120 V. Total protein was visualized by stain-free activation using the ChemiDoc™ MP system to verify equal loading.

Protein Transfer. Proteins were transferred to nitrocellulose membranes using the Trans-Blot Turbo system with the Mixed MW protocol (7 minutes, 2.5 A, up to 25 V). Transfer efficiency and uniformity were confirmed by total protein imaging.

Immunodetection. Membranes were blocked in 5% milk in TBS-T for 1 hour at room temperature, incubated overnight at 4 °C with primary antibodies, washed, and incubated with HRP-conjugated secondary antibodies for 1 hour. Protein bands were visualized using Clarity™ Western ECL substrate on a ChemiDoc™ MP imaging system.

Stripping and Re-probing. If required, membranes were stripped using ReBlot Plus Strong Stripping Solution for 15 minutes, washed, re-blocked, and re-incubated with additional primary antibodies.

Densitometric Analysis. Quantification was carried out using ImageLab 6.1, with signal normalization to total protein stain, ensuring accurate comparison across samples.

2.2.6 siRNA Knockdown and Plasmid Overexpression

Following the fatty-acid loading phase, differentiated HepaRG cells were subjected to genetic modulation using either siRNA-mediated knockdown or plasmid-based overexpression. All transfections were performed before hypoxia, reoxygenation, or Erastin exposure, ensuring that subsequent stress treatments were applied to genetically modified cells.

siRNA-Mediated Knockdown of UCA1, EGOT, H19, and NEAT1. Gene silencing of the lncRNAs UCA1, EGOT, H19, and NEAT1 was performed using gene-specific siRNAs obtained from Invitrogen, Thermo Fisher Scientific (USA). After PA/OA treatment, cells were washed with PBS and incubated in serum-free, antibiotic-free HepaRG medium. For each well of a 6-well plate, siRNA was diluted in 250 µL Opti-MEM, and Lipofectamine 2000 (Invitrogen, USA) was diluted in a separate 250 µL Opti-MEM aliquot and incubated for 5 minutes. The siRNA and Lipofectamine mixtures were combined in a 1:1 ratio, gently mixed, and incubated for 10 minutes to allow complex formation. The final concentration of siRNA per well was 100 nM. A total of 500 µL siRNA–lipid complex was added dropwise to each well containing 1.5 mL serum-free medium, and cells were incubated for 24 hours to allow effective knockdown. The medium was then replaced with standard differentiation medium.

NEAT1 Overexpression. For overexpression studies, a plasmid encoding the full-length human NEAT1 transcript (VectorBuilder,

USA) was transfected using ROTI®-Fect PLUS (Carl Roth, Germany). After steatosis induction, HepaRG cells were washed with PBS and maintained in serum-free, antibiotic-free medium. For each well, 2 µg plasmid DNA was diluted in 250 µL Opti-MEM, and ROTI®-Fect PLUS reagent was diluted in an additional 250 µL Opti-MEM according to the manufacturer's recommendations. Both solutions were combined, gently mixed, and incubated for 10–15 minutes to allow complex formation. A total of 500 µL plasmid–lipid complexes was added dropwise to each well containing 1.5 mL serum-free medium. After 24 hours of incubation, the NEAT1-overexpressing cells were used for the subsequent experimental procedures.

2.2.7 Erastin-Induced Ferroptosis

Erastin-induced ferroptosis was conducted in differentiated HepaRG cells after lncRNA knockdown or overexpression and before hypoxia–reoxygenation treatment. Erastin (Sigma-Aldrich, Germany) was dissolved in DMSO to prepare a 10 mM stock solution, which was aliquoted and stored at −20 °C protected from light. Immediately before use, the stock solution was diluted in pre-warmed HepaRG differentiation medium to obtain the desired working concentrations. The final DMSO concentration was kept constant across all treatments and controls and did not exceed 0.1% (v/v). Vehicle control cells for these experiments were treated with the same final concentration of DMSO but without Erastin and were processed in parallel using identical protocols.

For functional experiments following lncRNA knockdown or overexpression, a single working concentration of 20 μM Erastin was applied. Differentiated HepaRG cells in 6-well plates, previously subjected to PA/OA treatment and siRNA-mediated knockdown or plasmid-based overexpression, were washed once with PBS and incubated in fresh differentiation medium containing 20 μM Erastin for 24 hours under standard culture conditions. After this 24-hour Erastin exposure, cells were washed with PBS, supplied with fresh differentiation medium, and subsequently subjected to the hypoxia (48 h, <0.5% O_2) and reoxygenation (24 h) protocol described above, in order to investigate the impact of ferroptosis priming on ischemia–reperfusion-like injury.

For cell viability assays, NEAT1-overexpressing HepaRG cells were seeded into 96-well plates at 1 × 10^4 cells/well. After completion of PA/OA loading and NEAT1 overexpression, cells were treated with Erastin at 5, 10, 20, 40, or 100 μM for 24 hours at 37 °C in a humidified 5% CO_2 incubator. Vehicle control wells received differentiation medium containing the same final concentration of DMSO without Erastin. At the end of the 24-hour incubation, cell viability was measured according to the manufacturer's instructions.

2.2.8 Cell Viability Assay

Cell viability was determined using the CytoTox-Glo™ Cytotoxicity Assay (Promega, USA) following NEAT1 overexpression, PA/OA-induced steatosis, and 24-hour Erastin exposure. NEAT1-

overexpressing HepaRG cells were seeded into white 96-well plates at 1×10^4 cells per well and treated with 5, 10, 20, 40, or 100 μM Erastin prior to viability assessment. The assay was performed according to the manufacturer's instructions. The CytoTox-Glo™ Reagent was freshly prepared by combining the AAF-Glo™ substrate with the assay buffer. After Erastin treatment, 50 μL of the CytoTox-Glo™ reagent was added directly to each well, mixed briefly, and incubated for 15 minutes at room temperature to measure dead-cell protease activity, which generates a stable luminescent signal. Luminescence was recorded using a microplate reader. To determine total cell number, 50 μL of Lysis Reagent (digitonin-containing buffer) was added to each well, mixed gently, and incubated for another 15 minutes. A second luminescence reading was then performed to quantify total cellular protease activity. Cell viability was calculated as recommended by the manufacturer:

Viability = Total luminescence − Dead-cell luminescence.

All measurements included background (no-cell) controls, untreated controls, and DMSO vehicle controls.

2.2.9 RT² lncRNA PCR Array Screening of Candidate lncRNAs

A panel of 114 lncRNAs previously reported to be associated with ischemia–reperfusion injury, liver disease, or regulated cell death was selected for initial screening. Total RNA was extracted from HepaRG cells exposed to normoxia, hypoxia, PA/OA-induced

steatosis, combined hypoxia–steatosis, and reoxygenation. For each condition, 1 µg RNA was processed using the RT² First Strand Kit (Qiagen, USA) according to the manufacturer's instructions. cDNA was combined with RT² SYBR Green ROX qPCR Mastermix and loaded onto the Human LncFinder RT² lncRNA PCR Array (Qiagen, USA). Real-time PCR was performed on the LightCycler® 480 II platform using standard cycling conditions (95 °C for 10 min, followed by 40 cycles of 95 °C for 15 s and 60 °C for 60 s). Melting curve analysis was performed to confirm amplification specificity. Cq values were exported and analyzed using the LightCycler® 480 Software, applying the ΔΔCq method for relative quantification. Genes with fold change ≥2 or ≤−2, and passing all built-in array quality controls, were considered significantly regulated. Differentially expressed lncRNAs were subsequently compared with ferroptosis-associated lncRNAs from ncFO and programmed cell death–related lncRNAs from LncPCD, yielding the final candidate set (UCA1, H19, EGOT, and NEAT1) selected for functional validation.

2.2.10 Bioinformatics Analysis

Differentially expressed lncRNAs identified in the RT² lncRNA PCR Array were cross-referenced with ncFO, a curated database containing 178 experimentally validated ferroptosis-associated lncRNAs (http://www.jianglab.cn/ncFO/). lncRNAs showing upregulation (fold change ≥2) or downregulation (fold change ≤−2) in the array were intersected with the ncFO set to identify

ferroptosis-related transcripts. This analysis yielded seven upregulated (H19, UCA1, PVT1, LUCAT1, LINC00673, ZFAS1, MALAT1) and nine downregulated lncRNAs (TUG1, XIST, NEAT1, DANCR, CPS1-IT1, CCAT1, FTX, OIP5-AS1, HULC). To further refine candidates across additional programmed cell death pathways, differentially expressed lncRNAs were compared with entries in the LncPCD database (http://spare4.hospital.studio:9000/lncPCD/Home.jsp), which contains 1081 lncRNAs associated with apoptosis, necroptosis, ferroptosis and autophagy. Intersection analysis identified nine consistently upregulated and twelve consistently downregulated lncRNAs. lncRNAs appearing in both ncFO and LncPCD datasets and showing robust fold-changes in the RT² Array were considered biologically relevant. Based on expression consistency across hypoxia, steatosis and reoxygenation, together with disease relevance from published studies, four lncRNAs—UCA1, H19, EGOT and NEAT1—were selected for functional validation. All downstream processing was performed in R (version 4.3.3). Packages employed included dplyr and tidyr for data preprocessing, ggplot2, ggpubr, pheatmap and ComplexHeatmap for visualization, VennDiagram for intersection analysis, EnhancedVolcano for fold-change plotting, and readxl/data.table for data import and handling. External transcriptomic validation was conducted using microarray dataset GSE14951 from the NCBI GEO repository, in which UCA1 was confirmed to be upregulated in post-reperfusion human liver tissue,

supporting its relevance in ischemia–reperfusion settings.

2.2.11 Statistical Analysis

All statistical analyses were performed using GraphPad Prism (version 9.0, GraphPad Software, USA) unless otherwise specified. For RT-qPCR and Western blot quantification, data were first assessed for normal distribution and homogeneity of variance. Comparisons involving more than two experimental variables were analyzed using two-way repeated-measures ANOVA, followed by Bonferroni's post hoc multiple comparisons test, as applied throughout the analyses of lncRNA expression. For comparisons between two groups, a two-tailed unpaired Student's t-test was used when appropriate. For cell viability assays (CytoTox-Glo™), luminescence values were collected in technical triplicates and normalized according to the manufacturer's recommended formula (total luminescence − dead-cell luminescence). Group differences across multiple erastin concentrations were analyzed using two-way ANOVA with Bonferroni correction. Dose–response curves were plotted to evaluate concentration-dependent reductions in viability following NEAT1 overexpression under normal and fatty conditions. External transcriptomic validation (GSE14951) was performed using publicly available processed data, and statistical significance between reperfused and non-reperfused human liver samples was evaluated using a two-tailed unpaired t-test. All quantitative data are presented as mean ± standard deviation

(SD). Statistical significance was defined as $p \leq 0.05$. Levels of significance are indicated as follows: $p \leq 0.05$, ** $p \leq 0.01$, *** $p \leq 0.001$, **** $p \leq 0.0001$, consistent with the presentation in the Results section.

3. Results

3.1 Hypoxia-related lncRNAs in hepatocytes

Recently, research has highlighted a significantly higher mortality rate among patients receiving marginal donor livers with IRI compared to those with non-marginal donor livers and normal donors182. We examined the data to find the cause of this difference. The results show that lncRNAs, a type of small biological molecule, are important for cell death in marginal donor livers183–185. Subsequently, we identified 114 candidate lncRNAs associated with cell death or liver diseases based on comprehensive literature analysis174,183,185–194. To investigate the response of hepatocytes under ischemic conditions akin to those in marginal donor livers, we subjected the HepaRG cell line to 48-hour hypoxia treatment. Concurrently, to simulate conditions of marginal donor livers, we treated the cell line with palmitic acid/oleic acid (PA/OA) (Figure 7A). Post-treatment, Oil-Red O staining revealed increased cytoplasmic lipid accumulation in the treated HepaRG cells (Figure 7B). Subsequently, we collected these cells and assessed the expression of the identified lncRNAs. Utilizing RT2 lncRNA PCR Array, we analyzed the expression profiles of the 114 candidate lncRNAs (Table 2). The resulting heatmap depicted differential expression of these lncRNAs under various conditions (Figure 7C). Notably, under combined adipogenic and hypoxic treatments, 11 lncRNAs exhibited significantly elevated expression levels,

namely, EGOT, LOC100507156, BOK-AS1, H19, DLGAP1-AS1, UCA1, PVT1, LUCAT1, LINC00673, ZFAS1, and MALAT1, with fold changes exceeding 2. Conversely, 17 lncRNAs showed decreased expression, including TUG1, PWAR5, HNF4A-AS1, XIST, NEAT1, PRINS, DANCR, CPS1-IT1, TMEM161B-AS1, IPW, CCAT1, FTX, BDNF-AS, GNAS-AS1, NRON, OIP5-AS1, and HULC, with fold changes less than -2 (Figure 7D).

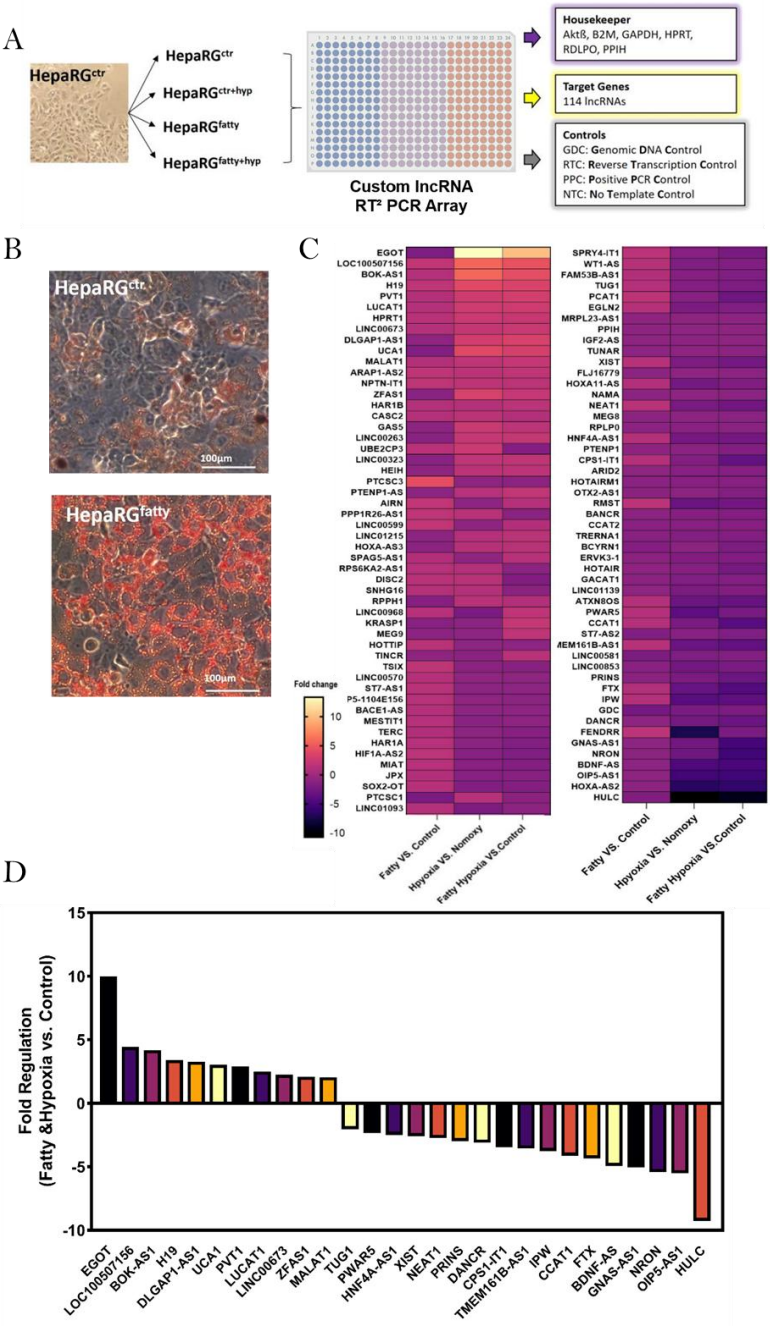
A
HepaRGctr
HepaRGctr
HepaRGctr+hyp
HepaRGfatty
HepaRGfatty+hyp
Custom lncRNA
RT² PCR Array
Housekeeper
Akt8, B2M, GAPDH, HPRT,
RDLPO, PPIH
Target Genes
114 lncRNAs
Controls
GDC: Genomic DNA Control
RTC: Reverse Transcription Control
PPC: Positive PCR Control
NTC: No Template Control
B
HepaRGctr
100µm
HepaRGfatty
100µm
C
EGOT
LOC100507156
BOK-AS1
H19
PVT1
LUCAT1
HPRT1
LINC00673
DLGAP1-AS1
UCA1
MALAT1
ARAP1-AS2
NPTN-IT1
ZFAS1
HAR1B
CASC2
GAS5
LINC00263
UBE2CP3
LINC00323
HEIH
PTCSC3
PTENP1-AS
AIRN
PPP1R26-AS1
LINC00599
LINC01215
HOXA-AS3
SPAG5-AS1
RPS6KA2-AS1
DISC2
SNHG16
RPPH1
LINC00968
KRASP1
MEG9
HOTTIP
TINCR
TSIX
LINC00570
ST7-AS1
P5-1104E156
BACE1-AS
MESTIT1
TERC
HAR1A
HIF1A-AS2
MIAT
JPX
SOX2-OT
PTCSC1
LINC01093
Fold change
10
5
0
-5
-10
Fatty VS. Control
Hpyoxia VS. Nomoxy
Fatty Hypoxia VS.Control
SPRY4-IT1
WT1-AS
FAM53B-AS1
TUG1
PCAT1
EGLN2
MRPL23-AS1
PPIH
IGF2-AS
TUNAR
XIST
FLJ16779
HOXA11-AS
NAMA
NEAT1
MEG8
RPLP0
HNF4A-AS1
PTENP1
CPS1-IT1
ARID2
HOTAIRM1
OTX2-AS1
RMST
BANCR
CCAT2
TRERNA1
BCYRN1
ERVK3-1
HOTAIR
GACAT1
LINC01139
ATXN8OS
PWAR5
CCAT1
ST7-AS2
TMEM161B-AS1
LINC00581
LINC00853
PRINS
FTX
IPW
GDC
DANCR
FENDRR
GNAS-AS1
NRON
BDNF-AS
OIP5-AS1
HOXA-AS2
HULC
Fatty VS. Control
Hpyoxia VS. Nomoxy
Fatty Hypoxia VS.Control
D
Fold Regulation
(Fatty &Hypoxia vs. Control)
15
10
5
0
-5
-10
EGOT
LOC100507156
BOK-AS1
H19
DLGAP1-AS1
UCA1
PVT1
LUCAT1
LINC00673
ZFAS1
MALAT1
TUG1
PWAR5
HNF4A-AS1
XIST
NEAT1
PRINS
DANCR
CPS1-IT1
TMEM161B-AS1
IPW
CCAT1
FTX
BDNF-AS
GNAS-AS1
NRON
OIP5-AS1
HULC

Figure 7. RT² lncRNA PCR array. The HepaRG cells was treated with normal medium (HepaRG) oleic acid (HepaRG^{fatty}), hypoxia treatment (HepaRG^{hyp}), oleic acid as well as hypoxia treatment (HepaRG$^{fatty+hyp}$), reoxygenation (HepaRG^{ctr+Re}), oleic acid and reoxygenation (HepaRG$^{fatty+Re}$), RT^2 lncRNA PCR array was adopt to screen hypoxia relatied lncRNAs in 114 lncRNAs (A). Oil red O staining was shown to be effective for fatty treatment of HepaRG cells (B). Heatmap showing results for individual lncRNA in different groups (C). RT² PCR Array revealed 28 markedly dysregulated lncRNAs under steatosis plus hypoxia (D). Fold change > 2 or < -2 are considered significant.

By applying RT^2 lncRNA PCR array, we identified 28 significantly altered target lncRNAs from 114 candidate lncRNAs previously proven to be closely associated with ischemia-reperfusion injury or liver disease. Among them, 11 lncRNAs exhibited an upregulation in expression under steatosis and hypoxic treatment compared to the control group, while 17 lncRNAs demonstrated a downregulation.

3.2 Screening for cell death-related lncRNAs

To refine our selection of research targets from the 11 highly expressed and 17 lowly expressed lncRNAs, we utilized the ncRNAs associated with ncRNA–ferroptosis associations database (ncFO: http://www.jianglab.cn/ncFO/), encompassing a comprehensive network dataset. This database identified a total of 178 experimentally validated lncRNAs linked to ferroptosis. Integrating data from our RT^2 PCR Array with the ncFO database, we identified seven up- and nine down-regulated lncRNAs (Figure

8A and B), namely H19, UCA1, PVT1, LUCAT1, LINC00673, ZFAS1, MALAT1 , TUG1, XIST, NEAT1, DANCR, CPS1-IT1, CCAT1, FTX, OIP5-AS1, and HULC (Figure 8C). Furthermore, we expanded our analysis using the LncPCD database (http://spare4.hospital.studio:9000/lncPCD/Home.jsp), which catalogs lncRNAs associated with programmed cell death. This database encompasses 1081 lncRNAs linked to programmed cell death pathways. From this dataset, we identified nine up- and twelve down-regulated lncRNAs (Figure 8D and E), namely EGOT, H19, DLGAP1-AS1, UCA1, PVT1, LUCAT1, LINC00673, ZFAS1, MALAT1 , TUG1, XIST, NEAT1, DANCR, CPS1-IT1, CCAT1, FTX, BDNF-AS, GNAS-AS1, NRON, OIP5-AS1, and HULC (Figure 8F). Through a thorough review of existing literature, we narrowed our focus to four lncRNAs of particular interest: UCA1, H19, EGOT, and NEAT1 (Figure 8G)[120,146,150,160,168,195,196].

C

upregulated lncRNAs	downregulated lncRNAs
PVT1	NEAT1
UCA1	CCAT1
MALAT1	XIST
H19	HULC
ZFAS1	TUG1
LINC00673	OIP5-AS1
LUCAT1	FTX
	CPS1-IT1
	DANCR

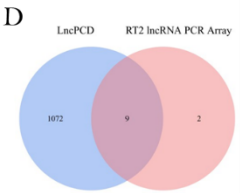

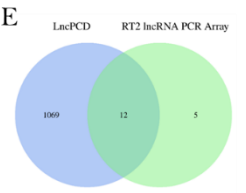

F

upregulated lncRNAs	downregulated lncRNAs
UCA1	NEAT1
H19	OIP5-AS1
ZFAS1	XIST
PVT1	TUG1
MALAT1	DANCR
LUCAT1	NRON
LINC00673	CCAT1
DLGAP1-AS1	BDNF-AS
EGOT	FTX
	HULC
	GNAS-AS1
	CPS1-IT1

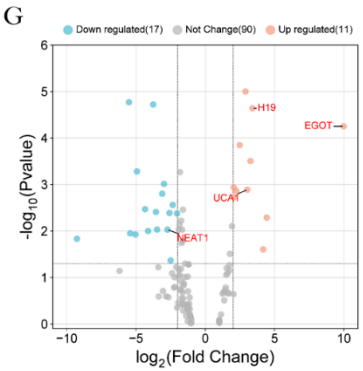

Figure 8. Selecting candidates by applying online database Database ncFO was adopted to combine with the results already obtained from RT^2 lncRNA PCR array, to obtain 7 ferroptosis related lncRNAs up-regulated and 9 ferroptosis related lncRNAs down-regulated (A, B, C). Database LncPCD was adopted to combine with the results already obtained from RT^2 lncRNA PCR array, resulting in 9 up-regulated and 12 down-regulated lncRNAs which associated with programmed cell death (D, E, F). Candidate lncRNAs presented in a volcano map (G). ncFO: A Comprehensive Resource of Curated and Predicted ncRNAs Associated with Ferroptosis. Genomics, Proteomics & Bioinformatics. 2022 Sep. DOI: 10.1016/j.gpb.2022.09.004. LncPCD: a manually curated database of experimentally supported associations between lncRNA-mediated programmed

cell death and diseases. Database (Oxford). 2023 Nov 27;2023:baad087. doi: 10.1093/database/baad087.

To refine the selection of candidates, we cross-referenced our RT² PCR array data with two curated databases: ncFO, which comprises 178 lncRNAs related to ferroptosis, and LncPCD, which encompasses 1,081 lncRNAs linked to programmed cell death. This integration revealed seven consistently upregulated and nine consistently downregulated lncRNAs from ncFO, and nine consistently upregulated and twelve consistently downregulated lncRNAs from LncPCD. Guided by the literature, we prioritised four key lncRNAs for further study: UCA1, H19, EGOT and NEAT1.

3.3 Investigation of lncRNA candidates

3.3.1 UCA1

UCA1 was located at chromosome 19p13.12 and initially discovered in bladder cancer[110]. Lu *et al.* propose that in Parkinson's disease, the expression of UCA1 is elevated and it regulates abnormal apoptosis and viability, which shows that UCA1 participates in the process of cell death[197]. Moreover, UCA1 has been implicated in the progression of various conditions including liver cirrhosis, hepatic malignancies, gastric cancers, endometrial cancer, myocardial infarction, and cerebral ischemia/reperfusion injury. For instance, Yan et al. demonstrated that UCA1 exacerbates acute ischemic stroke by suppressing miR-18a-5p, leading to increased apoptosis[122]. Additionally, Wang QS et al. found that lncUCA1 may protect cardiomyocytes from

hypoxia-induced apoptosis by inhibiting miR-143, thereby potentially preventing myocardial infarction[123]. However, the role of UCA1 in ischemia-reperfusion injury in marginal donor livers remains unclear.

Our initial screening assay revealed elevated expression of UCA1 in hypoxia- and steatosis-treated HepaRG cell lines (Figure 8G). To validate these findings, we conducted rt-PCR analysis, confirming that UCA1 RNA expression was significantly upregulated in the hypoxia-treated group, approximately three times higher than in the control group. Additionally, to mimic ischemia-reperfusion conditions, we assessed UCA1 RNA expression in the reoxygenation group, which showed a threefold decrease compared to the hypoxia group (Figure 9).

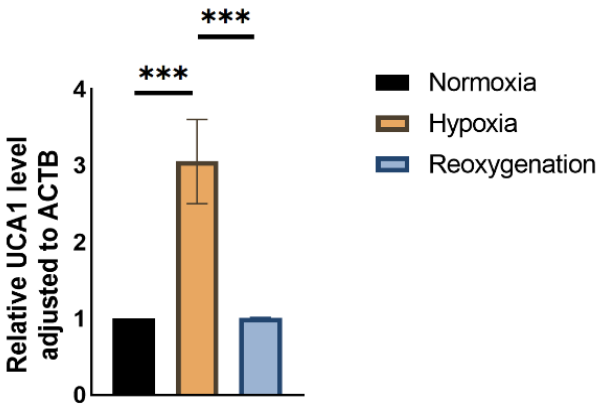

Figure 9. Validation of candidate lncRNA UCA1 by RT-qPCR. The RT^2 PCR Array results were verified by detecting the expression of UCA1 RNA. The HepaRG cells were treated under normal oxygen concentration (Normoxia), 24h

hypoxia treatment (Hypoxia), 24h reoxygenation (Reoxygenation group). Data were normalized to the housekeeper ACTB. (***p≤0.001).

Since we found that UCA1 showed high expression in the hypoxia group, in order to investigate the involvement of lncRNA UCA1 in the cell death process under hypoxia, correspondingly, we applied siRNA corresponding to UCA1 and silenced it, and the results showed that the silencing of UCA1 played a role in each group (Figure 10). Compared with the UCA1-silenced group, the RNA expression of UCA1 was higher in the non-silenced group, and this phenomenon was particularly obvious in the hypoxic group, where the silenced UCA1 RNA expression was about one-third of that in the non-silenced group.

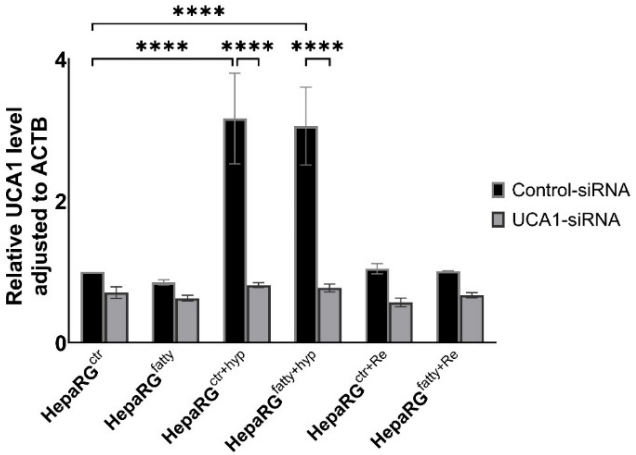

Figure 10. rt-PCR result of UCA1 silencing. After silencing of UCA1, the effect of under-expression was examined, and the results showed that RNA expression of UCA1 was different in different groups. The HepaRG cells was treated with

oleic acid (HepaRG^{fatty}), hypoxia treatment (HepaRG^{hyp}), oleic acid as well as hypoxia treatment (HepaRG$^{fatty+hyp}$), reoxygenation (HepaRG^{ctr+Re}), oleic acid and reoxygenation (HepaRG$^{fatty+Re}$). Data was normalized to the housekeeper ACTB. Statistical significance was determined by two-way repeated measures ANOVA with a Bonferroni multiple comparisons test (*p≤0.05, **p≤0.01, ***p≤0.001, ****p≤0.0001).

In order to screen the forms of cell death that lncRNA UCA1 may be involved in, we examined the expression of relevant enzymes regarding ferrroptosis, necrotic death, and apoptosis in different groups. We found that in the detection of xCT and FSP1, the relevant markers marking ferroptosis, the expression of the corresponding markers in the hypoxic group was significantly lower than that in the control group, however, a significant difference between the UCA1-silenced and non-silenced groups was detected only in the reoxygenated group for FSP1, and the expression of FSP1 was lower than that of the RNA of FSP1 in the group that underwent UCA1 silencing than in the non-silenced group (Figure 11A and B). The results of Western blot assays targeting the necroptosis marker pMLKL showed that no statistically significant differences in pMLKL protein expression were seen between the groups (Figure 11C). Western blotting results for the apoptosis marker Caspase 3 showed a decrease in Caspase 3 protein expression after UCA1 silencing in the hypoxia group, but the results were not statistically significantly different (Figure 11D).

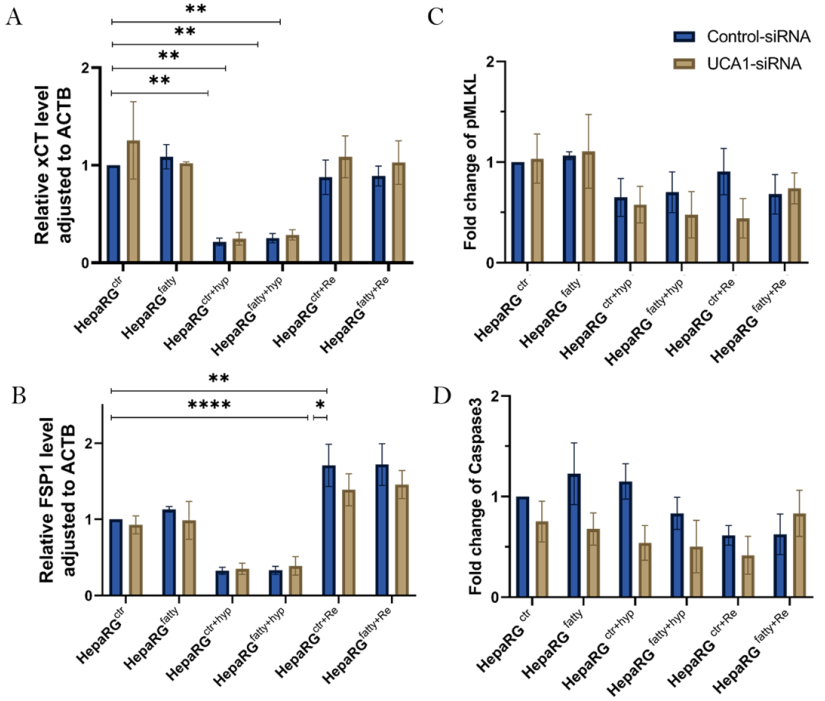

Figure 11. Relative expression of cell death regulating enzymes in HepaRG cell line with silenced UCA1. The HepaRG cells was treated with oleic acid (HepaRG^{fatty}), hypoxia treatment (HepaRG^{hyp}), oleic acid as well as hypoxia treatment (HepaRG$^{fatty+hyp}$), reoxygenation (HepaRG^{ctr+Re}), oleic acid and reoxygenation (HepaRG$^{fatty+Re}$), examining the RNA expression of SLC7A11/xCT (A), FSP1 (B) and the protein expression of pMLKL (C), Caspase-3 (D) to assess the forms of cell death that may be involved in different groups. Data was normalized to the housekeeper ACTB (A and B) or the total protein amount (C and D). Statistical significance was determined by two-way repeated measures ANOVA with a Bonferroni multiple comparisons test (*p≤0.05, **p≤0.01, ***p≤0.001, ****p≤0.0001).

The elevated expression of UCA1 in the hypoxia group was apparent. However, its specific mechanism in hepatocyte death does not appear to involve xCT, FSP1-mediated ferroptosis, Caspase 3-mediated apoptosis, or pMLKL-mediated necroptosis, since UCA1 silencing had no significant influence.

3.3.2 H19

Similar to UCA1, H19 expression was increased in HepaRG cell lines treated with hypoxia and steatosis (Figure 8G). To validate these observations, we conducted rt-PCR analysis and verified a substantial upregulation of H19 RNA expression in the hypoxia-treated group, approximately tenfold higher than in the control group. Furthermore, to mimic ischemia-reperfusion conditions, we evaluated H19 RNA expression in the reoxygenated group, revealing a decrease in H19 RNA expression in the reoxygenated group compared to the hypoxic group (Figure 12).

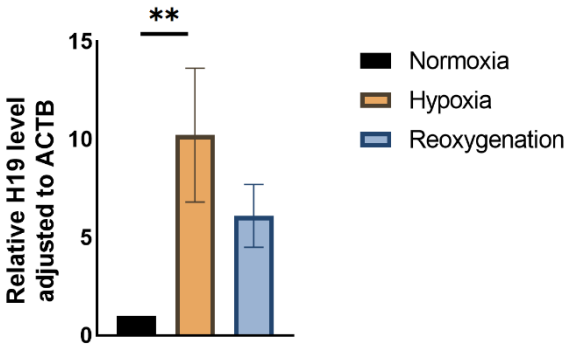

Figure 12. Validation of candidate lncRNA H19 by RT-qPCR. The RT^2 PCR

Array results were verified by detecting the expression of H19 RNA. The HepaRG cells was treated under normal oxygen concentration (Normoxia), 24h hypoxia treatment (Hypoxia), 24h reoxygenation (Reoxygenation group). Data were normalized to the housekeeper ACTB. (***p≤0.001).

We observed heightened expression of H19 in the hypoxic group. To investigate the involvement of the long non-coding RNA H19 in cell death under hypoxic conditions, we employed siRNA to silence H19. Our results demonstrated that silencing H19 had an impact across all groups. Specifically, compared to the non-silenced group, RNA expression of H19 was higher in the non-silenced group, with a notable difference observed in the hypoxic group where silenced H19 RNA expression was approximately one-sixth of that in the non-silenced group. Similarly, in the reoxygenation group, H19 RNA expression was elevated in the non-silenced group compared to the silenced group, with H19 RNA levels in the silenced group approximately one-fifth of those observed in the non-silenced group (Figure 13).

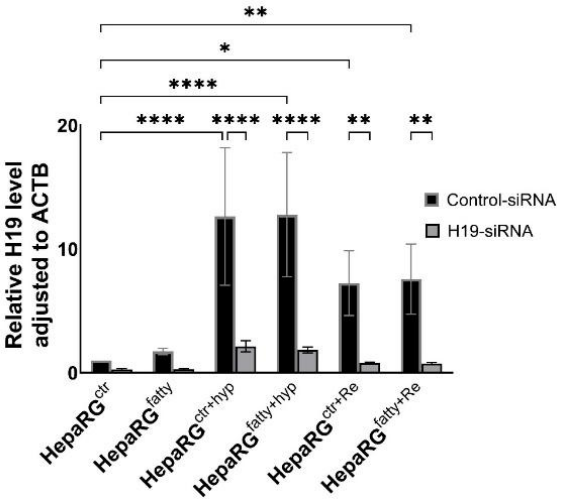

Figure 13. rt-PCR result of H19 silencing. After silencing of H19, the effect of under-expression was examined, and the results showed that RNA expression of H19 was different in different groups. The HepaRG cells was treated with oleic acid (HepaRGfatty), hypoxia treatment (HepaRGhyp), oleic acid as well as hypoxia treatment (HepaRGfatty+hyp), reoxygenation (HepaRGctr+Re), oleic acid and reoxygenation (HepaRGfatty+Re). Data was normalized to the housekeeper ACTB. Statistical significance was determined by two-way repeated measures ANOVA with a Bonferroni multiple comparisons test (*p≤0.05, **p≤0.01, ***p≤0.001, ****p≤0.0001).

To explore potential roles of lncRNA H19 in various forms of cell death, we assessed the expression of enzymes associated with ferroptosis, necrosis, and apoptosis across different experimental groups. Our findings revealed that in the hypoxia group, markers of ferroptosis (xCT, Gpx4, and FSP1) exhibited significantly lower expression compared to the control group. Upon reoxygenation, expression of ferroptosis markers increased relative to the hypoxia

group, returning to levels similar to those before hypoxia treatment. Notably, in the reoxygenation group, there was a significant difference in Gpx4 expression between the H19-silenced and non-silenced groups, with Gpx4 levels lower in the H19-silenced group (Figure 14A-C). Assessment of the necroptotic marker pMLKL showed increased expression upon H19 silencing, particularly pronounced in the reoxygenation group where pMLKL protein levels in the H19-silenced group were approximately three times higher than in the control group (Figure 14D). Western blot analysis targeting the apoptosis marker Caspase 3 revealed that Caspase 3 protein expression decreased in the hypoxia group after H19 silencing, reaching about half the level observed in the non-silenced group (Figure 14E).

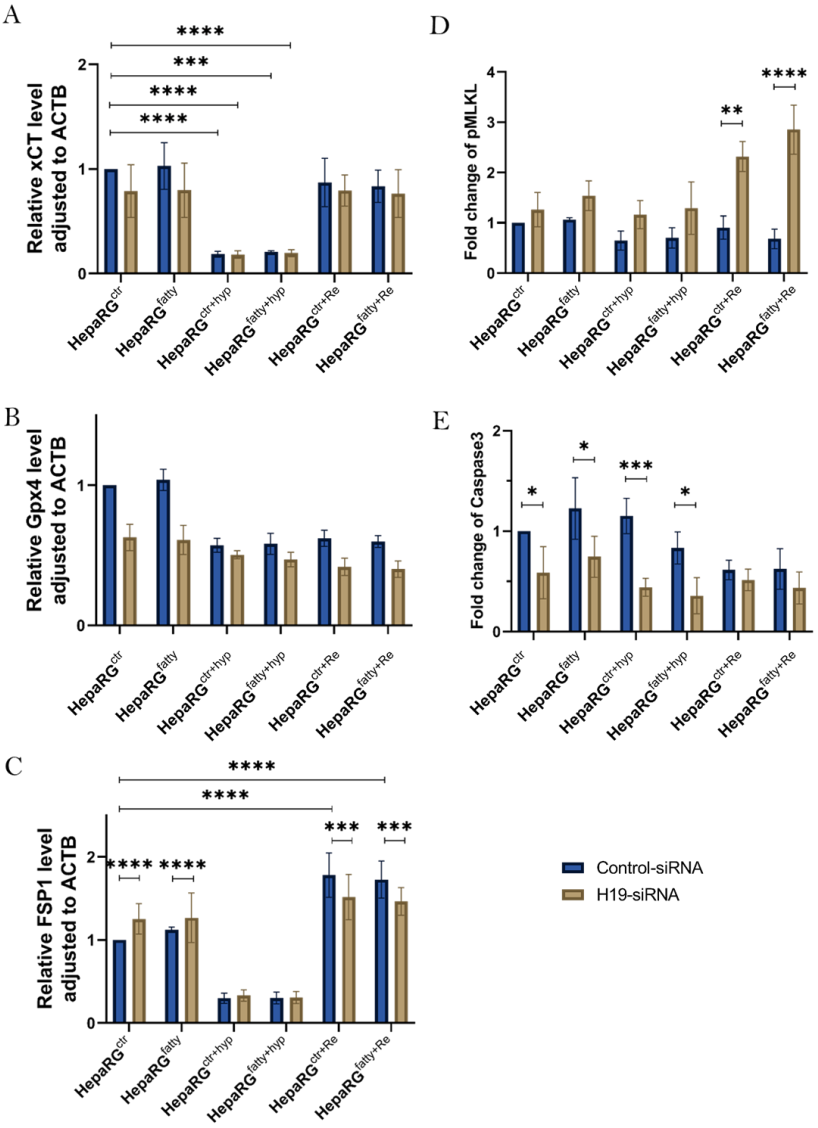

Figure 14. Relative expression of cell death regulating biomarkers in HepaRG cell line with silenced H19. The HepaRG cells was treated with oleic acid (HepaRG^{fatty}), hypoxia treatment (HepaRG^{hyp}), oleic acid as well as hypoxia

treatment (HepaRG$^{fatty+hyp}$), reoxygenation (HepaRG^{ctr+Re}), oleic acid and reoxygenation (HepaRG$^{fatty+Re}$), examining the RNA expression of SLC7A11/xCT (A), Gpx4 (B), FSP1 (C), and the protein expression of pMLKL (D) and Caspaase-3 (E) to assess the forms of cell death that may be involved in different groups. Data was normalized to the housekeeper ACTB (A-C) or the total protein amount (D and E). Statistical significance was determined by two-way repeated measures ANOVA with a Bonferroni multiple comparisons test (*p≤0.05, **p≤0.01, ***p≤0.001, ****p≤0.0001).

The alterations observed in lncRNA H19 following hypoxia-reoxygenation in the HepaRG hepatocyte cell line indicate its role in the hepatocytic response to hypoxic stress. Our experimental findings suggest that H19 potentially participates in ferroptosis or necroptosis pathways in hepatocytes post-hypoxia.

3.3.3 EGOT

LncRNA EGOT is a newly discovered lncRNA, which is located on human 3p26.1 chromosome. Early studies have shown that EGOT is highly expressed in hepatocellular carcinoma and breast cancer[151,198]. Some studies have shown that EGOT can regulate autophagy of renal tubular cells induced by hypoxia, another study demonstrated that overexpression of EGOT in tumor cells elicited apoptosis[150,160]. Nevertheless, there are few definitive conclusions regarding the role of EGOT in HIRI.

We utilized RT-PCR to corroborate the findings from the RT^2 array PCR assay. Our analysis confirmed a notable upregulation of EGOT RNA expression in the hypoxia-treated cohort, exceeding

levels observed in the control group by a factor of approximately three. Furthermore, under simulated ischemia-reperfusion conditions, the reoxygenated group exhibited a marked three-fold reduction in EGOT RNA expression compared to the hypoxic group (Figure 15).

Figure 15. Validation of candidate lncRNA EGOT by RT-qPCR. The RT^2 PCR

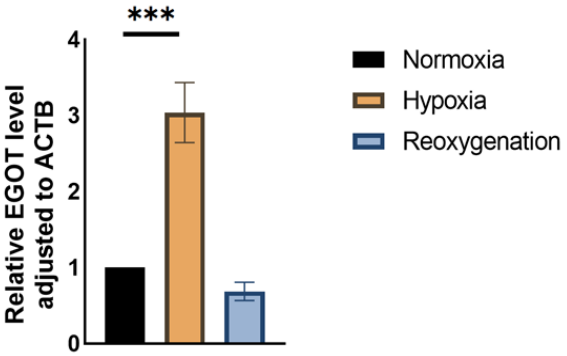

Array results were verified by detecting the expression of EGOT RNA. The HepaRG cells was treated under normal oxygen concentration (Normoxia), 24h hypoxia treatment (Hypoxia), 24h reoxygenation (reoxygenation group). Data was normalized to the housekeeper ACTB. (***p≤0.001).

Following the identification of elevated levels of EGOT expression in the cohort exposed to hypoxia, the subsequent investigation focused on the role of EGOT in the process of cell death under hypoxic and reoxygenated conditions. To this end, we employed specific siRNA to silence EGOT expression, revealing its impact across all experimental groups. Notably, EGOT RNA levels were significantly higher in the non-silenced group compared to the

EGOT-silenced group, with the most pronounced difference observed in the hypoxia-exposed subgroup, where silenced EGOT expression was approximately one-third that of the non-silenced counterpart. Despite the less pronounced reduction in the reoxygenation group following EGOT silencing when compared to the hypoxia group, the data nevertheless indicate a measurable silencing effect in the reoxygenation condition (Figure 16). The silencing effect of EGOT was thus substantiated in the hypoxia group and reoxygenation group.

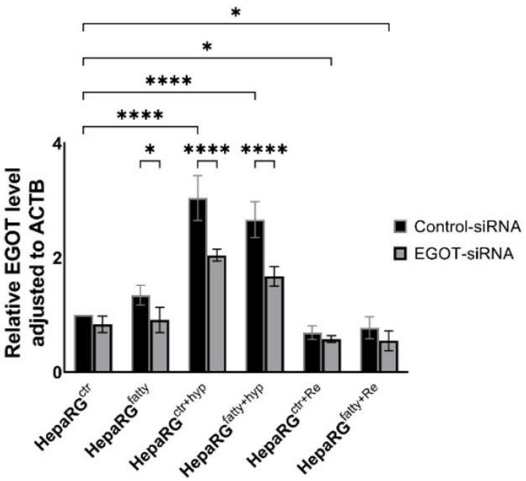

Figure 16. rt-PCR result of EGOT silencing. Following the silencing of EGOT, the impact of under-expression was investigated, revealing that RNA expression of EGOT varied among distinct groups. The HepaRG cells was treated with oleic acid (HepaRG^{fatty}), hypoxia treatment (HepaRG^{hyp}), oleic acid as well as hypoxia treatment (HepaRG$^{fatty+hyp}$), reoxygenation (HepaRG^{ctr+Re}), oleic acid and reoxygenation (HepaRG$^{fatty+Re}$). Data was normalized to the housekeeper ACTB. Statistical significance was determined by two-way repeated measures ANOVA with a Bonferroni multiple comparisons test (*p≤0.05, **p≤0.01, ***p≤0.001,

****p≤0.0001).

To investigate the potential involvement of Long non-coding RNA EGOT in various modes of cell death, we assessed the expression of enzymes associated with ferroptosis, necrosis, and apoptosis across different experimental conditions. Our findings revealed significantly lower levels of ferroptosis markers (xCT, FSP1) in the hypoxia-exposed group compared to the control group (Figure 17A and B). Following reoxygenation, EGOT expression increased relative to the hypoxic stat. Particularly noteworthy was the difference in xCT RNA levels between EGOT-silenced and non-silenced groups, with reduced xCT expression observed after EGOT downregulation, particularly evident in the reoxygenated setting. Analysis of the necroptotic marker pMLKL indicated that EGOT silencing led to increased pMLKL protein expression, notably pronounced in the reoxygenation + fatty group, where pMLKL levels in the EGOT-silenced group exceeded those in the corresponding control group by more than four-fold (Figure 17C). Additionally, Western blot analysis of the apoptosis marker Caspase 3 demonstrated a general decrease in Caspase 3 protein expression in the hypoxia group following EGOT silencing (Figure 17D).

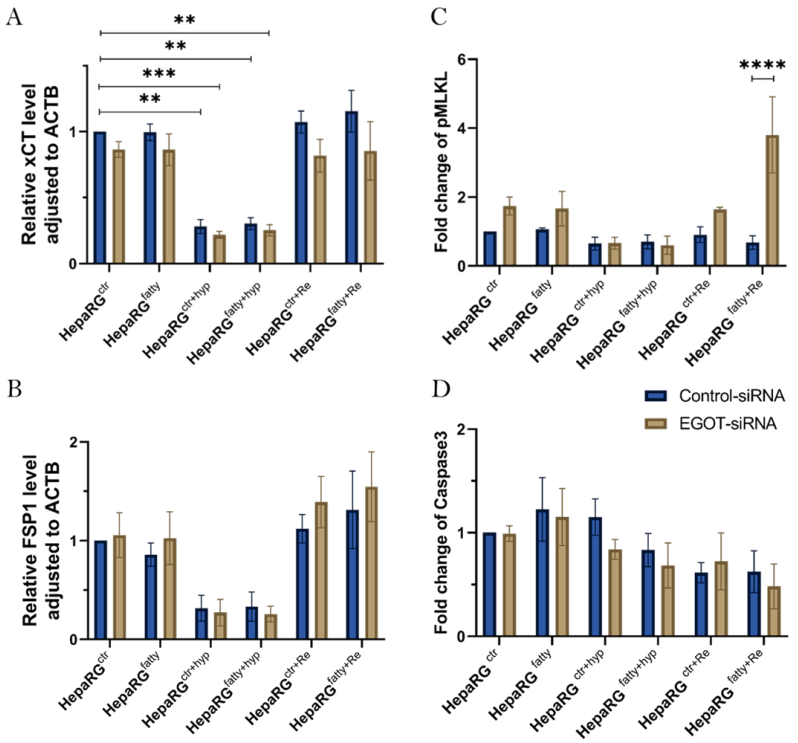

Figure 17. Relative expression of cell death regulating biomarkers in HepaRG cell line with silenced EGOT. The cell death was assessed in the control, HepaRG^{fatty} (palmitic acid, oleic acid) ,HepaRG$^{fatty+hyp}$(palmitic acid, oleic acid and hypoxia treatment 24h), HepaRG^{ctr+Re} (reoxygenation 24h), HepaRG$^{fatty+Re}$ (palmitic acid, oleic acid, reoxygenation 24h) group by examining the RNA expression of SLC7A11/xCT (A), FSP1 (B), as well as the protein expression of pMLKL (C) and Caspaase-3 (D). Statistical significance was determined by two-way repeated measures ANOVA with a Bonferroni multiple comparisons test (*p≤0.05, **p≤0.01, ***p≤0.001, ****p≤0.0001).

EGOT also exhibited results consistent with RT^2 PCR array screening. The experimental findings indicate that EGOT

potentially participates in the initial hypoxic phase of HIRI via the ferroptotic pathway, as well as in the cell death mechanism during the reoxygenation phase of HIRI through the necroptotic pathway.

3.3.4 NEAT1

Based on our integrated screening strategy combining RT² PCR array analysis with ferroptosis- and programmed cell death–associated databases, NEAT1 was selected for further validation as a candidate lncRNA potentially involved in hepatocyte responses to hypoxia and ischemia–reperfusion stress. RT^2 PCR Array test screening revealed a decrease in NEAT1 expression in HepaRG cell lines treated with hypoxia and steatosis (Figure 8G). To substantiate these observations, we conducted rt-PCR analysis, confirming a significant reduction in NEAT1 RNA expression in the hypoxia-treated group, approximately half that observed in the control group. Furthermore, to simulate ischemia-reperfusion conditions, we evaluated NEAT1 RNA expression in the reoxygenation group, which showed a decrease compared to the hypoxia group (Figure 18).

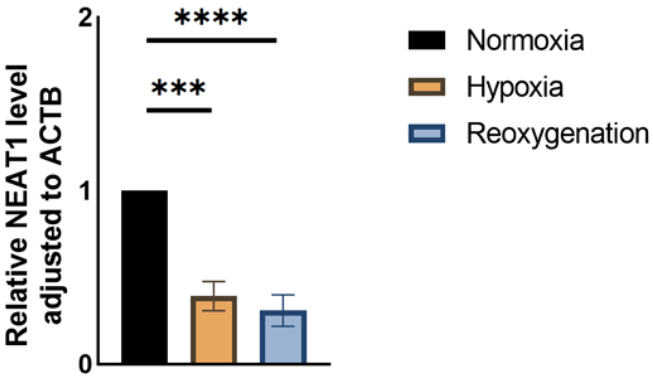

Figure 18. Validation of candidate lncRNA NEAT1 by RT-qPCR. The RT^2 PCR Array results were verified by detecting the expression of NEAT1 RNA. The HepaRG cells was treated under normal oxygen concentration (Normoxia), 24h hypoxia treatment (Hypoxia), 24h reoxygenation (Reoxygenation group). Data was normalized to the housekeeper ACTB. (***p≤0.001, ****p≤0.0001).

From Figure 18, it is evident that NEAT1 RNA expression levels were low in both the hypoxia group and the reoxygenation group. To investigate the role of NEAT1 in cell death under hypoxic and reoxygenation conditions, we subsequently introduced a NEAT1-expressing plasmid to induce NEAT1 overexpression (Figure 19A). Our results demonstrated that elevated NEAT1 expression exerted an influence across all experimental groups. Specifically, compared to the control plasmid group, the NEAT1 overexpression group exhibited significantly increased NEAT1 RNA levels, a difference particularly pronounced in the hypoxia and reoxygenation groups. NEAT1 RNA expression after high-expression was more than twice that of the control plasmid group.

In untreated HepaRG cells, NEAT1-siRNA decreased NEAT1 levels by approximately half relative to controls ($p < 0.01$) (Figure 19B). A similar reduction was observed in fatty acid–treated cells ($p < 0.01$) and in cells exposed to hypoxia ($p < 0.05$). In the combined fatty acid and hypoxia condition, NEAT1 levels were also lower in the NEAT1-siRNA group, although the magnitude of reduction was smaller. These results indicate that NEAT1 knockdown is effective across normoxic, hypoxic, and lipid-loaded environments, with statistically significant decreases in transcript abundance in all conditions.

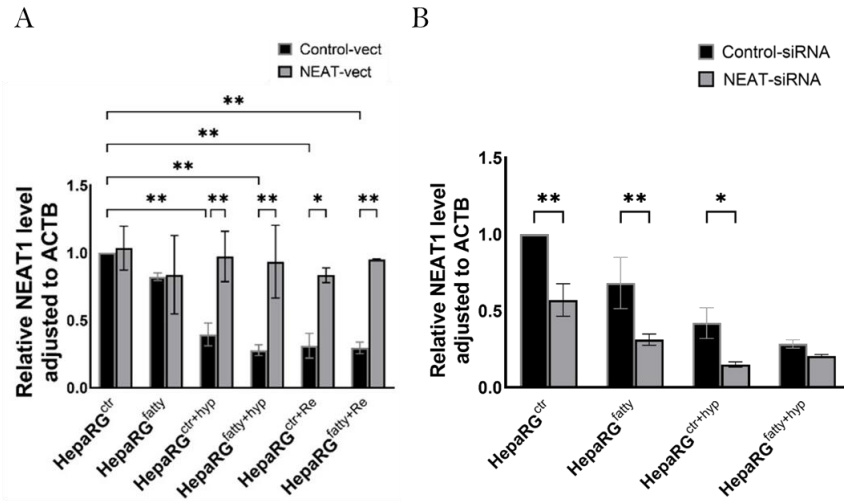

Figure 19. RT-qPCR result of NEAT1 overexpressing (A) and silencing (B). After overexpressing of NEAT1, the effect of was examined, and the results showed that RNA expression of NEAT1 was different in different groups. The HepaRG cells was treated with oleic acid ($HepaRG^{fatty}$), hypoxia treatment ($HepaRG^{hyp}$), oleic acid as well as hypoxia treatment ($HepaRG^{fatty+hyp}$), reoxygenation ($HepaRG^{ctr+Re}$), oleic acid and reoxygenation ($HepaRG^{fatty+Re}$).

Data was normalized to the housekeeper ACTB. Statistical significance was determined by two-way repeated measures ANOVA with a Bonferroni multiple comparisons test (*p≤0.05, **p≤0.01).

Gidlöf et al. found that NEAT1 may be downregulated after hypoxia[203], thereby participating in the hypoxia-protective mechanism of hypoxic cardiomyocytes in mice, which is consistent with our findings from RT² screening and validation using the HepaRG cell line, showing a decrease in NEAT1 after 24 h of hypoxia. According to recent studies, NEAT1 can participate in ferroptosis in multiple organs through different mechanisms. Zhang et al. reported that NEAT1 expression increases during ferroptosis in HCC cells[204]. They showed that NEAT1 upregulation promotes ferroptosis in HCC cells. Exosomal NEAT1 also promotes ferroptosis in brain microvascular endothelial cells through the miR-9-5p/TFRC/GOT1 axis[205]. This effect aggravates sepsis-associated encephalopathy. To clarify the targets of ferroptosis involving lncRNA NEAT1, we examined the expression of ferroptosis-related enzymes across different experimental groups (Figure 20). Following NEAT1 overexpression, we observed an increase in xCT expression, particularly notable in the reoxygenation group where it was twice as high as in the control group (Figure 20A). However, the RNA expression assay of FSP1 yielded contrasting results between the hypoxia and reoxygenation groups post NEAT1 overexpression (Figure 20B). Specifically, NEAT1 overexpression led to increased

FSP1 RNA expression in the hypoxia group and decreased expression in the reoxygenation group. Additionally, Western bloting analysis revealed decreased FSP1 protein expression across all experimental groups following NEAT1 overexpression (Figure 20C).

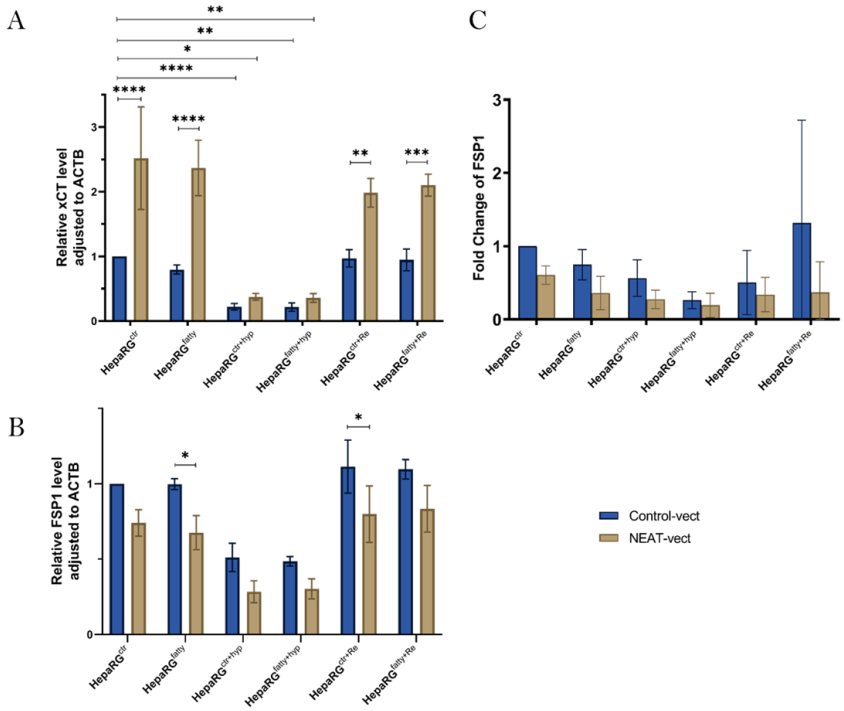

Figure 20. Relative expression of ferroptosis regulating biomarkers in HepaRG cell line after NEAT1 overexpressed. The ferroptosis was assessed in the control, HepaRG^{fatty} (palmitic acid, oleic acid) ,HepaRG$^{fatty+hyp}$(palmitic acid, oleic acid and hypoxia treatment 24h), HepaRG^{ctr+Re} (reoxygenation 24h) and HepaRG$^{fatty+Re}$ (palmitic acid, oleic acid, reoxygenation 24h) group by examining the RNA expression SLC7A11/xCT (A), FSP1 (B), as well as the protein expression of FSP1 (C). Statistical significance was determined by two-way

repeated measures ANOVA with a Bonferroni multiple comparisons test (*p≤0.05, **p≤0.01, ***p≤0.001, ****p≤0.0001).

System x_c^- is one among many amino acid transporters expressed in the plasma membrane of mammalian cells. This transporter is composed of xCT (SLC7A11), which is the substrate-specific subunit, and 4F2 heavy chain (SLC3A2). Inhibition of system x_c^- causes a rapid drop of intracellular glutathione level and ferroptosis[206]. Erastin was discovered as a potent and selective inhibitor of system x_c^- causing a novel iron-dependent form of non-apoptotic cell death, ferroptosis[207]. In our earlier study, we found that xCT expression in HepaRG cells dropped after hypoxia and recovered after reoxygenation. NEAT1 overexpression raised the level of xCT. Based on the work of Wu, Zhang, and Yu[92,208,209], we propose that NEAT1 may act as a regulator in ferroptosis. To investigate the effect of NEAT1 overexpression and knockdown on the mRNA expression of ferroptosis-related genes in HepaRG non-fatty and fatty cells under different treatment conditions (DMSO or Erastin), we treated HepaRG cells with Erastin to simulate ferroptotic conditions. This allowed us to assess how NEAT1 overexpression or knockdown influences the regulation of ferroptosis in both non-fatty and fatty cell environments. NEAT1 was then manipulated for overexpression and knockdown (Figure 21). The results showed that NEAT1 expression fell in all groups after knockdown, reaching about half of the control level, which confirmed that the silencing

was effective (Figure 21A). After overexpression, NEAT1 expression increased overexpression, especially in the erastin-treated ferroptosis group, where the level reached about 4–6 times that of the non-overexpressed cells (Figure 21B).

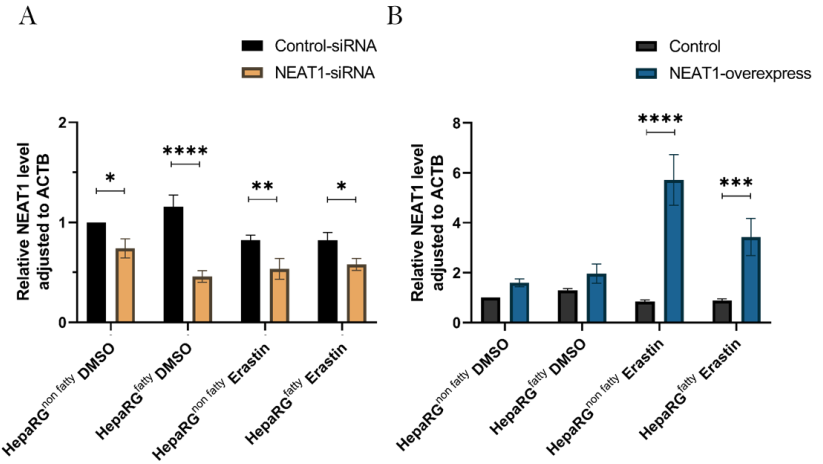

Figure 21. RT-qPCR analysis of NEAT1 knockdown and overexpression under ferroptosis. HepaRG cells were divided into non-fatty and fatty groups, followed by treatment with DMSO or erastin. This figure shows the groups under NEAT1 knockdown (A), and the groups under NEAT1 overexpression (B). Data were normalized to ACTB. Statistical analysis was performed using two-way ANOVA with Bonferroni multiple comparisons (*p≤0.05, **p≤0.01, ***p≤0.001, ****p≤0.0001).

To further explore the involvement of NEAT1 in ferroptosis, we transiently overexpressed NEAT1 in HepaRG cells using a vector and treated them with different concentrations of Erastin. Subsequently, we assessed cell viability and observed a gradual

decrease in activity across all groups treated with Erastin concentrations ranging from 20 μM to 100 μM (Figure 22). The results showed that at an Erastin concentration of 100 μM, NEAT1-overexpressing groups consistently exhibited lower cell viability compared with their respective control groups. Specifically, the NEAT1-overexpressing group without fatty acid treatment showed a 12.92% reduction in viability relative to the corresponding control group without fatty acid treatment, while the NEAT1-overexpressing group with fatty acid treatment exhibited a 21.88% reduction compared with the corresponding control group with fatty acid treatment. Moreover, cell viability in the fatty acid–treated NEAT1-overexpressing HepaRG cells was markedly lower than that in the untreated NEAT1-overexpressing HepaRG cells.

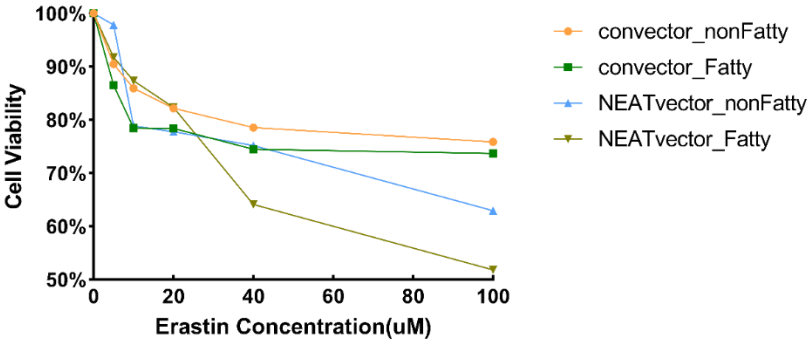

Figure 22. Cell viability assay of HepaRG cell line under ferroptosis induced by Erastin. HepaRG cell lines were treated with indicated doses of erastin, and cell viability was evaluated 48 hours post-treatment. The control group received treatment with blank plasmid, while the NEAT1vector group was treated with NEAT1 overexpression, each subjected to either control or fatty conditions.

As shown in Figure 23, non-fatty cells treated with DMSO showed a low baseline level of xCT, and NEAT1 overexpression significantly increased expression compared with control ($p<0.05$). In fatty cells under DMSO treatment, NEAT1 overexpression further elevated xCT levels ($p<0.05$). In non-fatty cells treated with Erastin, xCT expression increased, and NEAT1 overexpression led to a further rise ($p<0.01$). In fatty cells exposed to Erastin, the highest expression level was observed, and NEAT1 overexpression caused an additional increase ($p<0.001$). These findings suggest that NEAT1 may promote xCT expression and could contribute to antioxidant regulation during ferroptosis (Figure 23A). Analysis of GPX4 expression showed that NEAT1 overexpression significantly reduced mRNA levels in non-fatty HepaRG cells under DMSO treatment ($p<0.0001$) (Figure 23B). In fatty cells and in Erastin-treated groups, no statistically significant differences were detected ($p>0.05$). However, a downward trend of GPX4 expression was observed across these groups following NEAT1 overexpression. These findings suggest that NEAT1 may attenuate GPX4 expression to varying degrees. For SLC2A, NEAT1 overexpression resulted in a significant upregulation in both non-fatty and fatty cells ($p<0.01$, $p<0.001$) (Figure 23C). The increase was more obvious under Erastin treatment, particularly in fatty cells. This indicates that NEAT1 enhances SLC2A expression and may promote metabolic responses under stress. Regarding FSP1 expression, NEAT1 overexpression in non-fatty cells under DMSO treatment showed no significant difference

compared with controls ($p>0.05$) (Figure 23D). In fatty cells treated with DMSO, FSP1 expression decreased after NEAT1 overexpression, reaching statistical significance ($p<0.01$). In non-fatty cells treated with Erastin, NEAT1 overexpression led to a modest reduction, which was statistically significant ($p<0.05$). In fatty cells treated with Erastin, a significant decrease was also observed after NEAT1 overexpression ($p<0.05$). Overall, NEAT1 overexpression tended to reduce FSP1 expression, with the effect more evident in fatty cells, though the biological significance of these changes requires further investigation.

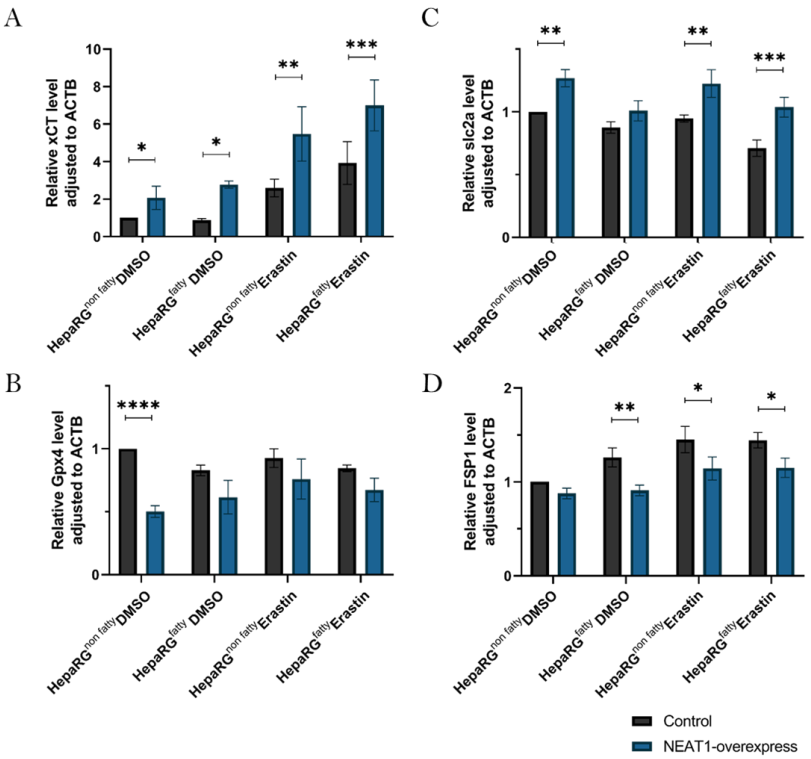

Figure 23. RT-qPCR results of ferroptosis-related markers in HepaRG cells after Erastin treatment with overexpressed NEAT1. These four figures illustrate the relative expression levels of different genes in HepaRG non-fatty and fatty cells following DMSO or Erastin treatment, comparing the control group (Control) with the NEAT1 overexpression group (NEAT1-overexpress). NEAT1 overexpression elevated xCT expression in both non-fatty and fatty cells, with stronger effects under Erastin treatment (A). GPX4 expression decreased in non-fatty cells after NEAT1 overexpression, while other groups showed no significant changes but a downward trend (B). SLC2A expression increased in both cell types, with more pronounced changes under Erastin, especially in fatty cells (C). FSP1 expression was reduced across groups, with a greater reduction in fatty cells (D). Data were normalized to ACTB. Statistical analysis was performed

using two-way ANOVA with Bonferroni multiple comparisons (*p≤0.05, **p≤0.01, ***p≤0.001, ****p≤0.0001).

Our previous results (Figure 23) showed that NEAT1 overexpression was associated with increased xCT and SLC2A expression, while GPX4 and FSP1 expression tended to decrease. These findings suggest that NEAT1 may participate in ferroptosis regulation by influencing both antioxidant defense and metabolic pathways. Since earlier studies have reported that NEAT1 promotes ferroptosis through the miR-362-3p/MIOX axis[204], they further examined the potential interaction sites. Both the 3′UTR of MIOX and NEAT1 were found to contain putative binding sites for miR-362-3p. We next examined the expression of miR-362 and MIOX in HepaRG cells under different conditions. As shown in Figure 24A, knockdown of NEAT1 significantly increased the expression of miR-362 compared with controls, suggesting that NEAT1 may normally suppress miR-362 levels. In Figure 24B, NEAT1 overexpression elevated MIOX mRNA expression, with the effect most pronounced under Erastin treatment. These findings are consistent with the proposed ceRNA mechanism, in which NEAT1 sponges miR-362 and thereby releases MIOX from its inhibition.

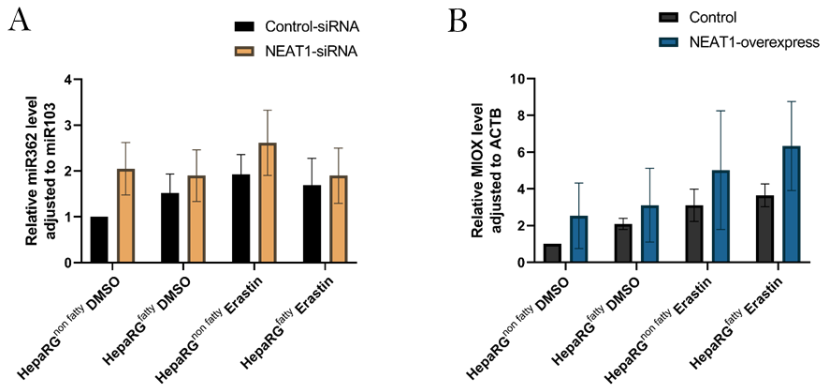

Figure 24. RT-qPCR analysis of the NEAT1/miR-362-3p/MIOX axis in HepaRG cells. NEAT1 knockdown increased miR-362 expression under different conditions (A), and NEAT1 overexpression elevated MIOX mRNA levels, with stronger effects under Erastin treatment (B). Data were normalized to miR103 (for miR-362) or ACTB (for MIOX). No statistically significant differences were observed among groups.

In summary, NEAT1 expression decreased after hypoxia and partially recovered with reoxygenation. Functional analysis showed that NEAT1 overexpression increased xCT and SLC2A expression, while GPX4 and FSP1 expression tended to decline. Cell viability assays demonstrated that NEAT1 overexpression reduced survival under Erastin treatment, with a stronger effect in fatty cells. Further analysis of the NEAT1/miR-362-3p/MIOX axis revealed that NEAT1 knockdown elevated miR-362, whereas NEAT1 overexpression enhanced MIOX expression, especially in the Erastin group. These findings suggest that NEAT1 may influence ferroptosis by regulating antioxidant defense, metabolic

activity, and the miR-362-3p/MIOX pathway.

4. Discussion

Hepatic ischemia–reperfusion injury is characterized by a dynamic transition from hypoxic stress to oxidative damage, during which multiple regulated cell death programs are engaged in a time- and context-dependent manner. In this setting, long non-coding RNAs have emerged as important modulators of stress adaptation and cell fate decisions. We investigated four hypoxia-responsive lncRNAs with potential roles in hepatocyte injury during ischemia/reperfusion. For each, we combined expression profiling, functional silencing, and pathway marker analysis to uncover distinct contributions to ferroptosis, apoptosis, and necroptosis. This strategy allowed direct comparison of lncRNAs that primarily reflect hypoxic stress responses with those that more actively bias cell death pathways during the reoxygenation phase.

4.1 UCA1

UCA1 is a long non-coding RNA originally identified in bladder cancer and later recognized as an important regulator of stress-induced cellular injury[109,115]. Increasing evidence indicates that UCA1 participates in the modulation of apoptosis, inflammation, and cell survival through miRNA-mediated and signaling-dependent mechanisms[110,116,118,156,210]. In neurological models of ischemic injury, UCA1 has been reported to aggravate neuronal damage by suppressing protective microRNAs such as miR-18a-5p, thereby enhancing apoptotic signaling and inflammatory

responses[122]. Conversely, in cardiomyocytes subjected to hypoxia–reoxygenation, UCA1 has been shown to attenuate apoptosis by targeting miR-143 and preserving mitochondrial integrity, suggesting a cytoprotective role under certain stress conditions[123]. These findings highlight the context-dependent nature of UCA1 function, with its downstream effects closely linked to regulation of programmed cell death pathways. Notably, although UCA1 has been implicated in liver diseases and viral hepatitis, its involvement in hepatocyte apoptosis and other forms of programmed cell death during hepatic ischemia–reperfusion injury remains poorly defined, particularly in marginal donor livers characterized by heightened susceptibility to ischemic stress.

Our experiments show that UCA1 is significantly upregulated in hepatocytes under hypoxia, with a marked reduction upon reoxygenation. Silencing UCA1 did not produce significant changes in ferroptosis markers (xCT, FSP1), apoptosis marker caspase-3, or necroptosis marker p-MLKL in hypoxic conditions, though minor alterations appeared during reoxygenation. These data suggest that UCA1 serves as a hypoxia-responsive lncRNA, but its direct impact on hepatocyte death pathways may be context-dependent.

In cardiomyocyte models, UCA1 exerts protective effects against hypoxia/reoxygenation-induced apoptosis. Overexpression of UCA1 inhibited miR-143, thereby activating the MDM2/p53 axis and reducing apoptosis in neonatal rat cardiomyocytes subjected to H/R injury[123]. Additionally, in H9C2 cells, UCA1 suppresses

endoplasmic reticulum stress and apoptosis under ischemia/reperfusion conditions[121]. These findings underscore UCA1's anti-apoptotic roles through miRNA sponging and stress pathway modulation. Further, recent evidence suggests that UCA1 delivered by mesenchymal stem cell–derived exosomes protect cardiomyocytes by preventing miR-143–mediated degradation of Bcl-2, strengthening its role in H/R injury mitigation[211]. In cancer contexts, UCA1 supports metabolic reprogramming. It upregulates hexokinase-2 via the mTOR-STAT3/miR-143 pathway, enhancing glycolysis and survival[212]. Such metabolic roles may also hold relevance in hepatocytes under ischemic stress, especially given their reliance on glycolytic shifts during oxygen deprivation. Applying these insights to our liver IRI model: UCA1 upregulation during hypoxia may represent an adaptive response. In hypoxia–reoxygenation models, UCA1 has been reported to attenuate apoptosis by sequestering miR-143 and modulating the downstream MDM2/p53 pathway, thereby influencing early activation of intrinsic apoptotic signaling[123]. Its negligible impact on ferroptosis/apoptosis markers in our in vitro setting might reflect a transient or indirect role, overshadowed upon reoxygenation when oxidative stress intensifies. Other lncRNAs like H19 or NEAT1 may carry a more direct influence on ferroptotic or necroptotic pathways. Using the publicly available GSE14951 dataset, we showed that UCA1 expression was elevated in human liver transplant biopsies following ischemia–reperfusion injury, suggesting potential clinical relevance.

although previous studies in cardiomyocytes reported a decrease of UCA1 expression under hypoxia/reoxygenation conditions, where its downregulation was associated with enhanced ER stress, mitochondrial dysfunction, and apoptosis[210]. Similar associations have been reported in cardiac ischemic injury, where UCA1 expression changes correlate with disease severity, supporting its potential as a non-invasive biomarker[120,123]. Tissue-specific outcomes likely stem from differential miRNA targets. In hepatocytes, UCA1 may sponge miR-143 or other yet-unidentified miRNAs, modulating survival signals or metabolic pathways. Such a ceRNA mechanism has been established in tumors and cardiomyocytes[121,213]. Moreover, UCA1's role in glycolysis control through HK2 upregulation (via mTOR-STAT3/miR-143) in cancer may be mirrored in hypoxic hepatocytes, aiding energy supply under oxygen deprivation. This may help explain the pronounced UCA1 response under hypoxia combined with steatosis—conditions that mimic marginal donor livers, which are highly vulnerable to IRI[182].

In summary, UCA1 acts as a hypoxia-responsive regulator. It displays protective properties via miR-143 sponging, ER stress suppression, and possibly metabolic regulation, but might not directly govern apoptosis, necroptosis, or ferroptosis in hepatocytes under current conditions. Its rapid induction in human IRI highlights its biomarker potential. Definitive functional roles will require in vivo validation, for example using hepatocyte-specific UCA1 gain- or loss-of-function mouse models. Single-cell RNA

sequencing of isolated hepatic cell populations could then be employed to delineate cell-type–specific transcriptional changes, identify differentially expressed genes and downstream miRNA regulators, and guide pathway enrichment analyses for focused mechanistic studies of programmed cell death in hepatic ischemia–reperfusion injury.

4.2 H19

H19 was the first lncRNA and first imprinted gene identified in eukaryotes as a hepatic fetal-specific non-translatable mRNA in the late 1980s[125]. H19, a maternally expressed and paternally imprinted 2.7 kb gene, resides close to the telomeric region of chromosome 11p15.5 and is reciprocally imprinted and regulated with its neighboring gene IGF2[127]. It is evident that H19 exhibits a highly conserved secondary structure. This finding indicates that the function of H19 is structure-dependent, suggesting a significant degree of evolutionary conservation[133]. The function of H19 can be dissected into two major functions: firstly, a reservoir of miR-675 that suppresses its targets[130], and secondly, a modulator of micro-RNAs or proteins via their binding. During the last three decades, H19 has been well characterized as a multitasking lncRNA. The aberrant expression of H19 has been linked to various human cancers, including gastric, liver, and pancreatic cancers[135,143,214,215]. In gastric cancer cells H19 RNA was shown to interact with P53 protein, causing its partial inactivation[216]. We also have shown that hypoxia

triggers *H19* expression in *p53* deficient cell lines[217]. H19 plays a role under hypoxic regulation, as illustrated in Figure 25, hypoxia leads to upregulation of h19, which ultimately causes DNA damage. Further investigation is required to determine the impact of H19 in HIRI.

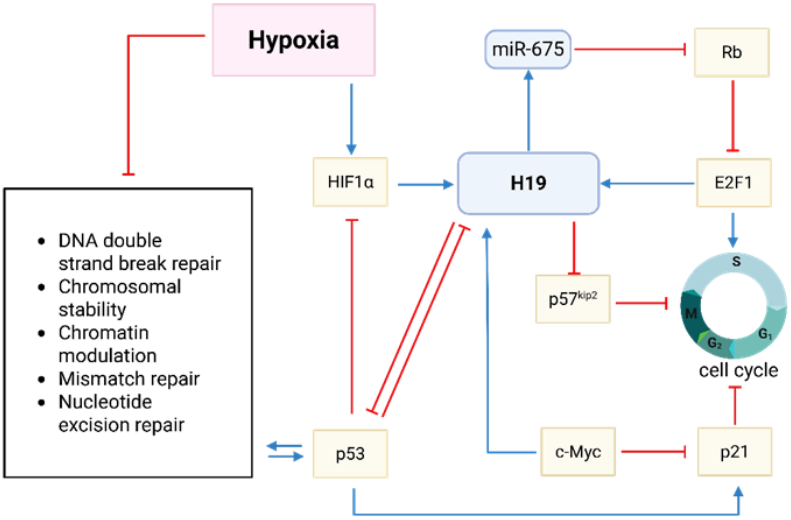

Figure 25. Regulation of H19 under hypoxia. H19 plays a critical role in cell proliferation and the response to hypoxic stress. Hypoxia induces H19 expression under hypoxic stress in p53 mutated cells, in which HIF1α, which is essential to H19 upregulation, as well as H19 itself, are not repressed by P53. Since hypoxia is a mutagenic condition, it can also induce p53 mutations and cause the H19 response. H19 promotes cell cycle progression through Rb suppression by its miR-675 or by $p57^{kip2}$ (CDKN1C) suppression or c-Myc activation.

Our study demonstrated that H19 was markedly upregulated in hepatocytes subjected to hypoxia, while reoxygenation reduced

its expression. Silencing H19 led to reduced GPX4 and caspase-3 levels and increased pMLKL expression, suggesting that H19 may participate in ferroptosis, apoptosis, and necroptosis. These results indicate that H19 has a multifaceted role in hepatocyte response to ischemic stress.

Previous work has shown that H19 is a maternally expressed imprinted lncRNA that is highly active during embryogenesis and reactivated under stress conditions[218]. H19 functions as a precursor for miR-675, which originates within its first exon and is processed to the mature form in both human and mouse cells[219]. Hypoxia can drive H19 expression through HIF-1α. In glioblastoma models, HIF-1α directly binds the H19 promoter and, with SP1, enhances H19 transcription; H19 and HIF-1α levels correlate in tumors[144]. This mechanism supports our observation that H19 increases in hypoxic hepatocytes. H19's effect in I/R is tissue-specific. In the brain, I/R elevates H19 in microglia and triggers pyroptosis and neuroinflammation by disturbing the NLRP3/NLRP6 inflammasome balance[146]. In the heart, H19 has been reported to modulate autophagy; in acute myocardial infarction models, altering H19 changes Beclin-1/ATG7 and impacts injury severity[139]. These findings align with the re-oxygenation data showing cell-death pathway shifts when H19 is suppressed. Multiple lines of evidence link H19 to ferroptosis control through miRNA axes that govern lipid peroxidation machinery. In an intracerebral hemorrhage model, knocking down H19 increased GPX4 and SLC7A11 and reduced iron-dependent

lipid damage; H19 acted via the miR-106b-5p/ACSL4 axis[139]. This axis provides a plausible explanation for our finding that H19 silencing alters GPX4 in hepatocytes during re-oxygenation. H19 can also couple iron handling to oxidative stress: ferritin heavy-chain (FTH1) silencing upregulates H19 and miR-675, linking the H19/miR-675 module to iron-metabolism shifts relevant to ferroptosis[220,221]. Direct evidence that H19 controls necroptosis is limited. However, H19 can activate NF-κB signaling in glioma, including under oxidative stress, where it confers temozolomide resistance—clear proof of H19→NF-κB pathway engagement[222]. NF-κB and STAT3 pathways intersect with programmed cell-death decisions, including necroptosis, in multiple contexts; reviews and mechanistic studies describe NF-κB/STAT3 crosstalk with apoptosis, autophagy, and necroptosis signaling modules[223–225]. Given our pMLKL rise after H19 silencing, we infer that H19 may influence necroptosis indirectly via inflammatory and redox nodes rather than as a dedicated necroptotic effector. H19 is dysregulated across liver conditions. In NAFLD/NASH and cholestasis, hepatic H19 rises and modulates lipogenesis, bile-acid signaling, and fibrogenic responses; H19 is discussed as a diagnostic/prognostic biomarker and potential target[226]. These disease associations support a model in which H19 is a stress-responsive regulator in hepatocytes.

Taken together, prior work depicts H19 as an imprinted, conserved lncRNA that integrates hypoxia signals and miRNA programs (especially miR-675) to tune growth and stress responses. In

ischemic injury, H19's net effect depends on cell type and the balance of autophagy, inflammasome activity, and iron-lipid peroxidation pathways[146,227]. Our data fit this framework: hypoxia upregulates H19, while re-oxygenation unmasks its role across death programs—ferroptosis via GPX4-related antioxidant control, apoptosis via caspase-3, and a possible check on necroptosis reflected by pMLKL release.

To clarify these context-dependent effects, future studies should combine in vivo H19 modulation with analyses of human liver specimens during ischemia–reperfusion. Single-cell RNA sequencing of human hepatic samples collected at defined ischemic and reperfusion stages could delineate cell-type–specific H19 regulation and identify ferroptosis-, apoptosis-, and necroptosis-related transcriptional programs. Integration of differential expression with pathway enrichment analyses may further highlight key downstream regulators, including the H19–miR-675 axis, which could then be functionally validated using targeted gain- or loss-of-function approaches.

4.3 EGOT

EGOT is a long non-coding RNA initially described in eosinophil differentiation and later identified as a highly inducible stress-responsive transcript[228]. A substantial body of evidence demonstrates that EGOT expression is robustly induced by viral infection, pathogen-associated molecular patterns, inflammatory cytokines, and hypoxic stress through activation of NF-κB,

PI3K/AKT, and MAPK signaling pathways[157,158,229]. Functionally, EGOT has been shown to regulate interferon-stimulated gene expression, inflammatory cytokine production, and autophagy-related processes[159,160]. In renal tubular cells, EGOT negatively modulates hypoxia-induced autophagy by interacting with RNA-binding protein HuR and autophagy-related genes such as ATG7 and ATG16L1[160], whereas in hepatic and immune contexts EGOT has been linked to inflammation, antiviral responses, and tumor progression[156,157,198]. These findings position EGOT as an important regulator at the intersection of stress signaling, inflammation, and programmed cell death, particularly autophagy. Nevertheless, its role in coordinating hepatocyte death or survival during hepatic ischemia–reperfusion injury—where dysregulated autophagy and inflammation are key pathological features—has not yet been systematically investigated.

Our study found that EGOT expression increased significantly under hypoxia in hepatocytes, while reoxygenation reduced its levels. Silencing EGOT led to lower xCT expression, reduced ferroptosis resistance, and higher pMLKL protein abundance, particularly under reoxygenation with fatty acid loading, where pMLKL was increased more than fourfold compared to controls. Caspase-3 expression was also reduced upon EGOT knockdown, suggesting that EGOT may intersect with apoptosis as well. Together, these findings indicate that EGOT participates in ferroptosis and necroptosis pathways during IRI, with potential additional effects on apoptosis regulation.

EGOT was first described—then named EGO—as a non-coding RNA required for eosinophil granule protein expression during eosinophil development[149]. The locus sits antisense within intronic sequences of the ITPR1 gene, establishing EGOT as an intronic antisense lncRNA[156]. In renal tubular cells, hypoxia-induced autophagy is associated with downregulation of EGOT; HuR (ELAVL1) helps stabilize EGOT at baseline and modulates autophagy gene expression under stress[160]. This result differs from our hepatocyte data, pointing to cell-type specificity in hypoxia responses of EGOT. Direct reports that EGOT controls ferroptosis are lacking. We therefore interpret our xCT decrease and heightened lipid-peroxidation susceptibility after EGOT silencing as indirect evidence that EGOT buffers antioxidant defenses, analogous to other hypoxia-responsive lncRNAs that regulate the system Xc^-/GSH axis (e.g., H19)[230]. This inference fits our data but requires formal validation with ferroptosis-specific assays and rescue experiments in hepatocytes. The marked rise of pMLKL after EGOT knockdown suggests necroptosis involvement during reoxygenation. Although we did not find prior studies showing a direct EGOT RIPK1/RIPK3/MLKL axis, the observed NF-κB linkage provides a plausible route, because inflammatory NF-κB signaling often shapes necroptotic thresholds. Our hepatocyte findings thus place EGOT upstream of cell-death choice under oxidative and inflammatory stress[229]. In clinical and disease settings, EGOT is dysregulated across cancers and infections, in some cases associating with prognosis and therapy

response[152,154,156]. These observations, along with our hepatocyte findings, suggest that EGOT may function as a stress-responsive regulator, potentially coordinating Ca^{2+} release and autophagy via ITPR1, modulating inflammatory signaling, and influencing susceptibility to ferroptosis and necroptosis during ischemia/reperfusion

Altogether, EGOT is a hypoxia-responsive lncRNA with multi-pathway effects in hepatocytes subjected to I/R. Prior work establishes its genomic context (ITPR1 intronic antisense), autophagy control via ITPR1, tumor-context roles, and antiviral induction. Our data add potential regulation of ferroptosis (xCT/antioxidant defense) and necroptosis (pMLKL). Future studies should integrate in vivo modulation of EGOT during hepatic ischemia–reperfusion with analyses of human liver specimens. Single-cell transcriptomic profiling could define cell-type–specific EGOT regulation and link inflammatory and calcium-associated signaling programs to ferroptotic and necroptotic gene signatures. Integration of differential expression with pathway enrichment analyses may further clarify how EGOT coordinates redox balance, lipid peroxidation, and cell death through its connections to xCT-dependent antioxidant defense and ITPR1-related calcium signaling.

4.4 NEAT1

LncRNA NEAT1 is a highly conserved intergenic lncRNA, which was first discovered in mammalian genome-wide screening[165]. Studies have shown that NEAT1 is associated with the

development of a variety of human diseases, including non-cancerous lesions such as sepsis and neurodegenerative lesions, as well as a variety of cancers such as hepatocellular carcinoma[168,178,199–202]. NEAT1 often shows abnormal expression during inflammation. It is important in controlling gene activity at both the epigenetic and transcriptional levels[166]. Various aspects of hepatic cancers, including cell proliferation, migration, angiogenesis, apoptosis, and EMT, have been associated with the heightened expression of NEAT1[180,183,201]. Research indicates that NEAT1 participates in the ferroptosis pathway via SLC7A11[181]. Further studies are required to clarify the mechanism through which NEAT1 functions via the ferroptosis pathway in HIRI.

In our models, NEAT1 decreased under hypoxia and remained low during reoxygenation. NEAT1 overexpression increased xCT but reduced GPX4 and FSP1, and it enhanced erastin sensitivity. These data indicate a role for NEAT1 in redox control and ferroptosis susceptibility during ischemia/reperfusion, with possible effects on apoptosis and other death programs.

Tumor hypoxia induces NEAT1 via HIF-2α, which promotes paraspeckle formation and survival under low oxygen[169]. Reviews of hypoxic control of the noncoding genome confirm HIF-2-dependent NEAT1 induction and link it to stress adaptation. Our hepatocyte data differ, showing NEAT1 reduction during hypoxia and reoxygenation. Isoform-specific regulation and tissue context may explain this discrepancy; NEAT1_2 is the principal paraspeckle scaffold, and its dynamics can diverge from NEAT1_1

across cell types and stimuli[177,231]. In fulminant hepatic failure, NEAT1 is upregulated; it recruits EZH2 to silence LATS2 and increases hepatocyte apoptosis, indicating a pathogenic role in acute liver injury[196]. In a cellular hepatic ischemia/reperfusion model, NEAT1 is overexpressed and promotes apoptosis and inflammatory signaling, reducing proliferation[180]. These studies support the concept that NEAT1 contributes to injury in stressed liver, though the direction of change may vary with insult and model. Ferroptosis is an iron-dependent form of cell death driven by lipid peroxidation. Erastin initiates ferroptosis by blocking system Xc^- and depleting glutathione[84,232]. FSP1 suppresses ferroptosis by regenerating coenzyme Q10 and acts in parallel to GPX4[233]. Two lines of evidence connect NEAT1 to ferroptosis. In hepatocellular carcinoma, NEAT1 promotes ferroptosis through a miR-362-3p/MIOX axis, where it sponges miR-362-3p, derepresses MIOX, elevates ROS, and enhances erastin/RSL3 killing in vitro and in vivo[204]. In non-small cell lung cancer, NEAT1 modulates ferroptosis sensitivity via ACSL4. NEAT1 silencing combined with erastin reduces ACSL4, SLC7A11, and GPX4 more than erastin alone, increasing lipid peroxidation; conversely, NEAT1 overexpression blunts this effect[208]. These findings show that NEAT1 can either promote or protect against ferroptosis depending on cell type and the pathway node engaged.

The combination of SLC7A11 upregulation with GPX4 and FSP1 downregulation that we observed suggests an overall shift toward ferroptosis in hepatocytes. While increased SLC7A11 would

normally support glutathione synthesis and suppress ferroptosis[234], GPX4 is a selenoprotein whose synthesis requires SECIS-dependent incorporation of selenocysteine and is vulnerable to translational bottlenecks under stress[235,236]. Thus, SLC7A11 and GPX4 expression can be uncoupled during oxidative stress. At the same time, loss of FSP1, which regenerates coenzyme Q10 to trap lipid radicals independently of GPX4, removes an additional protective barrier[233]. LncRNA-mediated regulation of FSP1 has been demonstrated for LINC01133, which stabilizes AIFM2/FSP1 mRNA via FUS binding[233], providing a precedent that NEAT1 might also affect FSP1 expression or stability. Although these mechanisms remain hypotheses in hepatocytes, they offer plausible explanations for the marker profile we observed. The net effect of these changes was increased erastin sensitivity, consistent with reports that NEAT1 can promote ferroptosis in liver cancer cells[204]. However, contrasting findings also exist in infection-induced injury, NEAT1 knockdown activated the NRF2–GPX4 pathway and suppressed ferroptosis[233]. Such discrepancies emphasize the strong context-dependence of NEAT1 function, likely influenced by isoform usage, chromatin interactions, and the specific miRNA networks engaged. From a translational perspective, ferroptosis is recognized as a contributor to HIRI and a potential therapeutic target[237,238]. Our findings suggest that NEAT1 may shape hepatocyte susceptibility to ferroptotic injury by tilting the balance between upstream cystine transport and downstream lipid peroxide defenses.

Profiling NEAT1 expression together with ferroptosis markers such as GPX4, SLC7A11, and FSP1 may help predict graft vulnerability during liver transplantation and guide the development of lncRNA-based interventions. Further studies should delineate NEAT1 isoform-specific dynamics (NEAT1_1 and NEAT1_2) under hypoxia–reoxygenation and define how paraspeckle-dependent nuclear programs regulate stress-responsive transcription in hepatocytes. This could be achieved using hepatocyte-specific NEAT1 gain- and loss-of-function mouse models, complemented by analyses of human liver ischemia–reperfusion specimens. Coupling these models with cell-type–resolved transcriptomic profiling would help clarify how NEAT1 controls ferroptosis-related pathways, including SLC7A11-mediated cystine transport and GPX4/FSP1-dependent lipid peroxide detoxification, as well as its interaction with inflammatory signaling and downstream cell death programs during hepatic ischemia–reperfusion injury.

Taken together, our analysis supports a model in which hypoxia-responsive lncRNAs shape hepatocyte vulnerability to hepatic ischemia–reperfusion injury through distinct points of entry into regulated cell death pathways. UCA1 behaved predominantly as a rapid hypoxia-inducible transcript with limited direct impact on canonical ferroptosis, apoptosis, or necroptosis markers under the conditions tested, consistent with a role in stress adaptation or context-specific modulation. In contrast, H19 and EGOT showed

clearer coupling to cell-death–associated programs across the hypoxia–reoxygenation transition, reflecting their multi-pathway influence on antioxidant defense and necroptotic signaling nodes. NEAT1 emerged as the strongest modulator of ferroptosis-linked susceptibility in our system, reshaping the balance between upstream cystine transport and downstream lipid peroxide detoxification and thereby amplifying sensitivity to ferroptotic challenge, particularly under lipid-loaded conditions that emulate marginal donor livers. Collectively, these findings reinforce the concept that hepatic ischemia–reperfusion injury is governed by coordinated and time-dependent engagement of multiple regulated death programs, and suggest that coordinated assessment of hypoxia-responsive lncRNAs together with regulated cell death markers in liver graft biopsies may provide a molecular framework to stratify injury severity and identify grafts at heightened risk during transplantation.

5. References

1. Devarbhavi H, Asrani SK, Arab JP, Nartey YA, Pose E, Kamath PS. Global burden of liver disease: 2023 update. *J Hepatol*. 2023;79(2):516-537. doi:10.1016/j.jhep.2023.03.017

2. Jennings RB, Sommers HM, Smyth GA, Flack HA, Linn H. Myocardial necrosis induced by temporary occlusion of a coronary artery in the dog. *Arch Pathol*. 1960;70:68-78.

3. Toledo-Pereyra LH, Simmons RL, Najarian JS. Protection of the ischemic liver by donor pretreatment before transplantation. *Am J Surg*. 1975;129(5):513-517. doi:10.1016/0002-9610(75)90308-6

4. Ames A, Wright RL, Kowada M, Thurston JM, Majno G. Cerebral ischemia. II. The no-reflow phenomenon. *Am J Pathol*. 1968;52(2):437-453.

5. Flores J, DiBona DR, Beck CH, Leaf A. The role of cell swelling in ischemic renal damage and the protective effect of hypertonic solute. *J Clin Invest*. 1972;51(1):118-126. doi:10.1172/JCI106781

6. Caldwell-Kenkel JC, Currin RT, Tanaka Y, Thurman RG, Lemasters JJ. Reperfusion injury to endothelial cells following cold ischemic storage of rat livers. *Hepatol Baltim Md*. 1989;10(3):292-299. doi:10.1002/hep.1840100307

7. Lambotte L, d'Udekem Y, Amrani M, Taper H. Free radicals and liver ischemia-reperfusion injury. *Transplant Proc*. 1988;20(5):977.

8. Jaeschke H. Mechanisms of reperfusion injury after warm ischemia of the liver. *J Hepatobiliary Pancreat Surg*. 1998;5(4):402-408. doi:10.1007/s005340050064

9. Teoh NC, Farrell GC. Hepatic ischemia reperfusion injury: pathogenic mechanisms and basis for hepatoprotection. *J*

Gastroenterol Hepatol. 2003;18(8):891-902. doi:10.1046/j.1440-1746.2003.03056.x

10. Li J, Li RJ, Lv GY, Liu HQ. The mechanisms and strategies to protect from hepatic ischemia-reperfusion injury. *Eur Rev Med Pharmacol Sci*. 2015;19(11). Accessed March 25, 2024. http://www.europeanreview.org/wp/wp-content/uploads/2036-2047.pdf

11. Hirao H, Nakamura K, Kupiec-Weglinski JW. Liver ischaemia-reperfusion injury: a new understanding of the role of innate immunity. *Nat Rev Gastroenterol Hepatol*. 2022;19(4):239-256. doi:10.1038/s41575-021-00549-8

12. Peng Y, Yin Q, Yuan M, et al. Role of hepatic stellate cells in liver ischemia-reperfusion injury. *Front Immunol*. 2022;13:891868. doi:10.3389/fimmu.2022.891868

13. Montalvo-Jave EE, Escalante-Tattersfield T, Ortega-Salgado JA, Piña E, Geller DA. Factors in the pathophysiology of the liver ischemia-reperfusion injury. *J Surg Res*. 2008;147(1):153-159. doi:10.1016/j.jss.2007.06.015

14. Peralta C, Bartrons R, Riera L, et al. Hepatic preconditioning preserves energy metabolism during sustained ischemia. *Am J Physiol Gastrointest Liver Physiol*. 2000;279(1):G163-171. doi:10.1152/ajpgi.2000.279.1.G163

15. Lentsch AB, Kato A, Yoshidome H, McMasters KM, Edwards MJ. Inflammatory mechanisms and therapeutic strategies for warm hepatic ischemia/reperfusion injury. *Hepatology*. 2000;32(2):169-173. doi:10.1053/jhep.2000.9323

16. Caraceni P, Domenicali M, Vendemiale G, et al. The reduced tolerance of rat fatty liver to ischemia reperfusion is associated with mitochondrial oxidative injury. *J Surg Res*. 2005;124(2):160-168. doi:10.1016/j.jss.2004.10.007

17. Kim JS, Wang JH, Lemasters JJ. Mitochondrial permeability transition in rat hepatocytes after anoxia/reoxygenation: role of Ca2+-dependent mitochondrial formation of reactive oxygen species. *Am J Physiol - Gastrointest Liver Physiol*. 2012;302(7):G723. doi:10.1152/ajpgi.00082.2011

18. Xu L, Ge F, Hu Y, Yu Y, Guo K, Miao C. Sevoflurane Postconditioning Attenuates Hepatic Ischemia-Reperfusion Injury by Limiting HMGB1/TLR4/NF-κB Pathway via Modulating microRNA-142 in vivo and in vitro. *Front Pharmacol*. 2021;12:646307. doi:10.3389/fphar.2021.646307

19. Colletti LM, Remick DG, Burtch GD, Kunkel SL, Strieter RM, Campbell DA. Role of tumor necrosis factor-alpha in the pathophysiologic alterations after hepatic ischemia/reperfusion injury in the rat. *J Clin Invest*. 1990;85(6):1936-1943. doi:10.1172/JCI114656

20. Wanner GA, Ertel W, Müller P, et al. Liver ischemia and reperfusion induces a systemic inflammatory response through Kupffer cell activation. *Shock Augusta Ga*. 1996;5(1):34-40. doi:10.1097/00024382-199601000-00008

21. Shan Z, Ju C. Hepatic Macrophages in Liver Injury. *Front Immunol*. 2020;11:322. doi:10.3389/fimmu.2020.00322

22. Hasegawa T, Malle E, Farhood A, Jaeschke H. Generation of hypochlorite-modified proteins by neutrophils during ischemia-reperfusion injury in rat liver: attenuation by ischemic preconditioning. *Am J Physiol Gastrointest Liver Physiol*. 2005;289(4):G760-767. doi:10.1152/ajpgi.00141.2005

23. Bamboat ZM, Balachandran VP, Ocuin LM, Obaid H, Plitas G, DeMatteo RP. Toll-like receptor 9 inhibition confers protection from liver ischemia-reperfusion injury. *Hepatol Baltim Md*. 2010;51(2):621-632. doi:10.1002/hep.23365

24. Tsung A, Klune JR, Zhang X, et al. HMGB1 release induced

by liver ischemia involves Toll-like receptor 4–dependent reactive oxygen species production and calcium-mediated signaling. *J Exp Med*. 2007;204(12):2913. doi:10.1084/jem.20070247

25. Brenner C, Galluzzi L, Kepp O, Kroemer G. Decoding cell death signals in liver inflammation. *J Hepatol*. 2013;59(3):583-594. doi:10.1016/j.jhep.2013.03.033

26. Zwacka RM, Zhang Y, Halldorson J, Schlossberg H, Dudus L, Engelhardt JF. CD4(+) T-lymphocytes mediate ischemia/reperfusion-induced inflammatory responses in mouse liver. *J Clin Invest*. 1997;100(2):279-289. doi:10.1172/JCI119533

27. Casillas-Ramírez A, Mosbah IB, Ramalho F, Roselló-Catafau J, Peralta C. Past and future approaches to ischemia-reperfusion lesion associated with liver transplantation. *Life Sci*. 2006;79(20):1881-1894. doi:10.1016/j.lfs.2006.06.024

28. M EM, Mb JC, J R, C P. Current knowledge on oxidative stress in hepatic ischemia/reperfusion. *Free Radic Res*. 2013;47(8). doi:10.3109/10715762.2013.811721

29. Caldwell CC, Tschoep J, Lentsch AB. Lymphocyte function during hepatic ischemia/reperfusion injury. *J Leucoc Biol*. 2007;82(3):457-464.

30. Peralta C, Jiménez-Castro MB, Gracia-Sancho J. Hepatic ischemia and reperfusion injury: effects on the liver sinusoidal milieu. *J Hepatol*. 2013;59(5):1094-1106. doi:10.1016/j.jhep.2013.06.017

31. Kaltenmeier C, Yazdani HO, Handu S, Popp B, Geller D, Tohme S. The Role of Neutrophils as a Driver in Hepatic Ischemia-Reperfusion Injury and Cancer Growth. *Front Immunol*. 2022;13:887565. doi:10.3389/fimmu.2022.887565

32. Peralta C, Fernández L, Panés J, et al. Preconditioning protects against systemic disorders associated with hepatic ischemia-reperfusion through blockade of tumor necrosis factor-induced P-selectin up-regulation in the rat. *Hepatol Baltim Md*. 2001;33(1):100-113. doi:10.1053/jhep.2001.20529

33. Lesurtel M, Graf R, Aleil B, et al. Platelet-derived serotonin mediates liver regeneration. *Science*. 2006;312(5770):104-107. doi:10.1126/science.1123842

34. Tamura T, Kondo T, Pak S, et al. Interaction between Kupffer cells and platelets in the early period of hepatic ischemia-reperfusion injury--an in vivo study. *J Surg Res*. 2012;178(1):443-451. doi:10.1016/j.jss.2011.12.010

35. McConnell MJ, Kostallari E, Ibrahim SH, Iwakiri Y. The evolving role of liver sinusoidal endothelial cells in liver health and disease. *Hepatol Baltim Md*. 2023;78(2):649-669. doi:10.1097/HEP.0000000000000207

36. Puche JE, Saiman Y, Friedman SL. Hepatic stellate cells and liver fibrosis. *Compr Physiol*. 2013;3(4):1473-1492. doi:10.1002/cphy.c120035

37. Khandoga A, Hanschen M, Kessler JS, Krombach F. CD4+ T cells contribute to postischemic liver injury in mice by interacting with sinusoidal endothelium and platelets. *Hepatol Baltim Md*. 2006;43(2):306-315. doi:10.1002/hep.21017

38. Tang SP, Mao XL, Chen YH, Yan LL, Ye LP, Li SW. Reactive Oxygen Species Induce Fatty Liver and Ischemia-Reperfusion Injury by Promoting Inflammation and Cell Death. *Front Immunol*. 2022;13:870239. doi:10.3389/fimmu.2022.870239

39. Bogdanos DP, Gao B, Gershwin ME. Liver Immunology. *Compr Physiol*. 2013;3(2):567-598. doi:10.1002/cphy.c120011

40. Weibel ER, Stäubli W, Gnägi HR, Hess FA. Correlated

morphometric and biochemical studies on the liver cell. I. Morphometric model, stereologic methods, and normal morphometric data for rat liver. *J Cell Biol*. 1969;42(1):68-91. doi:10.1083/jcb.42.1.68

41. Gujral JS, Bucci TJ, Farhood A, Jaeschke H. Mechanism of cell death during warm hepatic ischemia-reperfusion in rats: apoptosis or necrosis? *Hepatol Baltim Md*. 2001;33(2):397-405. doi:10.1053/jhep.2001.22002

42. Galluzzi L, Vitale I, Aaronson SA, et al. Molecular mechanisms of cell death: recommendations of the Nomenclature Committee on Cell Death 2018. *Cell Death Differ*. 2018;25(3):486-541. doi:10.1038/s41418-017-0012-4

43. Festjens N, Vanden Berghe T, Vandenabeele P. Necrosis, a well-orchestrated form of cell demise: Signalling cascades, important mediators and concomitant immune response. *Biochim Biophys Acta BBA - Bioenerg*. 2006;1757(9):1371-1387. doi:10.1016/j.bbabio.2006.06.014

44. Shojaie L, Iorga A, Dara L. Cell Death in Liver Diseases: A Review. *Int J Mol Sci*. 2020;21(24):9682. doi:10.3390/ijms21249682

45. Zheng Y, Xu X, Chi F, Cong N. Pyroptosis: A Newly Discovered Therapeutic Target for Ischemia-Reperfusion Injury. *Biomolecules*. 2022;12(11):1625. doi:10.3390/biom12111625

46. Cao JY, Dixon SJ. Mechanisms of ferroptosis. *Cell Mol Life Sci*. 2016;73(11):2195-2209. doi:10.1007/s00018-016-2194-1

47. Mao B, Yuan W, Wu F, Yan Y, Wang B. Autophagy in hepatic ischemia-reperfusion injury. *Cell Death Discov*. 2023;9(1):115. doi:10.1038/s41420-023-01387-0

48. de Bont CM, Boelens WC, Pruijn GJM. NETosis, complement, and coagulation: a triangular relationship. *Cell Mol Immunol*.

2019;16(1):19-27. doi:10.1038/s41423-018-0024-0

49. Goswami J, Waring H, Tsung A, Huang H. Cell Death in Ischemia-Reperfusion-Induced Liver Injury. In: Ding WX, Yin XM, eds. *Cellular Injury in Liver Diseases*. ~181. Springer International Publishing; 2017:173-193. doi:10.1007/978-3-319-53774-0_8

50. Nishimura Y, Lemasters JJ. Glycine blocks opening of a death channel in cultured hepatic sinusoidal endothelial cells during chemical hypoxia. *Cell Death Differ*. 2001;8(8):850-858. doi:10.1038/sj.cdd.4400877

51. Zhang H, Yan Q, Wang X, et al. The Role of Mitochondria in Liver Ischemia-Reperfusion Injury: From Aspects of Mitochondrial Oxidative Stress, Mitochondrial Fission, Mitochondrial Membrane Permeable Transport Pore Formation, Mitophagy, and Mitochondria-Related Protective Measures. *Oxid Med Cell Longev*. 2021;2021(1):6670579. doi:10.1155/2021/6670579

52. Scaffidi P, Misteli T, Bianchi ME. Release of chromatin protein HMGB1 by necrotic cells triggers inflammation. *Nature*. 2002;418(6894):191-195. doi:10.1038/nature00858

53. Schwabe RF, Luedde T. Apoptosis and necroptosis in the liver: a matter of life and death. *Nat Rev Gastroenterol Hepatol*. 2018;15(12):738-752. doi:10.1038/s41575-018-0065-y

54. Eguchi A, Wree A, Feldstein AE. Biomarkers of liver cell death. *J Hepatol*. 2014;60(5):1063-1074. doi:10.1016/j.jhep.2013.12.026

55. Tang SP, Mao XL, Chen YH, Yan LL, Ye LP, Li SW. Reactive Oxygen Species Induce Fatty Liver and Ischemia-Reperfusion Injury by Promoting Inflammation and Cell Death. *Front Immunol*. 2022;13:870239. doi:10.3389/fimmu.2022.870239

56. Jaeschke H, Lemasters JJ. Apoptosis versus oncotic necrosis in hepatic ischemia/reperfusion injury. *Gastroenterology*. 2003;125(4):1246-1257. doi:10.1016/S0016-5085(03)01209-5

57. Schulze-Bergkamen H, Schuchmann M, Fleischer B, Galle PR. The role of apoptosis versus oncotic necrosis in liver injury: Facts or faith? *J Hepatol*. 2006;44(5):984-993. doi:10.1016/j.jhep.2006.02.004

58. Gong XY, Zhang Y. Protective effect of miR-20a against hypoxia/reoxygenation treatment on cardiomyocytes cell viability and cell apoptosis by targeting TLR4 and inhibiting p38 MAPK/JNK signaling. *Vitro Cell Dev Biol - Anim*. 2019;55(10):793-800. doi:10.1007/s11626-019-00399-4

59. Gautheron J, Gores GJ, Rodrigues CMP. Lytic cell death in metabolic liver disease. *J Hepatol*. 2020;73(2):394-408. doi:10.1016/j.jhep.2020.04.001

60. Dugbartey GJ. Cellular and molecular mechanisms of cell damage and cell death in ischemia-reperfusion injury in organ transplantation. *Mol Biol Rep*. 2024;51(1):473. doi:10.1007/s11033-024-09261-7

61. Zhou Z, Chen Q, Wan L, Zheng D, Li Z, Wu Z. Dexmedetomidine protects hepatic cells against oxygen-glucose deprivation/reperfusion injury via lncRNA CCAT1. *Cell Biol Int*. 2018;42(9):1250-1258. doi:10.1002/cbin.10996

62. Zhang Y, Zhang H, Zhang Z, et al. LncRNA MALAT1 cessation antagonizes hypoxia/reoxygenation injury in hepatocytes by inhibiting apoptosis and inflammation via the HMGB1-TLR4 axis. *Mol Immunol*. 2019;112:22-29. doi:10.1016/j.molimm.2019.04.015

63. Li X, Yi S, Deng Y, et al. MiR-124 protects human hepatic L02 cells from H2O2-induced apoptosis by targeting Rab38 gene. *Biochem Biophys Res Commun*. 2014;450(1):148-153.

doi:10.1016/j.bbrc.2014.05.085

64. Li H, Lin W, Zhang G, et al. BMSC-exosomes miR-25-3p Regulates the p53 Signaling Pathway Through PTEN to Inhibit Cell Apoptosis and Ameliorate Liver Ischemia–reperfusion Injury. *Stem Cell Rev Rep*. 2023;19(8):2820-2836. doi:10.1007/s12015-023-10599-x

65. George J, Lu Y, Tsuchishima M, Tsutsumi M. Cellular and molecular mechanisms of hepatic ischemia-reperfusion injury: The role of oxidative stress and therapeutic approaches. *Redox Biol*. 2024;75:103258. doi:10.1016/j.redox.2024.103258

66. Degterev A, Huang Z, Boyce M, et al. Chemical inhibitor of nonapoptotic cell death with therapeutic potential for ischemic brain injury. *Nat Chem Biol*. 2005;1(2):112-119. doi:10.1038/nchembio711

67. Linkermann A, Green DR. Necroptosis. *N Engl J Med*. 2014;370(5):455-465. doi:10.1056/NEJMra1310050

68. Grootjans S, Vanden Berghe T, Vandenabeele P. Initiation and execution mechanisms of necroptosis: an overview. *Cell Death Differ*. 2017;24(7):1184-1195. doi:10.1038/cdd.2017.65

69. Zhuang C, Chen F. Small-Molecule Inhibitors of Necroptosis: Current Status and Perspectives. *J Med Chem*. 2020;63(4):1490-1510. doi:10.1021/acs.jmedchem.9b01317

70. Han W, Li L, Qiu S, et al. Shikonin circumvents cancer drug resistance by induction of a necroptotic death. *Mol Cancer Ther*. 2007;6(5):1641-1649. doi:10.1158/1535-7163.MCT-06-0511

71. Wu X, Zhao X, Li F, et al. MLKL-mediated endothelial necroptosis drives vascular damage and mortality in systemic inflammatory response syndrome. *Cell Mol Immunol*. 2024;21(11):1309-1321. doi:10.1038/s41423-024-01217-y

72. Wang Q, Yang F, Duo K, et al. The Role of Necroptosis in

Cerebral Ischemic Stroke. *Mol Neurobiol*. 2024;61(7):3882-3898. doi:10.1007/s12035-023-03728-7

73. Adameova A, Horvath C, Abdul-Ghani S, Varga ZV, Suleiman MS, Dhalla NS. Interplay of Oxidative Stress and Necrosis-like Cell Death in Cardiac Ischemia/Reperfusion Injury: A Focus on Necroptosis. *Biomedicines*. 2022;10(1):127. doi:10.3390/biomedicines10010127

74. Jun W, Benjanuwattra J, Chattipakorn SC, Chattipakorn N. Necroptosis in renal ischemia/reperfusion injury: A major mode of cell death? *Arch Biochem Biophys*. 2020;689:108433. doi:10.1016/j.abb.2020.108433

75. Huang Z, Mou T, Luo Y, et al. Inhibition of miR-450b-5p ameliorates hepatic ischemia/reperfusion injury via targeting CRYAB. *Cell Death Dis*. 2020;11(6):1-14. doi:10.1038/s41419-020-2648-0

76. Hong JM, Kim SJ, Lee SM. Role of necroptosis in autophagy signaling during hepatic ischemia and reperfusion. *Toxicol Appl Pharmacol*. 2016;308:1-10. doi:10.1016/j.taap.2016.08.010

77. Ni HM, Chao X, Kaseff J, et al. Receptor-Interacting Serine/Threonine-Protein Kinase 3 (RIPK3)–Mixed Lineage Kinase Domain-Like Protein (MLKL)–Mediated Necroptosis Contributes to Ischemia-Reperfusion Injury of Steatotic Livers. *Am J Pathol*. 2019;189(7):1363-1374. doi:10.1016/j.ajpath.2019.03.010

78. Baidya R, Crawford DHG, Gautheron J, Wang H, Bridle KR. Necroptosis in Hepatosteatotic Ischaemia-Reperfusion Injury. *Int J Mol Sci*. 2020;21(16):5931. doi:10.3390/ijms21165931

79. Conrad M, Angeli JPF, Vandenabeele P, Stockwell BR. Regulated necrosis: disease relevance and therapeutic opportunities. *Nat Rev Drug Discov*. 2016;15(5):348-366. doi:10.1038/nrd.2015.6

80. Yang F, Shang L, Wang S, et al. TNFα-Mediated Necroptosis Aggravates Ischemia-Reperfusion Injury in the Fatty Liver by Regulating the Inflammatory Response. *Oxid Med Cell Longev*. 2019;2019:2301903. doi:10.1155/2019/2301903

81. Khan MR, Wu M, Liu G. Tumor-suppressive or tumor-supportive: For p53, that is the question. *Mol Cell Oncol*. 2018;5(3):e1408537. doi:10.1080/23723556.2017.1408537

82. Wang K, Liu F, Liu CY, et al. The long noncoding RNA NRF regulates programmed necrosis and myocardial injury during ischemia and reperfusion by targeting miR-873. *Cell Death Differ*. 2016;23(8):1394. doi:10.1038/cdd.2016.28

83. Zuo H, Wang Y, Yuan M, et al. Small extracellular vesicles from HO-1-modified bone marrow-derived mesenchymal stem cells attenuate ischemia-reperfusion injury after steatotic liver transplantation by suppressing ferroptosis via miR-214-3p. *Cell Signal*. 2023;109:110793. doi:10.1016/j.cellsig.2023.110793

84. Dixon SJ, Lemberg KM, Lamprecht MR, et al. Ferroptosis: an iron-dependent form of nonapoptotic cell death. *Cell*. 2012;149(5):1060-1072. doi:10.1016/j.cell.2012.03.042

85. Li J, Cao F, Yin HL, et al. Ferroptosis: past, present and future. *Cell Death Dis*. 2020;11(2):88. doi:10.1038/s41419-020-2298-2

86. Feng H, Stockwell BR. Unsolved mysteries: How does lipid peroxidation cause ferroptosis? *PLoS Biol*. 2018;16(5):e2006203. doi:10.1371/journal.pbio.2006203

87. Linkermann A, Stockwell BR, Krautwald S, Anders HJ. Regulated cell death and inflammation: an auto-amplification loop causes organ failure. *Nat Rev Immunol*. 2014;14(11):759-767. doi:10.1038/nri3743

88. Stockwell BR. Ferroptosis turns 10: Emerging mechanisms,

physiological functions, and therapeutic applications. *Cell*. 2022;185(14):2401-2421. doi:10.1016/j.cell.2022.06.003

89. Friedmann Angeli JP, Schneider M, Proneth B, et al. Inactivation of the ferroptosis regulator Gpx4 triggers acute renal failure in mice. *Nat Cell Biol*. 2014;16(12):1180-1191. doi:10.1038/ncb3064

90. Kagan VE, Mao G, Qu F, et al. Oxidized arachidonic and adrenic PEs navigate cells to ferroptosis. *Nat Chem Biol*. 2017;13(1):81-90. doi:10.1038/nchembio.2238

91. Zilka O, Shah R, Li B, et al. On the Mechanism of Cytoprotection by Ferrostatin-1 and Liproxstatin-1 and the Role of Lipid Peroxidation in Ferroptotic Cell Death. *ACS Cent Sci*. 2017;3(3):232-243. doi:10.1021/acscentsci.7b00028

92. Xu Y, Li Y, Li J, Chen W. Ethyl carbamate triggers ferroptosis in liver through inhibiting GSH synthesis and suppressing Nrf2 activation. *Redox Biol*. 2022;53:102349. doi:10.1016/j.redox.2022.102349

93. Wu L, Tian X, Zuo H, et al. miR-124-3p delivered by exosomes from heme oxygenase-1 modified bone marrow mesenchymal stem cells inhibits ferroptosis to attenuate ischemia-reperfusion injury in steatotic grafts. *J Nanobiotechnology*. 2022;20(1):196. doi:10.1186/s12951-022-01407-8

94. Li X, Wu L, Tian X, et al. miR-29a-3p in Exosomes from Heme Oxygenase-1 Modified Bone Marrow Mesenchymal Stem Cells Alleviates Steatotic Liver Ischemia-Reperfusion Injury in Rats by Suppressing Ferroptosis via Iron Responsive Element Binding Protein 2. *Oxid Med Cell Longev*. 2022;2022:6520789. doi:10.1155/2022/6520789

95. Derrien T, Johnson R, Bussotti G, et al. The GENCODE v7 catalog of human long noncoding RNAs: analysis of their gene

structure, evolution, and expression. *Genome Res*. 2012;22(9):1775-1789. doi:10.1101/gr.132159.111

96. Djebali S, Davis CA, Merkel A, et al. Landscape of transcription in human cells. *Nature*. 2012;489(7414):101-108. doi:10.1038/nature11233

97. Amaral P, Carbonell-Sala S, De La Vega FM, et al. The status of the human gene catalogue. *Nature*. 2023;622(7981):41-47. doi:10.1038/s41586-023-06490-x

98. Cesana M, Cacchiarelli D, Legnini I, et al. A Long Noncoding RNA Controls Muscle Differentiation by Functioning as a Competing Endogenous RNA. *Cell*. 2011;147(2):358-369. doi:10.1016/j.cell.2011.09.028

99. Jeck WR, Sharpless NE. Detecting and characterizing circular RNAs. *Nat Biotechnol*. 2014;32(5):453-461. doi:10.1038/nbt.2890

100. Meng S, Zhou H, Feng Z, et al. CircRNA: functions and properties of a novel potential biomarker for cancer. *Mol Cancer*. 2017;16:94. doi:10.1186/s12943-017-0663-2

101. Ferrer J, Dimitrova N. Transcription regulation by long non-coding RNAs: mechanisms and disease relevance. *Nat Rev Mol Cell Biol*. 2024;25(5):396-415. doi:10.1038/s41580-023-00694-9

102. Deveson IW, Hardwick SA, Mercer TR, Mattick JS. The Dimensions, Dynamics, and Relevance of the Mammalian Noncoding Transcriptome. *Trends Genet TIG*. 2017;33(7):464-478. doi:10.1016/j.tig.2017.04.004

103. Marchese FP, Raimondi I, Huarte M. The multidimensional mechanisms of long noncoding RNA function. *Genome Biol*. 2017;18(1):206. doi:10.1186/s13059-017-1348-2

104. Statello L, Guo CJ, Chen LL, Huarte M. Gene regulation

by long non-coding RNAs and its biological functions. *Nat Rev Mol Cell Biol*. 2021;22(2):96-118. doi:10.1038/s41580-020-00315-9

105. Gao N, Li Y, Li J, et al. Long Non-Coding RNAs: The Regulatory Mechanisms, Research Strategies, and Future Directions in Cancers. *Front Oncol*. 2020;10. doi:10.3389/fonc.2020.598817

106. Mably JD, Wang DZ. Long non-coding RNAs in cardiac hypertrophy and heart failure: functions, mechanisms and clinical prospects. *Nat Rev Cardiol*. 2024;21(5):326-345. doi:10.1038/s41569-023-00952-5

107. Nemeth K, Bayraktar R, Ferracin M, Calin GA. Non-coding RNAs in disease: from mechanisms to therapeutics. *Nat Rev Genet*. 2024;25(3):211-232. doi:10.1038/s41576-023-00662-1

108. Mattick JS, Amaral PP, Carninci P, et al. Long non-coding RNAs: definitions, functions, challenges and recommendations. *Nat Rev Mol Cell Biol*. 2023;24(6):430-447. doi:10.1038/s41580-022-00566-8

109. Wang XS, Zhang Z, Wang HC, et al. Rapid identification of UCA1 as a very sensitive and specific unique marker for human bladder carcinoma. *Clin Cancer Res Off J Am Assoc Cancer Res*. 2006;12(16):4851-4858. doi:10.1158/1078-0432.CCR-06-0134

110. Xue M, Chen W, Li X. Urothelial cancer associated 1: a long noncoding RNA with a crucial role in cancer. *J Cancer Res Clin Oncol*. 2016;142(7):1407-1419. doi:10.1007/s00432-015-2042-y

111. Liang X, Qi M, Wu R, et al. Long non-coding RNA CUDR promotes malignant phenotypes in pancreatic ductal adenocarcinoma via activating AKT and ERK signaling

pathways. *Int J Oncol*. 2018;53(6):2671-2682. doi:10.3892/ijo.2018.4574

112. Neve B, Jonckheere N, Vincent A, Van Seuningen I. Epigenetic Regulation by lncRNAs: An Overview Focused on UCA1 in Colorectal Cancer. *Cancers*. 2018;10(11):440. doi:10.3390/cancers10110440

113. Huang J, Zhou N, Watabe K, et al. Long non-coding RNA UCA1 promotes breast tumor growth by suppression of p27 (Kip1). *Cell Death Dis*. 2014;5(1):e1008. doi:10.1038/cddis.2013.541

114. Jiang CR, Li TH. Circulating UCA1 is highly expressed in patients with systemic lupus erythematosus and promotes the progression through the AKT pathway. *Eur Rev Med Pharmacol Sci*. 2018;22(8):2364-2371. doi:10.26355/eurrev_201804_14828

115. Liu Z, Wang Y, Yuan S, et al. Regulatory role of long non-coding RNA UCA1 in signaling pathways and its clinical applications. *Oncol Lett*. 2021;21(5):404. doi:10.3892/ol.2021.12665

116. L C, L T, T L, et al. Downregulation of lncRNA UCA1 ameliorates the damage of dopaminergic neurons, reduces oxidative stress and inflammation in Parkinson's disease through the inhibition of the PI3K/Akt signaling pathway. *Int Immunopharmacol*. 2019;75. doi:10.1016/j.intimp.2019.105734

117. Z Z, H L, Z C, et al. Long non-coding RNA UCA1 relieves cardiomyocytes H9c2 injury aroused by oxygen-glucose deprivation via declining miR-122. *Artif Cells Nanomedicine Biotechnol*. 2019;47(1). doi:10.1080/21691401.2019.1652630

118. Gao M, Li C, Xu M, Liu Y, Liu S. LncRNA UCA1 attenuates autophagy-dependent cell death through blocking autophagic flux under arsenic stress. *Toxicol Lett*. 2018;284:195-204.

doi:10.1016/j.toxlet.2017.12.009

119. Wu W, Zhang S, Li X, Xue M, Cao S, Chen W. Ets-2 regulates cell apoptosis via the Akt pathway, through the regulation of urothelial cancer associated 1, a long non-coding RNA, in bladder cancer cells. *PloS One*. 2013;8(9):e73920. doi:10.1371/journal.pone.0073920

120. Chen Z, Liu R, Niu Q, Wang H, Yang Z, Bao Y. Morphine Postconditioning alleviates autophage in ischemia-reperfusion induced cardiac injury through up-regulating lncRNA UCA1. *Biomed Pharmacother*. 2018;108:1357-1364. doi:10.1016/j.biopha.2018.09.119

121. Chen J, Hu Q, Zhang B fang, Liu X pei, Yang S, Jiang H. Long noncoding RNA UCA1 inhibits ischaemia/reperfusion injury induced cardiomyocytes apoptosis via suppression of endoplasmic reticulum stress. *Genes Genomics*. 2019;41(7):803-810. doi:10.1007/s13258-019-00806-w

122. Yan J, Gao Y, Huang J, Gao W, Li Y, Lin B. Loss of lncRNA UCA1 ameliorates the injury managed by cerebral ischemia-reperfusion by sponging miR-18a-5p. *Folia Neuropathol*. 2023;61(1):77-87. doi:10.5114/fn.2022.122497

123. Qs W, J Z, X L. LncRNA UCA1 protects cardiomyocytes against hypoxia/reoxygenation induced apoptosis through inhibiting miR-143/MDM2/p53 axis. *Genomics*. 2020;112(1). doi:10.1016/j.ygeno.2019.04.009

124. Pachnis V, Belayew A, Tilghman SM. Locus unlinked to alpha-fetoprotein under the control of the murine raf and Rif genes. *Proc Natl Acad Sci*. 1984;81(17):5523-5527. doi:10.1073/pnas.81.17.5523

125. Brannan CI, Dees EC, Ingram RS, Tilghman SM. The product of the H19 gene may function as an RNA. *Mol Cell Biol*. 1990;10(1):28-36.

126. Rachmilewitz J, Goshen R, Ariel I, Schneider T, de Groot N, Hochberg A. Parental imprinting of the human H19 gene. *FEBS Lett*. 1992;309(1):25-28. doi:10.1016/0014-5793(92)80731-u

127. Raveh E, Matouk IJ, Gilon M, Hochberg A. The H19 Long non-coding RNA in cancer initiation, progression and metastasis – a proposed unifying theory. *Mol Cancer*. 2015;14(1):184. doi:10.1186/s12943-015-0458-2

128. Bartolomei MS, Zemel S, Tilghman SM. Parental imprinting of the mouse H19 gene. *Nature*. 1991;351(6322):153-155. doi:10.1038/351153a0

129. Matouk I, Raveh E, Ohana P, et al. The increasing complexity of the oncofetal h19 gene locus: functional dissection and therapeutic intervention. *Int J Mol Sci*. 2013;14(2):4298-4316. doi:10.3390/ijms14024298

130. Keniry A, Oxley D, Monnier P, et al. The H19 lincRNA is a developmental reservoir of miR-675 which suppresses growth and Igf1r. *Nat Cell Biol*. 2012;14(7):659-665. doi:10.1038/ncb2521

131. Drewell RA, Goddard CJ, Thomas JO, Surani MA. Methylation-dependent silencing at the H19 imprinting control region by MeCP2. *Nucleic Acids Res*. 2002;30(5):1139-1144. doi:10.1093/nar/30.5.1139

132. Dey BK, Pfeifer K, Dutta A. The H19 long noncoding RNA gives rise to microRNAs miR-675-3p and miR-675-5p to promote skeletal muscle differentiation and regeneration. *Genes Dev*. 2014;28(5):491-501. doi:10.1101/gad.234419.113

133. Yamamoto Y, Nishikawa Y, Tokairin T, Omori Y, Enomoto K. Increased expression of H19 non-coding mRNA follows hepatocyte proliferation in the rat and mouse. *J Hepatol*. 2004;40(5):808-814. doi:10.1016/j.jhep.2004.01.022

134. Ahmad I, Jasim SA, Sergeevna KN, et al. Emerging roles of long noncoding RNA H19 in human lung cancer. *Cell Biochem Funct*. 2024;42(4):e4072. doi:10.1002/cbf.4072

135. Li X, Liu R. Long non-coding RNA H19 in the liver-gut axis: A diagnostic marker and therapeutic target for liver diseases. *Exp Mol Pathol*. 2020;115:104472. doi:10.1016/j.yexmp.2020.104472

136. Darmadi D, Chugaeva UY, Saleh RO, et al. Critical roles of long noncoding RNA H19 in cancer. *Cell Biochem Funct*. 2024;42(3):e4018. doi:10.1002/cbf.4018

137. Wang Y, Liu W, Liu Y, et al. Long noncoding RNA H19 mediates LCoR to impact the osteogenic and adipogenic differentiation of mBMSCs in mice through sponging miR-188. *J Cell Physiol*. 2018;233(9):7435-7446. doi:10.1002/jcp.26589

138. Hofmann P, Sommer J, Theodorou K, et al. Long non-coding RNA H19 regulates endothelial cell aging via inhibition of STAT3 signalling. *Cardiovasc Res*. 2019;115(1):230-242. doi:10.1093/cvr/cvy206

139. Chen B, Wang H, Lv C, Mao C, Cui Y. Long non-coding RNA H19 protects against intracerebral hemorrhage injuries via regulating microRNA-106b-5p/acyl-CoA synthetase long chain family member 4 axis. *Bioengineered*. 12(1):4004-4015. doi:10.1080/21655979.2021.1951070

140. Luo H, Wang J, Liu D, et al. The lncRNA H19/miR-675 axis regulates myocardial ischemic and reperfusion injury by targeting PPARα. *Mol Immunol*. 2019;105:46-54. doi:10.1016/j.molimm.2018.11.011

141. Imig J, Brunschweiger A, Brümmer A, et al. miR-CLIP capture of a miRNA targetome uncovers a lincRNA H19–miR-106a interaction. *Nat Chem Biol*. 2015;11(2):107-114. doi:10.1038/nchembio.1713

142. Liang WC, Fu WM, Wang YB, et al. H19 activates Wnt signaling and promotes osteoblast differentiation by functioning as a competing endogenous RNA. *Sci Rep*. 2016;6(1):20121. doi:10.1038/srep20121

143. Wei LQ, Li L, Lu C, Liu J, Chen Y, Wu H. Involvement of H19/miR-326 axis in hepatocellular carcinoma development through modulating TWIST1. *J Cell Physiol*. 2019;234(4):5153-5162. doi:10.1002/jcp.27319

144. Wu W, Hu Q, Nie E, et al. Hypoxia induces H19 expression through direct and indirect Hif-1α activity, promoting oncogenic effects in glioblastoma. *Sci Rep*. 2017;7(1):45029. doi:10.1038/srep45029

145. Wang J, Zhao H, Fan Z, et al. Long Noncoding RNA H19 Promotes Neuroinflammation in Ischemic Stroke by Driving Histone Deacetylase 1-Dependent M1 Microglial Polarization. *Stroke*. 2017;48(8):2211-2221. doi:10.1161/STROKEAHA.117.017387

146. Wan P, Su W, Zhang Y, et al. LncRNA H19 initiates microglial pyroptosis and neuronal death in retinal ischemia/reperfusion injury. *Cell Death Differ*. 2020;27(1):176-191. doi:10.1038/s41418-019-0351-4

147. Cui C, Li Z, Wu D. The long non-coding RNA H19 induces hypoxia/reoxygenation injury by up-regulating autophagy in the hepatoma carcinoma cells. *Biol Res*. 2019;52(1):32. doi:10.1186/s40659-019-0239-2

148. Echevarría W, Leite MF, Guerra MT, Zipfel WR, Nathanson MH. Regulation of calcium signals in the nucleus by a nucleoplasmic reticulum. *Nat Cell Biol*. 2003;5(5):440-446. doi:10.1038/ncb980

149. Wagner LA, Christensen CJ, Dunn DM, et al. EGO, a novel, noncoding RNA gene, regulates eosinophil granule

protein transcript expression. *Blood*. 2007;109(12):5191-5198. doi:10.1182/blood-2006-06-027987

150. Wu Y, Liang S, Xu B, et al. Long noncoding RNA eosinophil granule ontogeny transcript inhibits cell proliferation and migration and promotes cell apoptosis in human glioma. *Exp Ther Med*. 2017;14(4):3817-3823. doi:10.3892/etm.2017.4949

151. Sp X, Jf Z, Sy S, et al. Downregulation of the long noncoding RNA EGOT correlates with malignant status and poor prognosis in breast cancer. *Tumour Biol J Int Soc Oncodevelopmental Biol Med*. 2015;36(12). doi:10.1007/s13277-015-3746-y

152. Qiu S, Chen G, Peng J, et al. LncRNA EGOT decreases breast cancer cell viability and migration via inactivation of the Hedgehog pathway. *FEBS Open Bio*. 2020;10(5):817-826. doi:10.1002/2211-5463.12833

153. Jin L, Quan J, Pan X, et al. Identification of lncRNA EGOT as a tumor suppressor in renal cell carcinoma. *Mol Med Rep*. 2017;16(5):7072-7079. doi:10.3892/mmr.2017.7470

154. Peng W, Wu J, Fan H, Lu J, Feng J. LncRNA EGOT Promotes Tumorigenesis Via Hedgehog Pathway in Gastric Cancer. *Pathol Oncol Res POR*. 2019;25(3):883-887. doi:10.1007/s12253-017-0367-3

155. Garitano-Trojaola A, Agirre X, Prósper F, Fortes P. Long non-coding RNAs in haematological malignancies. *Int J Mol Sci*. 2013;14(8):15386-15422. doi:10.3390/ijms140815386

156. Carnero E, Barriocanal M, Prior C, et al. Long noncoding RNA EGOT negatively affects the antiviral response and favors HCV replication. *EMBO Rep*. 2016;17(7):1013-1028. doi:10.15252/embr.201541763

157. Barriocanal M, Prior C, Suarez B, et al. Long Noncoding RNA EGOT Responds to Stress Signals to Regulate Cell Inflammation and Growth. *J Immunol Baltim Md 1950*. 2021;206(8):1932-1942. doi:10.4049/jimmunol.1900776

158. Zhang C, Pan S, Aisha A, Abudoukelimu M, Tang L, Ling Y. Recombinant human brain natriuretic peptide regulates PI3K/AKT/mTOR pathway through lncRNA EGOT to attenuate hypoxia-induced injury in H9c2 cardiomyocytes. *Biochem Biophys Res Commun*. 2018;503(3):1186-1193. doi:10.1016/j.bbrc.2018.07.023

159. Xu S, Wang P, Zhang J, et al. Ai-lncRNA EGOT enhancing autophagy sensitizes paclitaxel cytotoxicity via upregulation of ITPR1 expression by RNA-RNA and RNA-protein interactions in human cancer. *Mol Cancer*. 2019;18(1):89. doi:10.1186/s12943-019-1017-z

160. Wang IK, Palanisamy K, Sun KT, et al. The functional interplay of lncRNA EGOT and HuR regulates hypoxia-induced autophagy in renal tubular cells. *J Cell Biochem*. 2020;121(11):4522-4534. doi:10.1002/jcb.29669

161. Hutchinson JN, Ensminger AW, Clemson CM, Lynch CR, Lawrence JB, Chess A. A screen for nuclear transcripts identifies two linked noncoding RNAs associated with SC35 splicing domains. *BMC Genomics*. 2007;8:39. doi:10.1186/1471-2164-8-39

162. Souquere S, Beauclair G, Harper F, Fox A, Pierron G. Highly ordered spatial organization of the structural long noncoding NEAT1 RNAs within paraspeckle nuclear bodies. *Mol Biol Cell*. 2010;21(22):4020-4027. doi:10.1091/mbc.E10-08-0690

163. Sasaki YTF, Ideue T, Sano M, Mituyama T, Hirose T. MENε/β noncoding RNAs are essential for structural integrity of nuclear paraspeckles. *Proc Natl Acad Sci*. 2009;106(8):2525-

2530. doi:10.1073/pnas.0807899106

164. Wang Y, Chen LL. Organization and function of paraspeckles. *Essays Biochem*. 2020;64(6):875-882. doi:10.1042/EBC20200010

165. Clemson CM, Hutchinson JN, Sara SA, et al. An Architectural Role for a Nuclear Non-coding RNA: NEAT1 RNA is Essential for the Structure of Paraspeckles. *Mol Cell*. 2009;33(6):717-726. doi:10.1016/j.molcel.2009.01.026

166. Pan Y, Wang T, Zhao Z, et al. Novel Insights into the Emerging Role of Neat1 and Its Effects Downstream in the Regulation of Inflammation. *J Inflamm Res*. 2022;15:557-571. doi:10.2147/JIR.S338162

167. Hb I, Ah F. Unveiling the intricacies of paraspeckle formation and function. *Curr Opin Cell Biol*. 2024;90. doi:10.1016/j.ceb.2024.102399

168. Bu F tian, Wang A, Zhu Y, et al. LncRNA NEAT1: Shedding light on mechanisms and opportunities in liver diseases. *Liver Int*. 2020;40(11):2612-2626. doi:10.1111/liv.14629

169. Choudhry H, Harris AL, McIntyre A. The tumour hypoxia induced non-coding transcriptome. *Mol Aspects Med*. 2016;47-48(~272):35-53. doi:10.1016/j.mam.2016.01.003

170. My A, Ro S, A H, et al. Molecular Mechanisms of Tumorgenesis and Metastasis of Long Non-coding RNA (lncRNA) NEAT1 in Human Solid Tumors; An Update. *Cell Biochem Biophys*. 2024;82(2). doi:10.1007/s12013-024-01287-9

171. Li K, Wang Z. lncRNA NEAT1: Key player in neurodegenerative diseases. *Ageing Res Rev*. 2023;86:101878. doi:10.1016/j.arr.2023.101878

172. Jia D, He Y, Wang Y, et al. NEAT1: A Novel Long Non-coding RNA Involved in Mediating Type 2 Diabetes and its Various Complications. *Curr Pharm Des*. 2022;28(16):1342-1350. doi:10.2174/1381612828666220428093207

173. Almalki WH. NEAT1 in inflammatory infectious diseases: An integrated perspective on molecular modulation. *Pathol Res Pract*. 2024;254:154956. doi:10.1016/j.prp.2023.154956

174. Al-Hawary SIS, Kashikova K, Ioffe EM, et al. Pathological role of LncRNAs in immune-related disease via regulation of T regulatory cells. *Pathol Res Pract*. 2023;249:154709. doi:10.1016/j.prp.2023.154709

175. Yan K, Fu Y, Zhu N, et al. Repression of lncRNA NEAT1 enhances the antitumor activity of CD8+T cells against hepatocellular carcinoma via regulating miR-155/Tim-3. *Int J Biochem Cell Biol*. 2019;110:1-8. doi:10.1016/j.biocel.2019.01.019

176. Kong Y, Huang T, Zhang H, et al. The lncRNA NEAT1/miR-29b/Atg9a axis regulates IGFBPrP1-induced autophagy and activation of mouse hepatic stellate cells. *Life Sci*. 2019;237:116902. doi:10.1016/j.lfs.2019.116902

177. T Y, S S, T C, et al. Functional Domains of NEAT1 Architectural lncRNA Induce Paraspeckle Assembly through Phase Separation. *Mol Cell*. 2018;70(6). doi:10.1016/j.molcel.2018.05.019

178. R L, Ar H, Si H, Ah F. Functional dissection of NEAT1 using genome editing reveals substantial localization of the NEAT1_1 isoform outside paraspeckles. *RNA N Y N*. 2017;23(6). doi:10.1261/rna.059477.116

179. Ren L, Chen S, Liu W, Hou P, Sun W, Yan H. Downregulation of long non-coding RNA nuclear enriched abundant transcript 1 promotes cell proliferation and inhibits

cell apoptosis by targeting miR-193a in myocardial ischemia/reperfusion injury. *BMC Cardiovasc Disord*. 2019;19(1):192. doi:10.1186/s12872-019-1122-3

180. Wang L, Qu P, Yin W, Sun J. Lnc-NEAT1 induces cell apoptosis and inflammation but inhibits proliferation in a cellular model of hepatic ischemia/reperfusion injury. *J Int Med Res*. 2021;49(3):300060519887251. doi:10.1177/0300060519887251

181. Wang M, Cheng H, Wu H, et al. Gambogenic acid antagonizes the expression and effects of long non-coding RNA NEAT1 and triggers autophagy and ferroptosis in melanoma. *Biomed Pharmacother Biomedecine Pharmacother*. 2022;154:113636. doi:10.1016/j.biopha.2022.113636

182. Eggenhofer E, Groell A, Junger H, et al. Steatotic Livers Are More Susceptible to Ischemia Reperfusion Damage after Transplantation and Show Increased γδ T Cell Infiltration. *Int J Mol Sci*. 2021;22(4):2036. doi:10.3390/ijms22042036

183. Zhu SF, Yuan W, Du YL, Wang BL. Research progress of lncRNA and miRNA in hepatic ischemia-reperfusion injury. *Hepatobiliary Pancreat Dis Int HBPD INT*. 2023;22(1):45-53. doi:10.1016/j.hbpd.2022.07.008

184. Christou CD, Tsoulfas G. The Role of microRNA in Hepatic Ischemia/Reperfusion Injury. *MicroRNA*. 9(4):248-254.

185. Shao JL, Wang LJ, Xiao J, Yang JF. Non-coding RNAs: The potential biomarker or therapeutic target in hepatic ischemia-reperfusion injury. *World J Gastroenterol*. 2023;29(33):4927-4941. doi:10.3748/wjg.v29.i33.4927

186. Bai X feng, Niu R ze, Liu J, et al. Roles of noncoding RNAs in the initiation and progression of myocardial ischemia–reperfusion injury. *Epigenomics*. 2021;13(09):715-743.

187. Cao Y, Liu J, Lu Q, et al. An update on the functional roles of long non-coding RNAs in ischemic injury (Review). *Int J Mol Med*. 2022;50(1):91. doi:10.3892/ijmm.2022.5147

188. Ghafouri-Fard S, Shoorei H, Taheri M. Non-coding RNAs participate in the ischemia-reperfusion injury. *Biomed Pharmacother*. 2020;129:110419.

189. Gong C, Zhou X, Lai S, Wang L, Liu J. Long noncoding RNA/circular RNA-miRNA-mRNA axes in ischemia-reperfusion injury. *BioMed Res Int*. 2020;2020. Accessed March 28, 2024. https://www.hindawi.com/journals/bmri/2020/8838524/

190. Li Q, Li Z, Fan Z, Yang Y, Lu C. Involvement of non-coding RNAs in the pathogenesis of myocardial ischemia/reperfusion injury. *Int J Mol Med*. 2021;47(4):1-1.

191. Lu M, Dong X, Zhang Z, Li W, Khoshnam SE. Non-coding RNAs in ischemic stroke: roles in the neuroinflammation and cell death. *Neurotox Res*. 2020;38:564-578.

192. Marinescu MC, Lazar AL, Marta MM, Cozma A, Catana CS. Non-coding RNAs: prevention, diagnosis, and treatment in myocardial ischemia–reperfusion injury. *Int J Mol Sci*. 2022;23(5):2728.

193. Xiong W, Qu Y, Chen H, Qian J. Insight into long noncoding RNA–miRNA–mRNA axes in myocardial ischemia-reperfusion injury: the implications for mechanism and therapy. *Epigenomics*. 2019;11(15):1733-1748.

194. Bao MH, Szeto V, Yang BB, Zhu S zhen, Sun HS, Feng ZP. Long non-coding RNAs in ischemic stroke. *Cell Death Dis*. 2018;9(3):281. doi:10.1038/s41419-018-0282-x

195. Lumkul L, Jantaree P, Jaisamak K, et al. Combinatorial Gene Expression Profiling of Serum HULC, HOTAIR, and UCA1 lncRNAs to Differentiate Hepatocellular Carcinoma from

Liver Diseases: A Systematic Review and Meta-Analysis. *Int J Mol Sci*. 2024;25(2):1258. doi:10.3390/ijms25021258

196. Wang Q, Liu L, Zhang S, et al. Long noncoding RNA NEAT1 suppresses hepatocyte proliferation in fulminant hepatic failure through increased recruitment of EZH2 to the LATS2 promoter region and promotion of H3K27me3 methylation. *Exp Mol Med*. 2020;52(3):461-472. doi:10.1038/s12276-020-0387-z

197. Lu M, Sun WL, Shen J, et al. LncRNA-UCA1 promotes PD development by upregulating SNCA. *Eur Rev Med Pharmacol Sci*. 2018;22(22):7908-7915. doi:10.26355/eurrev_201811_16417

198. Lu Y, Yang Z, Zhang J, et al. RNA-binding protein QKI promotes the progression of HCC by interacting with long non-coding RNA EGOT. *Int Immunopharmacol*. 2024;136:112297. doi:10.1016/j.intimp.2024.112297

199. Liu B, Ren H, Chen J. LncRNA NEAT1 correlates with Th1 and Th17 and could serve as an assistant biomarker in sepsis. *Biomark Med*. 2021;15(13):1177-1186. doi:10.2217/bmm-2020-0906

200. An H, Williams NG, Shelkovnikova TA. NEAT1 and paraspeckles in neurodegenerative diseases: A missing lnc found? *Non-Coding RNA Res*. 2018;3(4):243-252. doi:10.1016/j.ncrna.2018.11.003

201. Saleh RO, Alkhafaji AT, Mohammed JS, et al. LncRNA NEAT1 in the pathogenesis of liver-related diseases. *Cell Biochem Funct*. 2024;42(3):e4006. doi:10.1002/cbf.4006

202. Li K, Yao T, Zhang Y, Li W, Wang Z. NEAT1 as a competing endogenous RNA in tumorigenesis of various cancers: Role, mechanism and therapeutic potential. *Int J Biol Sci*. 2021;17(13):3428-3440. doi:10.7150/ijbs.62728

203. Gidlöf O, Bader K, Celik S, et al. Inhibition of the long non-coding RNA NEAT1 protects cardiomyocytes from hypoxia in vitro via decreased pri-miRNA processing. *Cell Death Dis*. 2020;11(8):677. doi:10.1038/s41419-020-02854-7

204. Zhang Y, Luo M, Cui X, O'Connell D, Yang Y. Long noncoding RNA NEAT1 promotes ferroptosis by modulating the miR-362-3p/MIOX axis as a ceRNA. *Cell Death Differ*. 2022;29(9):1850-1863. doi:10.1038/s41418-022-00970-9

205. Wei X biao, Jiang W qiang, Zeng J hao, et al. Exosome-Derived lncRNA NEAT1 Exacerbates Sepsis-Associated Encephalopathy by Promoting Ferroptosis Through Regulating miR-9-5p/TFRC and GOT1 Axis. *Mol Neurobiol*. 2022;59(3):1954-1969. doi:10.1007/s12035-022-02738-1

206. Koppula P, Zhuang L, Gan B. Cystine transporter SLC7A11/xCT in cancer: ferroptosis, nutrient dependency, and cancer therapy. *Protein Cell*. 2021;12(8):599-620. doi:10.1007/s13238-020-00789-5

207. Dolma S, Lessnick SL, Hahn WC, Stockwell BR. Identification of genotype-selective antitumor agents using synthetic lethal chemical screening in engineered human tumor cells. *Cancer Cell*. 2003;3(3):285-296. doi:10.1016/s1535-6108(03)00050-3

208. Wu H, Liu A. Long non-coding RNA NEAT1 regulates ferroptosis sensitivity in non-small-cell lung cancer. *J Int Med Res*. 2021;49(3):300060521996183. doi:10.1177/0300060521996183

209. Yu Q, Li Y, Zhang N, et al. Silencing of lncRNA NEAT1 alleviates acute myocardial infarction by suppressing miR-450-5p/ACSL4-mediated ferroptosis. *Exp Cell Res*. 2024;442(2):114217. doi:10.1016/j.yexcr.2024.114217

210. Choudhry H. UCA1 overexpression promotes hypoxic

breast cancer cell proliferation and inhibits apoptosis via HIF-1α activation. *J Oncol*. 2021;2021:5512156. doi:10.1155/2021/5512156

211. Diao L, Zhang Q. Transfer of lncRNA UCA1 by hUCMSCs-derived exosomes protects against hypoxia/reoxygenation injury through impairing miR-143-targeted degradation of Bcl-2. *Aging*. 2021;13(4):5967-5985. doi:10.18632/aging.202520

212. Li Z, Li X, Wu S, Xue M, Chen W. Long non-coding RNA UCA1 promotes glycolysis by upregulating hexokinase 2 through the mTOR–STAT3/microRNA143 pathway. *Cancer Sci*. 2014;105(8):951-955. doi:10.1111/cas.12461

213. Song Z, Suo C, Liu Y, et al. Comprehensive evaluation of non-coding RNA-mediated autophagy regulation in myocardial ischemia-reperfusion injury. *Front Pharmacol*. 2025;16. doi:10.3389/fphar.2025.1581341

214. Wang C, Deng J, Deng H, et al. A Novel Sox9/lncRNA H19 Axis Contributes to Hepatocyte Death and Liver Fibrosis. *Toxicol Sci Off J Soc Toxicol*. 2020;177(1):214-225. doi:10.1093/toxsci/kfaa097

215. B A, Sn P, Z S, H G, H G. An updated review of the H19 lncRNA in human cancer: molecular mechanism and diagnostic and therapeutic importance. *Mol Biol Rep*. 2020;47(8). doi:10.1007/s11033-020-05695-x

216. Yang F, Bi J, Xue X, et al. Up-regulated long non-coding RNA H19 contributes to proliferation of gastric cancer cells. *FEBS J*. 2012;279(17):3159-3165. doi:10.1111/j.1742-4658.2012.08694.x

217. Matouk IJ, Mezan S, Mizrahi A, et al. The oncofetal H19 RNA connection: Hypoxia, p53 and cancer. *Biochim Biophys Acta BBA - Mol Cell Res*. 2010;1803(4):443-451. doi:10.1016/j.bbamcr.2010.01.010

218. Gabory A, Jammes H, Dandolo L. The H19 locus: Role of an imprinted non-coding RNA in growth and development. *BioEssays*. 2010;32(6):473-480. doi:10.1002/bies.200900170

219. Cai X, Cullen BR. The imprinted H19 noncoding RNA is a primary microRNA precursor. *RNA N Y N*. 2007;13(3):313-316. doi:10.1261/rna.351707

220. Di Sanzo M, Chirillo R, Aversa I, et al. shRNA targeting of ferritin heavy chain activates H19/miR-675 axis in K562 cells. *Gene*. 2018;657:92-99. doi:10.1016/j.gene.2018.03.027

221. Mahmoudi-Lamouki R, Kadkhoda S, Hussen BM, Ghafouri-Fard S. Emerging role of miRNAs in the regulation of ferroptosis. *Front Mol Biosci*. 2023;10. doi:10.3389/fmolb.2023.1115996

222. Duan S, Li M, Wang Z, Wang L, Liu Y. H19 induced by oxidative stress confers temozolomide resistance in human glioma cells via activating NF-κB signaling. *OncoTargets Ther*. 2018;11:6395-6404. doi:10.2147/OTT.S173244

223. Berghe TV, Linkermann A, Jouan-Lanhouet S, Walczak H, Vandenabeele P. Regulated necrosis: the expanding network of non-apoptotic cell death pathways. *Nat Rev Mol Cell Biol*. 2014;15(2):135-147. doi:10.1038/nrm3737

224. Verzella D, Pescatore A, Capece D, et al. Life, death, and autophagy in cancer: NF-κB turns up everywhere. *Cell Death Dis*. 2020;11(3):210. doi:10.1038/s41419-020-2399-y

225. Georgiadis V, Knight RA. Necroptosis: STAT3 kills? *Jak-Stat*. 2012;1(3):200-202. doi:10.4161/jkst.20968

226. Wang Y, Hylemon PB, Zhou H. Long non-coding RNA H19: A key player in liver diseases. *Hepatol Baltim Md*. 2021;74(3):1652-1659. doi:10.1002/hep.31765

227. Zhou M, Zou YG, Y.-Z. Xue, et al. Long non-coding RNA

H19 protects acute myocardial infarction through activating autophagy in mice. *Eur Rev Med Pharmacol Sci*. 2018;22(17):5647-5651. doi:10.26355/eurrev_201809_15831

228. Rose D, Stadler PF. Molecular Evolution of the Non-Coding Eosinophil Granule Ontogeny Transcript. *Front Genet*. 2011;2. doi:10.3389/fgene.2011.00069

229. Zhao Q, Liu J, Ouyang X, et al. Role of immune-related lncRNAs--PRKCQ-AS1 and EGOT in the regulation of IL-1β, IL-6 and IL-8 expression in human gingival fibroblasts with TNF-α stimulation. *J Dent Sci*. 2023;18(1):184-190. doi:10.1016/j.jds.2022.06.006

230. Tang D, Chen X, Kang R, Kroemer G. Ferroptosis: molecular mechanisms and health implications. *Cell Res*. 2021;31(2):107-125. doi:10.1038/s41422-020-00441-1

231. Nakagawa S, Naganuma T, Shioi G, Hirose T. Paraspeckles are subpopulation-specific nuclear bodies that are not essential in mice. *J Cell Biol*. 2011;193(1):31-39. doi:10.1083/jcb.201011110

232. Parker JL, Deme JC, Kolokouris D, et al. Molecular basis for redox control by the human cystine/glutamate antiporter system xc−. *Nat Commun*. 2021;12(1):7147. doi:10.1038/s41467-021-27414-1

233. Doll S, Freitas FP, Shah R, et al. FSP1 is a glutathione-independent ferroptosis suppressor. *Nature*. 2019;575(7784):693-698. doi:10.1038/s41586-019-1707-0

234. Feng L, Zhao K, Sun L, et al. SLC7A11 regulated by NRF2 modulates esophageal squamous cell carcinoma radiosensitivity by inhibiting ferroptosis. *J Transl Med*. 2021;19:367. doi:10.1186/s12967-021-03042-7

235. Friedmann Angeli JP, Conrad M. Selenium and GPX4, a

vital symbiosis. *Free Radic Biol Med*. 2018;127:153-159. doi:10.1016/j.freeradbiomed.2018.03.001

236. Xie Y, Kang R, Klionsky DJ, Tang D. GPX4 in cell death, autophagy, and disease. *Autophagy*. 19(10):2621-2638. doi:10.1080/15548627.2023.2218764

237. Guo S, Li Z, Liu Y, Cheng Y, Jia D. Ferroptosis: a new target for hepatic ischemia-reperfusion injury? *Free Radic Res*. 2024;58(6-7):396-416. doi:10.1080/10715762.2024.2386075

238. Yamada N, Karasawa T, Wakiya T, et al. Iron overload as a risk factor for hepatic ischemia-reperfusion injury in liver transplantation: Potential role of ferroptosis. *Am J Transplant*. 2020;20(6):1606-1618. doi:10.1111/ajt.15773

IV. Supplements

Table 2. List of 114 Candidate lncRNAs Implicated in Liver Pathophysiology.

No.	lncRNA Symbol	No.	lncRNA Symbol	No.	lncRNA Symbol
1	DLX6-AS1	39	TRERNA1	77	HAR1B
2	EMX2OS	40	ERVK3-1	78	PRINS
3	DIO3OS	41	PPP1R26-AS1	79	HOTAIRM1
4	PCGEM1	42	LINC00263	80	PTCSC1
5	KCNIP4-IT1	43	LINC01139	81	LINC00853
6	CDKN2B-AS1	44	NRON	82	GACAT1
7	FAS-AS1	45	ST7-AS1	83	CPS1-IT1
8	SIX3-AS1	46	PTENP1	84	FLJ16779
9	RBM5-AS1	47	WT1-AS	85	ARAP1-AS2
10	LINC-ROR	48	UCA1	86	MESTIT1
11	HIF1A-AS1	49	HOXA-AS3	87	LINC00599
12	LINC00520	50	TMEM161B-AS1	88	GNAS-AS1
13	LINC00635	51	KRASP1	89	FENDRR
14	TCF7	52	RPS6KA2-AS1	90	NEAT1
15	NTC	53	LINC00570	91	DISC2
16	TUSC7	54	PVT1	92	OIP5-AS1
17	MALAT1	55	DLGAP1-AS1	93	FTX
18	IPW	56	LINC00673	94	CCAT1
19	HOXA-AS2	57	ARID2	95	PCAT1
20	BDNF-AS	58	IGF2-AS	96	LINC00581
21	HOTAIR	59	ZFAS1	97	PWAR5
22	BOK-AS1	60	XIST	98	NPTN-IT1
23	TUNAR	61	BCYRN1	99	LINC00323
24	NAMA	62	HAR1A	100	SPAG5-AS1
25	PTCSC3	63	MRPL23-AS1	101	LINC01093
26	HIF1A-AS2	64	LUCAT1	102	DANCR
27	HNF4A-AS1	65	AIRN	103	TUG1

28	RP5-1104E15,6	66	PTENP1-AS	104	RMST
29	RPPH1	67	CCAT2	105	SOX2-OT
30	ST7-AS2	68	UBE2CP3	106	HOXA11-AS
31	ATXN8OS	69	LINC01215	107	HULC
32	TINCR	70	CASC2	108	OTX2-AS1
33	H19	71	LINC00968	109	SNHG16
34	JPX	72	PPIH	110	SPRY4-IT1
35	EGOT	73	TERC	111	BANCR
36	HOTTIP	74	MIAT	112	BACE1-AS
37	MEG9	75	GAS5	113	EGLN2
38	HEIH	76	TSIX	114	FAM53B-AS1